TITANIA-SILICA SOL-GEL COATINGS

ON GLASS

By

ADEAL SOBHE MATUK

A dissertation submitted to the

School of Graduate Studies

Rutgers, The State University of New Jersey

In partial fulfillment of the requirements

For the degree of

Doctor of Philosophy

Graduate Program in Materials Science & Engineering

Written under the direction of

Professor Lisa C. Klein

And approved by

_____

_____

_____

_____

_____

New Brunswick, New Jersey

October 2018

ABSTRACT OF THE DISSERTATION

Titania-Silica Sol-Gel Coatings on Glass

By ADEAL SOBHE MATUK

Dissertation Director:

Lisa C. Klein

Binary TiO_2-SiO_2 oxides are materials that have attracted attention due to their usefulness as heterogeneous catalysts and catalytic supports. Due to the large difference between their optical properties, in particular, band gap and refractive index, and their compatibility with respect to the deposition conditions, SiO_2 and TiO_2 appear well suited for these purposes. These materials have been synthesized by several techniques including chemical vapor deposition, sputtering and sol-gel. The sol-gel process is a versatile method to control the thickness, uniformity and thermal stability of high surface area materials. The sol-gel method presents many advantages such as utilization of simple equipment, high homogeneity and the possibility of using a variety of substrates of different sizes.

This thesis investigates the preparation of glass coatings from TiO_2-SiO_2 and Fe-doped TiO_2-SiO_2 by using the low-temperature sol-gel process. The TiO_2-SiO_2 sol was prepared from titanium (IV) butoxide $Ti(OCH_2CH_2CH_2CH_3)_4$, and tetraethylorthosilicate

(TEOS), (Si (OC_2H_5)$_4$). The steps involved in the fabrication of sol-gel derived thin films, such as sol preparation and substrate preparation are discussed. Physical and chemical characterization of the thin films are discussed in detail. UV-Visible spectroscopy, Scanning Electron Microscopy (SEM), X-ray diffraction (XRD), and Fourier transform infrared spectroscopy (FTIR) were used to measure transmittance, thickness of films, the identification of phases, and chemical structure.

Eleven different compositions, 3, 5, 7.9, 10, and 15% TiO_2, and iron (Fe) doped TiO_2- SiO_2 were investigated. Films with five compositions of SiO_2-TiO_2 were coated onto glass microscope slides using dip-coating method. Thin films in this study were subjected to heat treatment in a furnace at 100ºC for 24 hours. The samples with 1 and 3 dip-coatings of 10% TiO_2-90% SiO_2 and 15% TiO_2-85% SiO_2 with solution age 0, 5, 15, and 25 days exhibit higher transmittance than any of the other compositions, especially in the spectral region 400-600nm. Since the peak of the solar radiation spectrum lies in this important spectral region, the optical performance of these samples is promising, and these samples were studied further. Transmission spectra for different amounts of $Fe(NO_3)_3$ doped TiO_2-SiO_2 thin films show that the films with smaller amounts of $Fe(NO_3)_3$ 0.0001 % exhibited higher transmittance in the spectral region 450nm - 550nm. This dopant amount has negligible absorption. Also, the transmittance of the as-deposited films at 0 days for all layers 1 and 3 is higher than the transmittance of the films for the solution aged 25 days. The solution should not be aged, if practical. The thickness of films with 1 and 3 coatings on the glass substrate were measured in fresh and aged solutions. The results of thickness measurements are in agreement with the transmittance measurement results.

Based on XRD analysis, the synthesized powders are amorphous. No characteristic crystalline peaks are observed. Higher photocatalytic activity is predicted for samples which are amorphous. Also, the amount of Fe ions had little effect on the crystal structure of the TiO_2-SiO_2.

The FT-IR spectra of all samples look similar. Hydroxyl groups were observed in all samples at around 3300 cm^{-1} and at about 1630 cm^{-1}. Siloxane bonds were detected at 1051, 1130, and 795 cm^{-1}. The linkage between TiO_2-SiO_2 was confirmed by the band at 935 cm^{-1} which is attributed to the Si-O-Ti stretching mode. The spectral features of TiO_2 can be discerned at around 553 and 446 cm^{-1}, attributed to Ti-O and Ti-O-Ti bonds. The addition of iron is evidenced by the peak of the ν Fe-O vibration band at ~420 cm^{-1}.

Acknowledgments

Over the last five and half years of my graduate study at Rutgers University, I have learned great things not only about science and academics but also about the life, the truth, and the faith. I have truly enjoyed every moment of learning and I am grateful to have these kinds of experience in my life. After pass this years, I came to put an end to this journey. I met lots of good people and shared these years with great groups of people. I cannot mention all the names but every single person I have met contributed to this dissertation in different ways and I would like to acknowledge them.

First of all, I would like to thank ALLAH for everything and for his generosity and mercy in giving me the strength and the ability to overcome the difficulties which I faced throughout the period of my study.

I would like to express my greatest gratitude to my advisor, Prof. Lisa C. Klein, for her support, guidance, encouragement over the past five and half years. Many thanks for her patience, confidence and the opportunity she offered for me to gain professional experience and maturity. She has been more than a guide, a friend, and philosopher, to me. Thank you for the opportunity me to study and explore a small window in the vast, interesting field of Sol-Gel science. Most achievements during my Ph.D. study would not be possible without her excellent guidance and supports. I am proud to work under her supervision and on a project which is very interesting. A very special thanks are addressed to Prof. Andrei Jitianu for being supportive at all levels. He, who has extensive knowledge in various areas and a passion for research, always has been a paragon to me. It was a

privilege to work with such an excellent mentor, and a good friend as well. His ideas, advice and contributions were and will always be invaluable.

I wish to express my gratefulness to my committee members Prof. Richard Lehman, Prof. Adrian Mann, Prof. Andrei Jitianu, and Assistant Prof. Ashutosh Goel, for their time, comments, and helpful suggestions, all of which made this thesis better. Again, I especially record my deep appreciation and thanks to Assistant Prof. Dr. Ashutosh Goel and Prof. James Harrington for giving me the necessary permission to use their laboratory facilities whenever I needed. I would like to thank all the faculty and staff members in Materials Science & Engineering at Rutgers, The State University of New Jersey.

I would like to thank my entire family for their support throughout the period of my study. Mom, brothers, and sisters thank you for all your encouragement and support when I needed it, and for keeping me on track to finish my work. Also, I would like to thank my other half, my friend, my insight, and my wife, thank you for your help, support, belief, and patience.

Last but not the least, I want to thank all my relatives and friends back home for their encouragements and prayers.

Dedication

I would like to dedicate this work to the soul of my father, Mr. Sobhe Matuk our dream finally comes true.

To the best mom in the whole world, and brothers, sisters,

And to my wonderful dear wife,

For all of them, I dedicate this work to their never-ending love, encourage and support from far away.

Table of Contents

LIST OF FIGURES

List of Tables

Chapter One
Fundamentals

1.1 Thin film technology

Nanomaterials are defined by a length scale of less than 100 nm, either in one dimension (nanowires), two dimensions (thin films) or in 3 dimensions (nanoparticles), so a thin film is a two-dimensional material prepared by the process of condensation and growth of atoms, molecules or ions [1]. Due to their physical dimension, geometry, and microstructure, the properties of thin films are usually different from those of bulk materials. They are largely affected by the high surface-to-volume ratio and influence a number of phenomena such as gas adsorption, diffusion, and catalytic activity. Most thin films have thicknesses ranging from a monolayer to nanometer levels up to several micrometers.

In recent years, thin film technology has grown and it is used in an endless variety of applications based on the various functional properties. Worldwide, thin films are a major research area. Some applications include thin films used for many and varied purposes in electronics, microelectronics, optics, information storage, engineering, biomedical fields, catalysis, corrosion protection, and chemical sensors, displays, nuclear, space, and other applications [2-5]. These applications are possible because of the optical, magnetic, reflective, electrical, mechanical and other properties that thin films have.

Thin films can be metallic, ceramic, polymer or even metallic glass. Independent of the film chemical composition, the mechanical characteristics, optical properties, and film thickness, structure, functional characteristics, and performance are strongly

influenced by the method and deposition parameters. Preparation conditions are therefore strongly related to the coating technologies, so to produce coatings for a certain application, it is necessary to know all the parameters that influence a desired film property during the deposition process. For films produced by the sol-gel process dip coating technique, the relevant parameters which must be taken into consideration are the composition of the solution, the temperature, the withdrawing speed, the interaction with the surrounding atmosphere during withdrawal of the substrate and the reaction with the substrate during densification [1].

The substrate has also a significant effect and many factors should be taken into consideration [6]. Properties such as the cleaning, the roughness of the substrate and the surface energy have an effect on adhesion between the coating and the substrate. Also, the stability of the substrate with the temperature variations as well as at the different aging processes affects their properties.

The wide range of materials, techniques for preparation, and range of applications make this an interdisciplinary field. Some common methods for depositing the various types of thin films are electroplating, chemical vapor deposition (CVD) and physical vapor deposition (PVD) [7].

1.2 Deposition techniques

There are several techniques for the deposition of coatings on substrates and they play a very important role to achieve desired film properties. Many different methods are used to fabricate thin films and each process has its own parameters, which control the formation and the growth of the films, where the deposition of the same material by

different deposition methods usually leads to different coating properties. The techniques employed for thin-film deposition can be classified into two main categories based on the nature of the deposition process viz., physical or chemical [1,8,9]:

(1) Vapor deposition techniques: include two main classes:

(a) Physical vapor deposition (PVD), such as sputtering and evaporation.

(b) Chemical vapor deposition (CVD), such as hydrothermal methods, plasma spraying, and pulsed laser deposition, etc.

(2) Wet chemical deposition techniques: The main deposition methods for this technique are the spray and the sol-gel coatings.

Chemical vapor deposition (CVD) and sol-gel methods are less expensive, in most cases, than physical vapor deposition (PVD) because the equipment does not require vacuum.

1.2.1 Vapor deposition techniques

1.2.1.1 Physical Vapor Deposition (PVD)

Physical vapor deposition (PVD) is capable of preparing thin film materials with structural control at the atomic or nanometer scale. It is a popular method for depositing due to the lower temperatures during deposition where atoms are transferred from a source (target) to a substrate in the form of a vapor. This technique was originally used by Granqvist and Buhrman in 1976 and developed by Gleiter in 1981. There are two commonly used forms of PVD, which are sputtering and evaporation.

Sputtering processes produce a thin film by dislodging atoms from the source through the influence of gaseous ions. The basic principle for sputter depositing is the same for all sputtering technologies. What differs between the types of sputtering methods is the power supply. The processes used include DC, RF, magnetron and reactive sputtering. This method deposition was discovered by Grove in 1852 [10].

In evaporation deposition, source materials and the substrate are placed in a vacuum chamber. The source material is heated to the point where it starts to evaporate and the vapor condenses onto a cooler substrate to form a film. There are different types of evaporation, but the basic principles remain the same and there are various parameters that control this method and all them are important to optimize the film properties, such as substrate temperature, chemical composition of the source, deposition rate, and deposition pressure [6].

1.2.1.2 Chemical Vapor Deposition (CVD)

The CVD process deposits reactive gases at the surface of a substrate without the need for vacuum. The substrate is placed inside a reactor where a number of gases can be supplied depending on the film needed. The fundamental principle for the process is that a chemical reaction takes place between the source gases [1]. There are three basic CVD techniques: lo w pressure CVD which produces layers with excellent uniformity of thickness, plasma CVD (PCVD) and laser CVD (LCVD). Laser CVD (LCVD) and thermal CVD use high temperatures, where thermodynamic processes govern the nature of the resulting deposit, while plasma CVD (PCVD) can take place at lower temperatures [11, 12].

1.2.2 Wet Chemical Deposition Techniques

Wet chemical deposition techniques include techniques in which the material species to be deposited are dispersed in a liquid medium. It is based on the preparation of solutions made of crystalline nanoparticles fully redispersable in a solvent. The term "wet chemical methods" refers to a group of methods of powder and material production using liquid phase at one of the process stages, like liquid phase sol-gel process, hydrothermal synthesis, Pechini method, spray drying, aerosol spray pyrolysis, or cryochemical synthesis [13]. These techniques have the ability to produce coatings with high optical quality on transparent substrates like glass and polymeric substrates as well as homogeneous coatings on non-transparent substrates. These processes are attractive due to their simplicity, versatility, and availability of low-cost precursors. They combine the advantages of using particles and the possibility to sinter the coatings at low temperature [8]. The main differences between wet chemistry products and similar products of solid-phase synthesis are much smaller grains (crystallites) and, usually, lower temperature and shorter duration of phase formation. Using wet chemical synthesis, films can be prepared over a broad range of dimensional-morphological regimes by careful control of thermodynamic parameters and growth kinetics in liquid media under assistance of selected solvents, ligands, surfactants or catalyst additives [14-16].

1.2.2.1 Spray Pyrolysis

Spray pyrolysis is a processing technique to prepare thin and thick films, ceramic coatings, and powders. It is one of the most used methods to coat substrates in a mass production with low effective cost [17]. Spray pyrolysis represents a very simple effective

processing method that is easy to carry out, versatile and inexpensive because of the availability of various low-cost chemical solutions, does not need complicated equipment or require high-quality substrates or chemicals, making it an easy technique for preparing films of any composition [18,19]. The method has been employed for the deposition of dense films, porous films, and for powder production, and used to coat large substrates with different geometries. The process consists in generating fine droplets which are then thermally decomposed on a hot substrate to form ultrafine particles or thin films [20-22].

1.2.2.2 Sol-Gel

The sol-gel process is a versatile process using chemical solutions. It is attractive because it is a series of chemical reactions which can be halted at different stages, and these the chemical reactions can be tailored at the molecular level. The sol-gel process involves the transition of a system from a liquid "sol" into a solid "gel" phase. Ebelman produced the first silica gels in 1846 [23] and Cossa synthesized alumina gels in 1870 [24].

The sol-gel method is relatively simple and is a widely used technique for obtaining coatings on various substrates. It is one of the most important technologies for preparing thin films for commercial applications [25]. Some of its advantages are for particles production in a relatively shorter processing time at lower temperatures [26], with its high process speed, a variety of chemical precursors, suitability for continuous production, ability to control the microstructure of the deposited film such as the pore size and the surface area [27]. The low cost of the sol-gel method is one important reason for the wide practice of this process. The sol-gel process is discussed in more detail in subsequent chapters.

1.3 Surface and coating technology

A coating can be defined as a thin layer or cover of something. When the coating thickness is less than few micrometers, it can be described as a thin film. To apply coatings onto the substrates and ensure good adhesion, it is necessary to clean the surface of the substrates. Sol-gel coatings adhere to the substrate through chemical covalent bonding and mechanical adhesion. The surface reactivity may be modified by the appropriate choice of precursors [28]. As mentioned above, some applications for sol-gel films and coatings are electronic coatings, optical coatings, porous coatings, and protective coatings [29]. Reflective or colored coatings have been used as antireflective surfaces in solar applications. Coatings have been applied on glass in order to obtain various properties, which render the glass more useful. Appropriate compounds are coated as a thin film on the glass by a variety of techniques [30–32].

1.4 Methods Used to Apply Sol-Gel on Substrates

Coatings and films are the earliest applications of the sol-gel technology. Several methods exist for depositing thin films by applying sol-gel coatings on substrates, such as dip coating, spin coating, spraying, painting, and electrodeposition [26]. These include the relatively simple methods of dip coating and spin coating, which are the two most commonly used coating methods. In this project, a dip coating method was employed which offers several significant advantages over other deposition techniques due to the use of very simple equipment. In this method, the sol-gel dipping process is applied for the fabrication of optically transparent layers, the substrate is immersed in a liquid and then

withdrawn at a defined speed under controlled temperature and atmospheric conditions [33].

1.4.1 Dip coating method

The dip coating technique is a good method to prepare thin films with high optical quality and homogeneity, and it is a method which is usually used to coat a solid material with some other material by dipping objects in suspension. The suspension that contains colloidal particles is often called the sol [25]. The process involves the formation of a film through successive steps of immersion of substrate into the dip-coating solution and withdrawal of the substrate form the solution at a constant rate. After the substrate is removed from the solution, the solvent is evaporated [28].

1.4.1.1 Advantages of dip coating

The dipping process is simple, cheap and can be used to coat large substrates on both sides in one step at room temperature, planar and axially symmetric substrates such as tubes, pipes, rods, fibers, and any complex shapes, which are not easily handled by a more conventional coating process [8]. This is of considerable importance to commercial applications since, in many instances, the cost of the process increases with substrate size. A high degree of film uniformity can be obtained, and thickness of the films can be controlled easily. Dip coating allows the fabrication of multi-layers with widely varying optical characteristics compared to some the sol-gel coating techniques, such as spin coating and spray coating [28].

1.4.1.2 Dip Coating Process

Dip coating is a process where a clean substrate is immersed in a liquid and then withdrawn at a given speed under controlled temperature and atmospheric conditions. The environmental conditions such as temperature and humidity affect the quality of the coating [28]. The coating process is finished with thermal treatment stage. Typically, sol−gel-derived coatings are amorphous. If desired, in order to introduce crystallization, controlled heat treatment is applied. To remove the entrapped solvent, and any organic remaining, thin films are dried and calcined at appropriate temperatures [34].

The dip-coating technique may operate in two distinct modes: first, by lifting the substrate from the coating solution (withdrawing) and second, by maintaining the sample at a fixed position and drawing the liquid away at a constant rate. The withdrawal process is the more economically applicable and employed in this work.

The dip coating process [35,36,27] can be divided into five separate stages: immersion (dipping), start-up, deposition, the formation of the wet layer where the boundary layer is formed, drainage and evaporation stage. Figure 1 shows the different stages of the dip coating process. The evaporation depends on the solvents used and normally accompanies the start-up, deposition and drainage stages. This leads to aggregation and gelation of the wet layer and once it has collapsed fully, a dense film remains on the substrate.

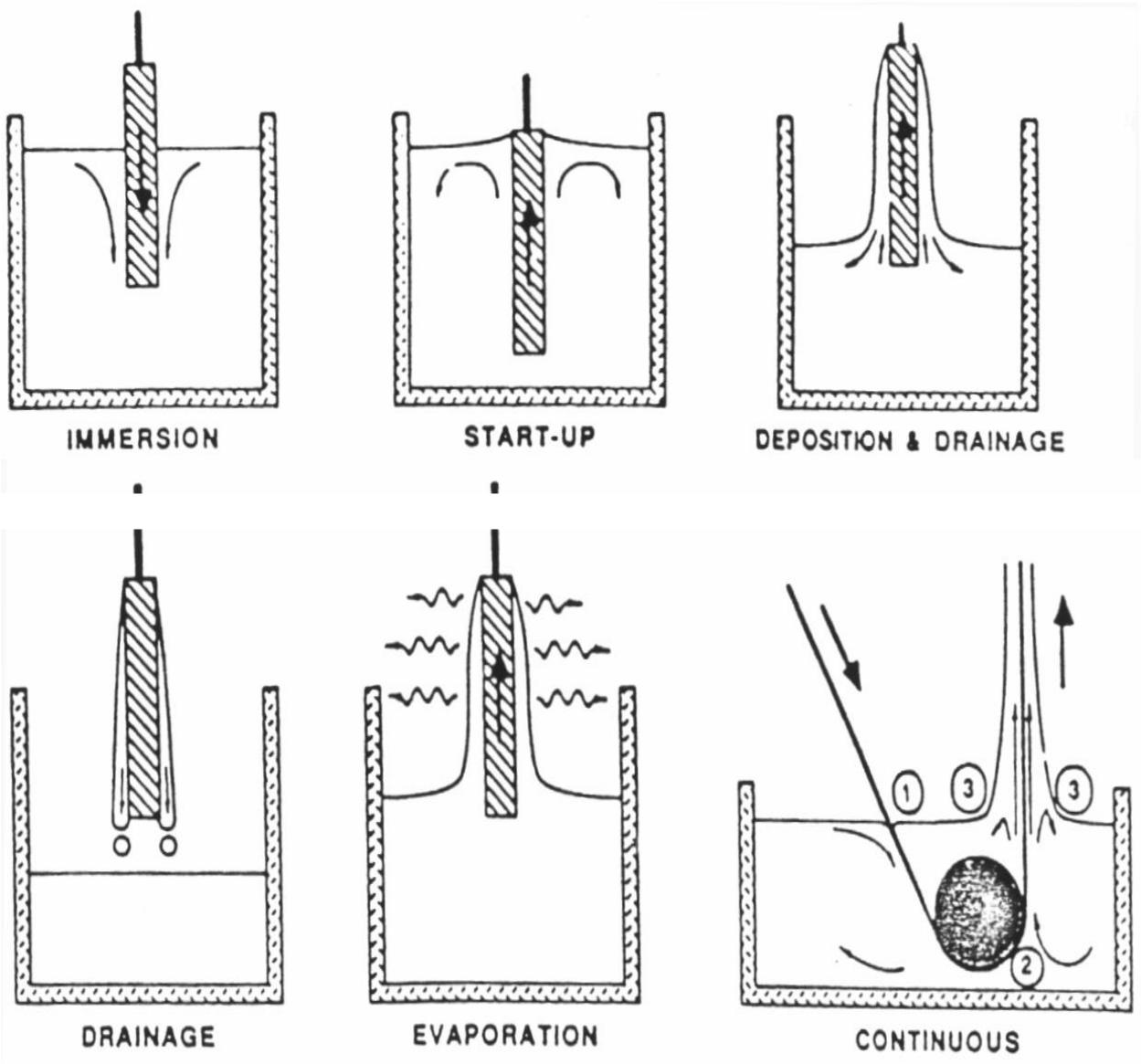

Figure 1-1: The different stages of the dip coating process [28]

In the deposition phase, the evaporation has the effect of making the coating rigid. The most significant factor in the evaporation effect is the amount of the diffusion of the vapor away from the film surface. The evaporation rate is independent of the liquid depth during dip coating. The movement of the substrate and convection could make the evaporation irregular [28].

In the dip coating process, there are five forces that have an effect on the film thickness, which may be in competition with each other. The net effect influences the position of the streamline and hence the film thickness. These forces are (1) viscous drag upward on the liquid by the moving substrate and the liquid container; (2) force due to gravity; (3) force due to surface tension; (4) inertial force of the boundary layer liquid arriving at the deposition region; and (5) disjoining or conjoining pressure.

The quality of the resultant thin films is dependent on the smooth removal of the liquid container. As a result, the dip coating apparatus usually is housed in a vibration-free chamber to minimize vibrations and avoid contact with the apparatus.

1.4.1.3 The thickness of the film

The thickness of the film is the result of the dividing of the upward- and the downward-moving layers. The inner layer of deposited liquid moves upward with the substrate and the outer layer is returned to the container. The film thickness is related to the position of the dividing border between the upward moving and the downward moving layers [29].

The thickness of the coating depends on the viscosity of the solution, the rate of solvent evaporation, and the substrate speed (υ). The liquid viscosity (η) and the substrate speed (υ) are the most important parameters and determine the deposited film thickness (h). It can be determined using the Landau-Levich equation that illustrates the relationship between film thickness and dip speed for Newtonian fluids [37].

$$h = 0.944 \frac{(\eta \upsilon)^{2/3}}{\gamma_{LV}^{\frac{1}{6}} (\rho . g)^{1/2}}$$

Where h is the film thickness, η is the liquid viscosity, υ is the withdrawal speed, γ_{LV} is the liquid-vapor surface tension, ρ is the density of the solution, and g is the acceleration due to gravity. The above equation shows that the faster the substrate is withdrawn, the thicker is the deposited film. In the case of sol-gel derived materials, if the viscosity and density of the solution remain constant, then the film thickness is proportional to the square root of the withdrawal speed [36].

1.5 Spin coating method

Another technique used for thin film deposition is spin coating [38]. This technique involves the deposition of thin films by centrifugal draining and evaporation. Spin coating is a popular method, which is characteristically used on flat substrates since the physics of application limit the coating uniformity. Thin films can be obtained by this process by depositing drops of the solution on the surface of a flat substrate, typically the center of the substrate and then spun it at high speeds letting the centrifugal force created to spread the coating on the surfaces and leave a uniform layer for subsequent processing stages and ultimate use[39].

There are four stages of forming thin films defined in the spin coating process, are described in Figure 2 [40]. The first stage is started by pouring coating solution (small substrate) or spraying it (big substrate) on the substrate. The basic requirement is that the amount of coating solution should be in excess and wet the surface completely during this stage. The second stage is started when the substrate is accelerated up to the desired

rotation speed. This rotation affects the uniformity and film properties, especially for the solution with high viscosity and volatile solvents. The third stage is keeping constant speed for the substrate spinning and fluid viscous forces dominate the fluid thinning behavior. Spin-coating speed is also can affect the microstructure of the film. The last stage is drying, during which the solvent is evaporated and at this point the coatings is effectively transformed into a gel.

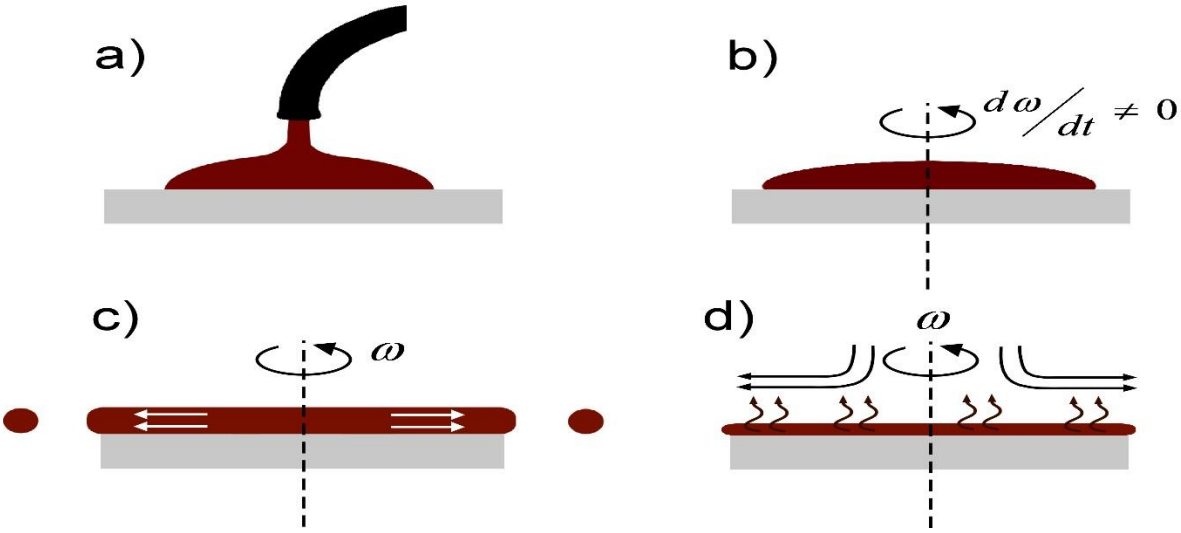

Figure 1-2: The different stages of the spin coating process

Spin coating is a method that enables covering objects of different shapes and sizes with uniform thin solid films and to control the film thickness with good reproducibility [41]. It is used for many applications to fabricate thin-film based devices, such as memory devices [42], thermoelectrics [43] and solar cells [44]. The thickness of the resulting films made by the spin coating method depends on the viscosity and concentration of the solution, rotation speed of the substrate, time of spinning.

Chapter Two

Introduction

2. Sol-Gel Technology

The sol-gel process is a versatile process using chemical solutions and it is particularly attractive because the chemical reactions can be tailored at the molecular level and provide new approaches and a better control in the preparation of nanomaterials. In general, the sol-gel process involves the generation of a colloidal suspension, "sols", which are subsequently converted to viscous gels and solid materials and involve chemical and physical processes such as hydrolysis, polymerization, drying, and densification. The sol-gel process consists first in preparing a solution of inorganic or organometallic precursors or metal oxide particles dispersed in a solvent.

There are many advantages to the sol-gel technique. One of these advantages is that it enables production of materials at low temperatures, lower than those used conventional melting techniques. Sol-gel process also facilitates production of a wide variety of thin films and coatings. This method allows fabrication of ceramic and glass materials in a wide variety of forms, ultra-fine or spherical shaped powders, coatings, ceramic fibers, microporous inorganic membranes, monolithic ceramics and glasses and extremely porous materials (aerogel) [28].

An added advantage of the sol-gel coating is that because of the small amounts of material required, the costs of precursors are relatively low. Sol-gel film deposition also offers the significant advantage over other film deposition techniques that require major

capital investment, such as chemical vapor deposition, physical vapor deposition, and sputtering. Adjustment of properties such as surface area, pore volume, and grain size are possible by the careful control of chemistry [45].

2.1 Sol-gel chemistry and sol-gel thin film deposition

The sol-gel process [28,46] is a low temperatures process via hydrolysis and condensation using metal organic precursors. In a typical sol-gel process, the main ingredients are a metal alkoxide precursor, water, a solvent and a catalyst. These basic ingredients are mixed thoroughly to achieve homogeneity on a molecular scale. Hydrolysis and condensation reactions lead to the formation of a viscous gel, which is an amorphous porous material containing liquid solvent in the pores. From this gel one can produce thin films which can be either porous or densified. The porous form is produced by curing a thin sol-gel-derived film at low temperatures (< 100°C), while the latter are fabricated via curing at elevated temperatures (> 400°C). This indicates that the sol-gel process has great flexibility and can be used for a variety of applications.

2.2 The Basic Sol-Gel Processes

The basic ingredients of the sol-gel process are mixed together. Hydrolysis and polycondensation of metal alkoxide precursors occur resulting in the formation stage of an interconnected rigid network known as a gel. This gel may be subjected to higher temperature, in order to densify the gel and to control its physical characteristics.

Basically, the sol-gel process involves a colloidal or polymeric solution that gels, is dried into different structures and can be further sintered. Figure (2-1) presents a scheme

of the different process routes leading from the sol to a variety of materials. Powders can be obtained by spray-drying of a sol. Gel fibers can be drawn directly from the sol, or thin films can be prepared by standard coating technologies such as dip- or spin-coating, spraying, etc.

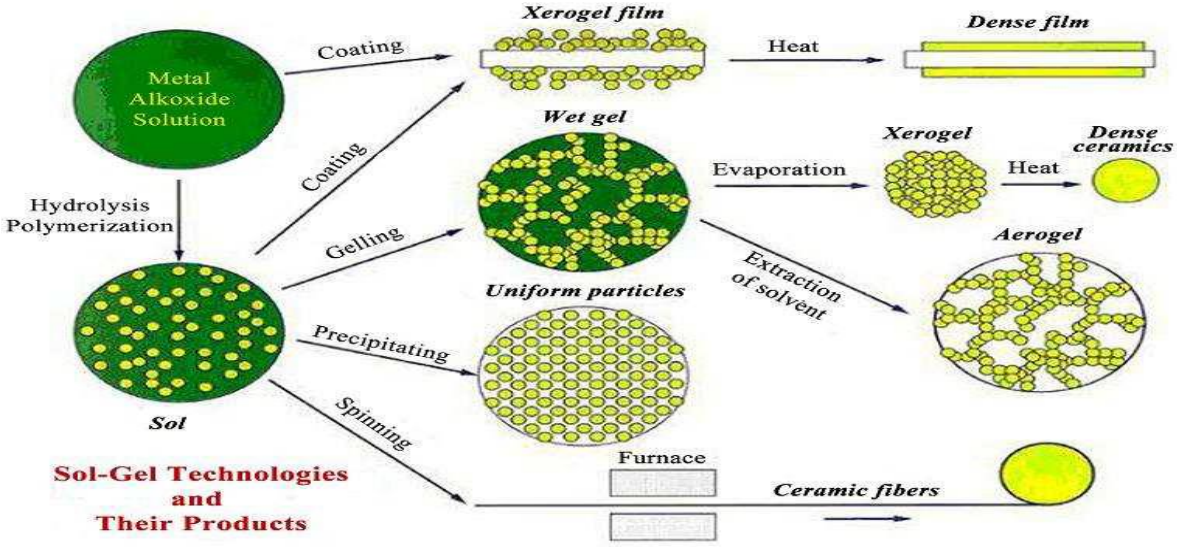

Figure 2-1: Scheme of the sol-gel processing options [28]

2.2.1 Solution – Hydrolysis & Condensation

A typical sol-gel is fabricated by the hydrolysis and polycondensation of metal alkoxides, typically silica-based. The alkoxysilanes are combined with water, alcohol, and a catalyst [47,48]. The first step in the sol-gel process is hydrolysis and is shown in equation (2-1). The hydrolysis reaction replaces alkoxide groups (OR) on the precursor with hydroxyl groups (OH). The general formula for hydrolysis reaction is [28]:

$$M\text{-}OR + HOH \rightarrow M\text{-}OH + ROH \qquad (2\text{-}1)$$

As the chemicals react further, condensation continues to occur. The condensation reactions that take place can have one of two forms in which a water or alcohol molecule is released. The condensation reactions, which are shown in equations (2-2) and (2-3) occur via a nucleophilic condensation reaction and produces (M – O – M), along with by-products of alcohol (ROH), or water.

$$\text{M-OH + RO-M} \rightarrow \text{M-O-M + ROH} \qquad \text{(2-2) alcohol reaction}$$

$$\text{M-OH + HO-M} \rightarrow \text{M-O-M + HOH} \qquad \text{(2-3) water reaction}$$

The alcohol is an important component in the sol-gel process because it participates in the reactions shown in equations (2-1) and (2-2). In the sol-gel process, the condensation reactions continue to build up long polymeric chains of (M – O – M) molecules which with time interlink to become a three-dimensional network which is known as a gel. The physical characteristics of this gel network depend upon the size of particles and extent of cross-linking prior to gelation. By controlling the synthesis conditions carefully, these reactions may lead to a variety of structures, and to different final states for the materials [49,50].

2.2.2 Ageing

Ageing is the term used to describe the process whereby after the ingredients have been mixed, the sol is allowed to continue the hydrolysis and condensation processes. Sometimes the chemical reactions continue even after the gel-point. The ageing process serves a number of purposes. Aging for sols used to produce monoliths is different to that of a sol being used for deposition of thin films. For coating sols, the main function of aging

is to increase the viscosity of the solution by accelerating cross-linking of polymers to ensure that dip-coating is possible.

2.2.3 Gelation

The solution undergoes hydrolyzes and condensation. The gel forms through polymerization. The formation of the gel is dependent on the original conditions of the hydrolysis and condensation reactions, such as temperature, precursor concentration, reaction medium and whether or not the catalyst was a base or acid.

2.2.4 Drying

To transform the weak bonds of the initial gel into a stronger network, the mixture of alcohol and water must be removed. This is done by drying. This removes most of the alcohol and water trapped in the pores. The resulting material is known as the xerogel, as shown in the Figure (2-2C) [51]. Depending on what the sol-gel is being used for the process can be modified according to produce powders, fibers, coatings, monoliths, or pores.

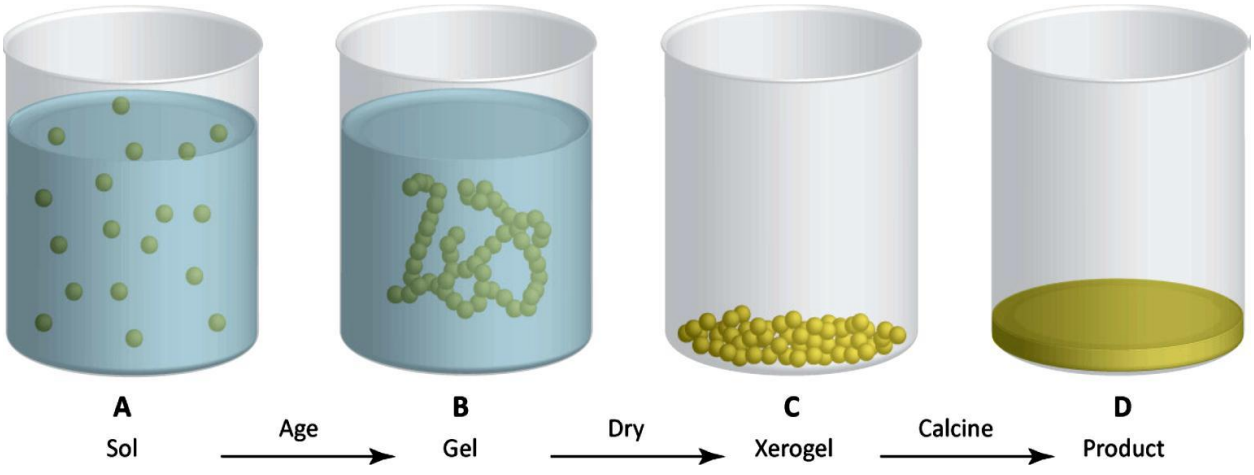

Figure 2-2: Schematic representation of the Sol-Gel process [51]

2.2.5 Calcination

The xerogel has poor mechanical strength and is non-crystalline. In order to strengthen and densify the material, the xerogel is heated at high temperature, usually around 500°C to produce a dense and, in some cases, crystalline product as shown in the Figure (2A-2D): [51].

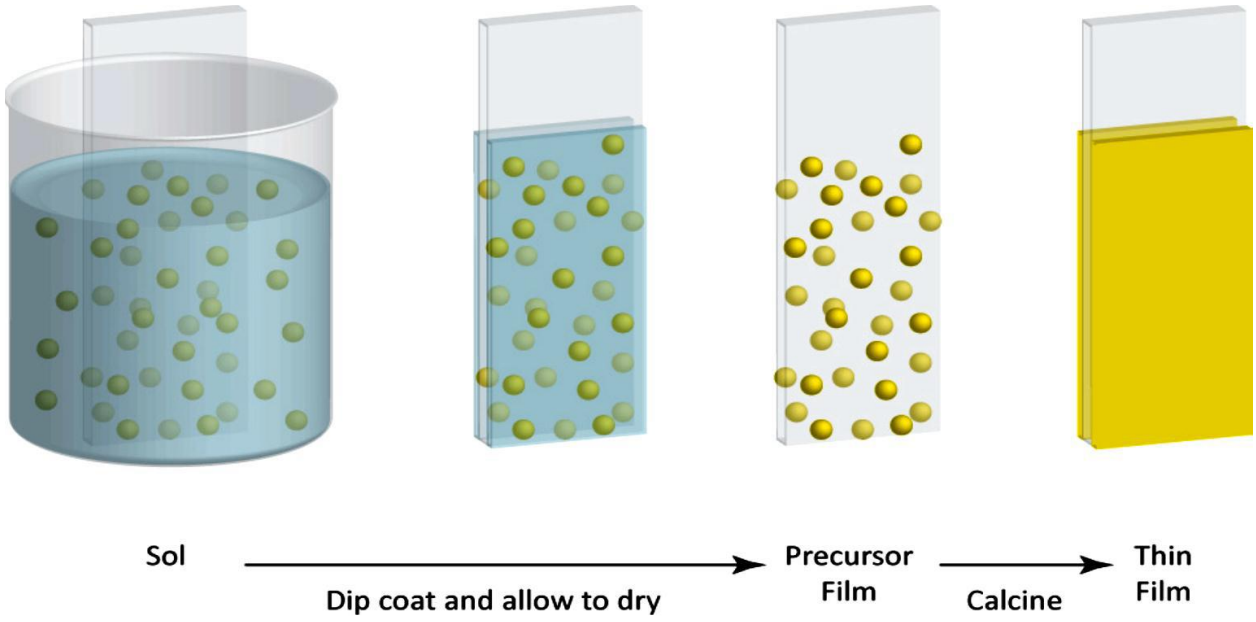

Figure 2-3: Schematic of the Sol-Gel preparation of thin film by dip coating [51]

The above sol-gel process yields a solid powder, rather than a thin film. In order to create a thin film coating by sol-gel, the process is modified so that the aged sol is deposited onto a suitable substrate. Deposition onto a substrate may be carried out either by immersing a substrate in the sol and removing at a constant vertical velocity (dip coating) or by dropping the liquid sol onto a spinning substrate (spin coating). The coated

substrates are then calcined to produce dense and crystalline thin films. This process is illustrated in the Figure (2-3) [51].

2.3 Titanium Dioxide

Titanium is one of the most common elements on earth. Titanium dioxide is an inorganic substance that is nonflammable, and not hazardous. It is a semiconducting transition metal oxides, which has various applications in paints and cosmetics. TiO_2 occurs naturally in some types of rock and also sands [52]. TiO_2 occurs naturally in three polymorphs called rutile, anatase, and brookite. A comparison of the properties of the three polymorphs is provided in Table (2-1). Rutile and anatase consist of a tetrahedral crystal system, but anatase has octahedrons that share four edges forming the four-fold axis form making it different from rutile [53]. Brookite consists of an orthorhombic crystal system [53]. The crystal structures of rutile, anatase, and brookite are shown in Figure (2-4). Rutile is the most common form of TiO_2. Rutile is odorless in nature and the most stable polymorph of TiO_2. Other polymorphs of TiO_2 can be changed to rutile polymorph by high temperature annealing, and the process is irreversible [54]. Rutile is deep red when viewed in transmitted light. The refractive index of rutile TiO_2 is 2.6. Rutile is transparent in visible light and is effective in absorbing of ultraviolet (UV) light. Hence, they are used in sunscreen lotions since they absorb UV light and help in protecting the skin [55]. The basic structural unit of rutile is shown in the Figure (2-4a).

Anatase is not stable at high temperatures and when annealed at temperatures above 550 C will transform to rutile TiO_2 [53]. Anatase is yellow to blue in color when viewed in transmitted light. The refractive index of anatase TiO_2 is 2.488. Anatase has a lower

absorption property compared to rutile. However, both rutile and anatase forms of TiO_2 are used in daily applications [55]. The basic growth unit possible for anatase is shown in the Figure (2-4b).

Brookite is yellowish brown to dark brown when viewed in transmitted light. The refractive index of brookite is 2.58 to 2.7 [55]. Brookite and rutile polymorphs of TiO_2 have a refractive index higher than that of a diamond, making them materials of high luster. Brookite transforms into rutile when annealed at temperatures above 750 C [56]. Brookite has mechanical properties that are similar to mechanical properties of rutile, but it is the least abundant polymorph of TiO_2 and hence has had very little commercial use. The basic structural unit of brookite is shown in the figure (2-4c).

In comparison with other polymorphs, anatase-TiO_2 is preferable for solar-cell applications because of its high electron mobility, low dielectric constant, and lower density [57]. Anatase-TiO_2 also has a slightly higher Fermi level, a lower capacity to adsorb oxygen, and a higher degree of hydroxylation compared with other phases. These properties increase the photoactivity of TiO_2 [58]. Based on charge-carrier dynamics, chemical properties, and activity of photocatalytic degradation of organic compounds, anatase-TiO_2 appears to be the most active photocatalytic polymorph [59].

Table 2-1: Comparison of the rutile, anatase, and brookite for different crystal structures of titania[55].

	Rutile	Anatase	Brookite
Crystal structure	**Tetragonal**	**Tetragonal**	**Orthorhombic**
Unit cell (Å)	a = b = 4.5936 c = 2.9587	a = b = 3.784 c = 9.515	a = 9.184 b = 5.447 c = 5.145
Color under transmitted light	deep red	yellow to blue	yellowish brown to dark brown
Molecule/cell	2	4	8
Volume/molecule ($Å^3$)	31.2160	34.061	32.172
Density (g/cm^3)	4.13	3.79	3.99
Unit cell volume ($Å^3$)	62.34	136.27	257.63
Refractive index	2.6	2.49	2.58
Ti-O bond length (Å)	1.949(4) 1.980(2)	1.937(4) 1.965(2)	1.87~2.04
O-Ti-O bond angle	81.2° 90.0°	77.7° 92.6°	81.2°~90.0°

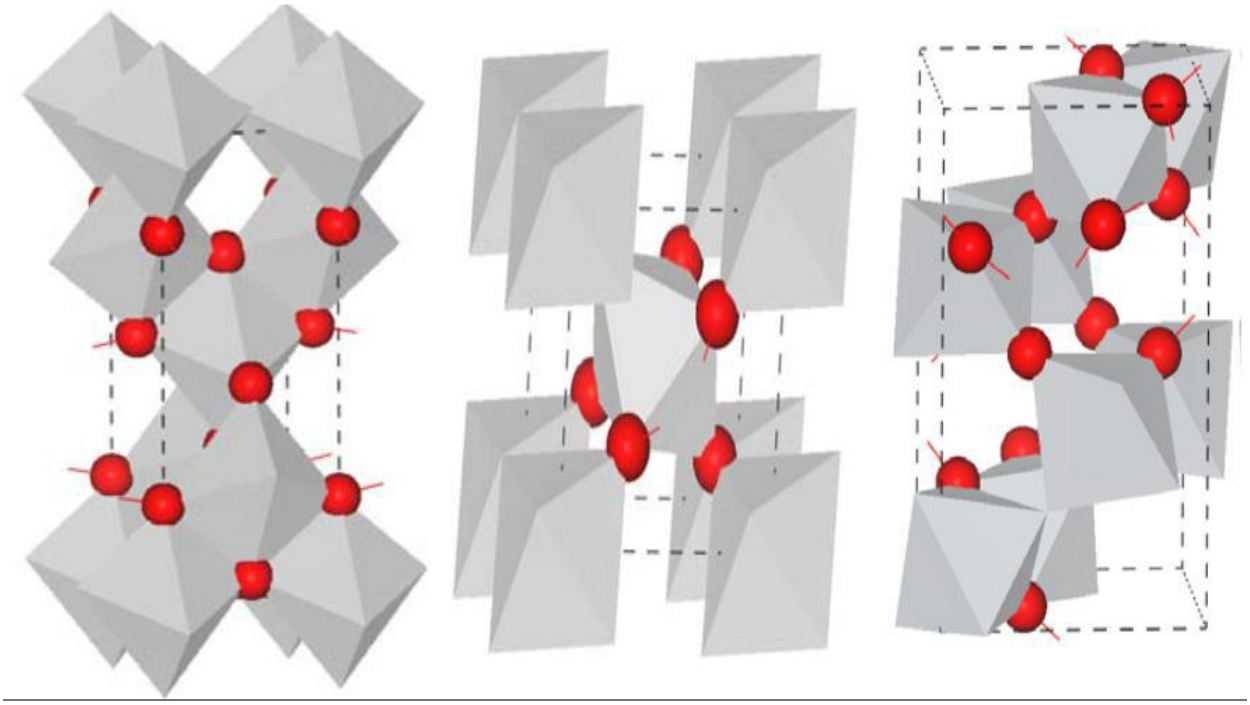

(b) Anatase	(a) Rutile	(c) Brookite

Figure 2-4: Crystal structures of titania (a) Rutile, (b) Anatase and (c) Brookite [60]

2.4 TiO_2 an interesting material

Titania has advantageous properties such as chemical stability, non-toxicity, and low cost, so it has received a great deal of attention. Titania has a very high refractive index (~2.4) and low visible absorptivity. It is favored in the field of coatings and in thin film optical devices, and also has the wide band gap (~3.2 eV) that can be exploited in the field of optical coatings combined with the high ultraviolet absorption. Wide band gap materials have the advantages of being able to operate at higher temperatures and having a longer carrier lifetime, reducing recombination loses. It also has an interesting property of self-cleaning where it prevents growth of bacteria and fungi when exposed to sunlight,

meaning buildings, which are constantly exposed to sunlight, can be protected by coated with a thin layer [61]. This is because the absorption range of TiO_2 is in the UV range of the solar spectrum that prevents any damage caused by UV light.

TiO_2 is used in wastewater purification [62], inorganic membranes, [63] and as catalyst supports. Titanium oxide is also being used in heterogeneous catalysis, as a photocatalyst, in solar cells for the production of hydrogen and electric energy [64-66]. Titania has excellent biocompatibility with respect to bone implants, and also finds applications in nanostructured form in Li-based batteries [67] and electrochromic devices [68]. Titanium is relatively cheap compared to other metals such as gold and platinum, making TiO_2 an interesting and attractive material.

2.5 Comparison with other materials

TiO_2 is the most promising material which can use as a photocatalyst compared with other materials, such as zinc oxide (ZnO) and silica (SiO_2), because it easily oxidizes hydrocarbons, and it is non-toxic. TiO_2 has been used together with SiO_2 and ZnO.

2.6 Silica dioxide SiO_2

The most abundant oxide on the earth is silica. It is synthesized into different shapes, like cylindrical pellets [69] or fibers [28]. Silica has high mechanical strength, and thermal stability. It is found in several polymorphs, each with its own structural characteristics, as well as chemical and physical properties. Generally, SiO_2 is made up of SiO_4 tetrahedral, where each silicon is bonded to four oxygen atoms and each oxygen atom is bounded with two silica atoms.

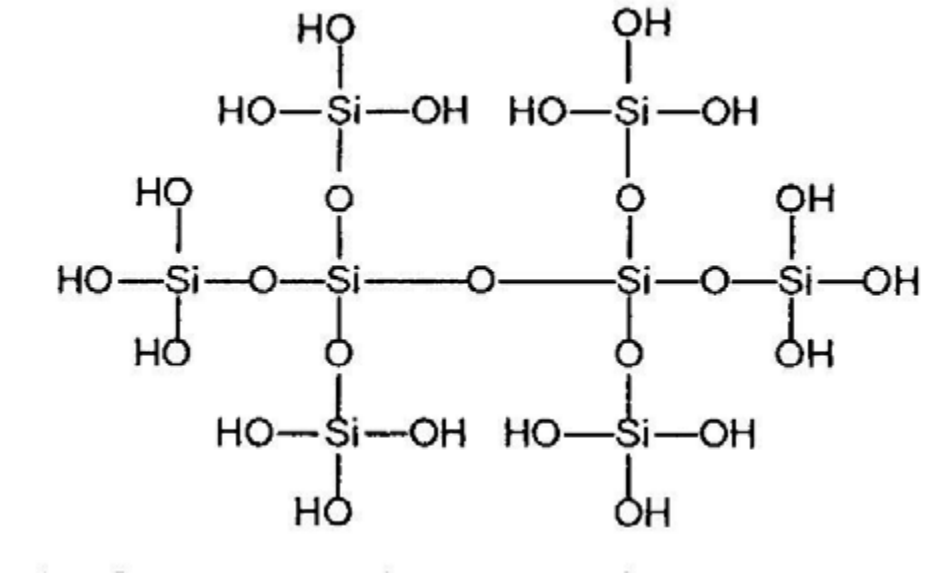

Figure 2-5: Linkages of SiO_2 tetrahedras [70]

The surface of silica has two types of functional groups: siloxane groups (Si – O – Si) and silanol groups (Si – O – H). The siloxane sites are considered nonreactive, while the silanol groups are the locale of activity for any process taking place on the surface [71].

2.7 SiO_2 an interesting material

Two of the most common alkoxides employed in the sol-gel process [72] are tetramethoxysilane, $Si(OCH_3)_4$, and tetraethoxysilane, $Si(OC_2H_5)_4$, known as TMOS and TEOS, respectively. Since these compounds and water are not miscible, a common solvent (generally, methyl or ethyl alcohol) has to be added to obtain an initially homogeneous liquid. TMOS has the advantage of rapid hydrolysis under a variety of conditions, but the toxic methanol produced can be hazardous to the eyes and lungs. Conversely, TEOS is hydrolysis rate limited [28], but produces less toxic ethanol during the reaction. Hydrolysis and polycondensation can be accelerated or slowed down by employing an appropriate acid

or base catalyst. These processes proceed simultaneously and are generally incomplete, as described above. Depending on the amount of water present, hydrolysis may go to completion or stop while the metal is only partially hydrolyzed.

2.8 Sol-gel synthesis of SiO_2

The chemical formula for TEOS is given by $Si(OC_2H_5)_4$, or $Si(OR)_4$ where the alkyl group R represents C_2H_5. Alkoxides are ideal chemical precursors for sol-gel synthesis because they react readily with water. The reaction is called hydrolysis because a hydroxyl ion becomes attached to the silicon atom as follows:

$$Si(OR)_4 + H_2O \rightarrow HO\text{-}Si(OR)_3 + R\text{-}OH \qquad (2\text{-}4)$$

Depending on the amount of water and catalyst present, hydrolysis may proceed to completion, so that all of the OR groups are replaced by OH groups as follows:

$$Si(OR)_4 + 4\ H_2O \rightarrow Si(OH)_4 + 4\ R\text{-}OH \qquad (2\text{-}5)$$

Any intermediate species ($(OR)_2$–Si-$(OH)_2$) or ($(OR)_3$–Si-(OH)) would be considered the result of partial hydrolysis. In addition, two partially hydrolyzed molecules can link together in a condensation reaction to form a siloxane [Si–O–Si] bond:

$$(OR)_3\text{–}Si\text{-}OH + HO\text{–}Si\text{-}(OR)_3 \rightarrow [(OR)_3Si\text{–}O\text{–}Si(OR)_3] + H\text{-}O\text{-}H \qquad (2\text{-}6)$$

$$(OR)_3\text{–}Si\text{-}OR + HO\text{–}Si\text{-}(OR)_3 \rightarrow [(OR)_3Si\text{–}O\text{–}Si(OR)_3] + R\text{-}OH \qquad (2\text{-}7)$$

Thus, polymerization is associated with the formation of a 1, 2, or 3- dimensional network of siloxane (Si – O – Si) bonds accompanied by the production of (H-O-H) and (R-O-H) species [73-76].

2.9 Mixed Oxides System

Regarding the possible strategies for synthesizing these materials, they include mixing Si and Ti alkoxides [77-80] by sol-gel methods [81]. However, some difficulties arise when Ti and Si alkoxides are mixed together, where the hydrolysis and condensation rates of the Ti alkoxides are much faster than that of the Si in presence of ambient water [77, 82]. As a result, the Ti alkoxides generally react rapidly with water and precipitate out of the reaction mixture before it can react with the Si into a network. There are two fundamental types of interaction between TiO_2 and SiO_2. There are physical forces of attraction, such as Van der Waals forces, and there is chemical bonding and creation of a Ti-O-Si bond [83,84].

2.10 Titania-silica composite materials

TiO_2-SiO_2 oxides composites have attracted attention due to their potential as heterogeneous catalysts and catalytic supports. They find good application in acid-catalyzed reactions and selective oxidation. Due to their low coefficient of thermal expansion over a wide temperature range, they are useful for optical applications [77]. Nanostructured SiO_2-TiO_2 is more effective as a photocatalyst than pure TiO_2 [85]. It can be used in solar energy collectors, and self-cleaning surface coatings [86].

Sol-gel synthesis is a popular way to synthesize TiO_2-SiO_2 thin films for their interesting optical properties, for integrated optic applications, for high thermal and chemical stability, low thermal expansion coefficients [87,88], tunable refractive index over a wide range [89,90], intrinsic antireflecting properties [91,92], enhanced photocatalytic activity[93,94], and superhyrophilicity and superhyrophobicity[95,96].

2.11 Properties of titania-silica composite materials

Composites made out of silica and titania can have the high stability from silica, the photocatalytic properties from titania and extra properties coming from chemical bonds between these two materials [83]. The production of silica can be cheaper than titania, so the costs of the photocatalyic material can then be significantly reduced. In addition to lower production costs, the durability increases as silica has a higher mechanical and thermal stability than titania. In addition to the lower costs and increased durability, the photocatalytic efficiency of the material can be increased with the addition of silica because silica has a large specific surface area and it is able to adsorb some pollutants and intermediates for a longer time than pure titania.

Both SiO_2 and TiO_2 are typical optical thin films with high transparency and low absorption in visible and near infrared regions. Because they are low cost, safe and abundant materials with high chemical, thermal and mechanical stabilities, they have been widely used for various optical applications, such as antireflective coatings [97,98], high reflecting, mirrors [99], photocatalyst [100] and integrated optical waveguides [101].

2.12 Titania-Silica Chemistry

The reaction of titania precursors with silica happens either directly with silanols or indirectly through hydrolysis of titania monomers ($Ti(OH)_4$) first and then subsequently by condensation [83]. Either way, the titania will form bonds with the silica through reaction:

$$\equiv Si - OH + R - Ti \equiv \rightarrow \equiv Si - O - Ti \equiv + HR \qquad (2\text{-}8)$$

Where R is a side group of a titania precursor or a hydroxyl group of a titania monomer. This condensation reaction between the titania precursor and the silica surface depends mostly on the hydroxyl groups of the silica [102] since the rest of the silica is very inert.

2.13 Fluorescence photobleaching

The interaction of electromagnetic radiation with matter is the basis of the photochemical processes that occur after photon absorption by photoactive molecules and the promotion of electrons from the ground to an excited state. At the excited state different processes will be occur before return to the ground state, one of these processes is photobleaching[103]. Photobleaching is defined as the photochemical destruction of a dye or a fluorophore when exposed to light, where the light induced change in a fluorophore resulting in the loss of its absorption of light of a particular wavelength. The loss of fluorescence signal is irreversible if the bleached fluorophore population is not replenished (e.g., via diffusion). Extent of photobleaching is dependent on the intensity and duration of exposure to exciting light.

Under high-intensity illumination conditions, the irreversible destruction or photobleaching of the excited fluorophore becomes the primary factor limiting fluorescence detect ability. The multiple photochemical reaction pathways responsible for photobleaching have been investigated and described in considerable detail. Photobleaching is loss of the ability of the fluorophore to fluoresce along the time that prevents long time experiments. The corresponding decay rate depends mainly on the amount of energy radiated over the specimen. Therefore a trade-off exists between the

needs of increasing the incident radiation to improve the signal to noise ratio of the signal and the needs of decreasing that radiation to minimize the fading effects [104].

Photobleaching occurs because each fluorophore has a limited number of excitation/emission cycles that it can undergo. After progressing through this number of cycles, the fluorophore will no longer release visible photons of light. So when talking about photobleaching the term photobleaching lifetime appears. It is defined as the total number of emitted photons before photobleaching process occurs. Each fluorophore has different photobleaching-characteristics. Its stability can be characterized by the average number of absorption emission cycles that the molecules of this fluorophore undergo before they are irreversibly photobleached. The number of cycles depends on the local environment and the molecular structure and is, therefore, a fluorophore specific property. The most severe limit for the emission intensity is set by photobleaching in the sample. The chromophores are not infinitely stable but are destroyed after a large number of absorption and emission cycles. Possible reasons are simultaneous multi-photon absorption, intersystem crossing, reactions from the triplet state and excited-state absorption [105, 106]. Finally the exact mechanism of photobleaching is assumed to be linked to a transition from the excited singlet state S1 to the excited triplet state T1. Through this transition the molecule will withdraw from the absorption-emission cycle and as the triplet state is relatively long-lived with respect to the singlet state, so it will be chemically more reactive [107].

Chapter Three

Literature Review

3.1 History of sol-gel technology

The sol-gel technique was described for the first time in 1846 by a French chemist Ebelman [108]. He observed the hydrolysis and polycondensation of tetraethylorthosilicate (TEOS), also known as tetraethoxysilane. In 1930 Geffcken and Berger succeeded to prepare a multicomponent oxide layer on industrial glasses using metal-containing precursors by sol-gel process and dip-coating technique. They received the first sol-gel patent in 1939, which covers the preparation of SiO_2 and TiO_2 for optical applications [109]. Later, they developed and improved this method. Sol-gel coating systems were studied extensively at Schott Glass starting in the 1950's. These preparations were for synthesis of single oxide optical coatings, especially TiO_2 and SiO_2, and mixed oxide materials. This work resulted in commercial products.

Roy and his colleagues changed the traditional sol-gel process into the synthesis of new ceramic oxides, making sol-gel silicate powders well known [110]. Roy and Roy [111] first reported the application of sol-gel technology to produce homogeneous multicomponent glasses. In 1956, Roy reported homogeneous powders by the sol-gel process [112]. In 1962 Schröder reported the preparation of amorphous single and mixed oxides layers of (SiO_2, TiO_2 and others) via hydrolysis and polycondensation of metal alkoxides [113] and in more detail in 1969[114].

In the late 1960s, Stober et al. [115] used the sol-gel method to prepare uniform mesoporous silica spheres. So-called Stober spheres are based on the hydrolysis of a silica precursor in an alcohol-ammonia solution. In 1971, a process for low-bulk density silica involving the hydrolysis of tetraethoxysilane (TEOS) in the presence of cationic surfactants was patented [116]. Later, both Schröder and Dislich investigated bulk gel preparation by an all alkoxide route described by Dislich in 1971[117] and resulting in a number of patents [118,119].

The sol-gel method became popular in the ceramics industry in the mid-1970's, and various types of inorganic glass were manufactured, based on this approach [120]. In the mid-1980's, the gel-to-glass conversion was considered the most interesting technological application for sol-gel processing and received the most attention by scientists such as Schmidt and Wilkes, who also started to synthesize organic-inorganic hybrid materials (OIHMs) [121-123].

Brinker and Scherer [28], in their comprehensive treatise on the physics and chemistry of sol-gel processing, have described several possibilities for sol-gel methods to synthesize a large number of preforms. The preparation of such materials involves using metal alkoxides, which go through hydrolysis and condensation polymerization reactions for the production of three dimensional structures consisting Si-O-Si polymers and oligomers. Since then, sol-gel technology has attracted a great deal of attention, especially in the fields of ceramics, polymer chemistry, organic and inorganic chemistry, physics and played an indispensable role in preparing novel OIHMs [28,124].

3.2 Titania-silica composite materials

In 1986 Anpo et al. [125] reported that the photocatalytic activity of TiO_2 can be enhanced by introducing SiO_2. In 1991 Anderson et al. [126] made TiO_2-SiO_2 glasses containing 8, 18, and 41 mol% TiO_2. They reported that Ti^{4+} ions are 4 fold coordinated for the sample containing 8 mol% TiO_2. The sample containing 18 mol% has 4 fold and 6 fold coordination. In 1992 Satoh et.al [127] fabricated TiO_2-SiO_2 bulk glasses from silicon and titanium alkoxides. In 1995 Liu and Cheng [128] produced a TiO_2-SiO_2 mixed oxide via coprecipitation and revealed that the SiO_2 inhibits the growth of TiO_2 crystals, resulting in amorphous TiO_2 within the SiO_2 matrix.

Anderson and Bard [129,130] reported higher photocatalytic activities for TiO_2-SiO_2 sol-gel derived photocatalysts with respect to pure TiO_2 photocatalysts. They also found that there is a strong synergy between both materials TiO_2 and SiO_2 and as a combined oxide. A higher photocatalytic decomposition rate was found with TiO_2-SiO_2 composites versus a pure TiO_2 slurry for substances that are easily adsorbed to the SiO_2 surface. The presence of an adsorbent increased efficiency by increasing the concentration of the substance near the TiO_2 sites. They also reported that degradation rates were lower compared to a slurry of pure TiO_2 for substances that are not readily adsorbed to the surface of SiO_2. So, the TiO_2-SiO_2 material demonstrated a more effective use of the TiO_2 sites than for TiO_2 alone. They found that there is an ideal ratio for TiO_2-SiO_2 composite which is reported to be 30 wt%/70 wt%.

In 1997 Orignac et al. [131] used the sol-gel method to prepare SiO_2/TiO_2 films from solutions containing different concentrations of ethanol and found that the porosity

volume fraction can reach a minimum when the ethanol volume ratio is near four. In 1999 Machida et al. [132] found that the addition of 10–30 mol% of SiO_2 into a TiO_2 film yields optimum photo-induced superhydrophilicity, which lasts for a certain time in the dark. In another study, Jung and Park [133] found that 30 wt % TiO_2 was optimum for the mineralization of trichloroethylene. Moreover, they reported that high porosity and large pore size in the SiO_2 facilitated the transfer of reactants, resulting in a higher rate of degradation than a slurry of Degussa P25 alone. In 2001 Chun et al. [134] used a different preparation, but their results also indicated that 30 wt% TiO_2 is an optimum. In addition, they showed results for two organic compounds with different characteristics, indicating that there is a strong correlation between adsorption of the compound on mixed oxide surface and the destruction of that compound.

Yu et al. [135, 136] found that addition of SiO_2 had a suppressive effect on the crystal growth of TiO_2, because the contact between TiO_2 particles was barred by SiO_2 during their growth process. Yu et al. [137] reported that as the amount of SiO_2 increased, the grain size in the resultant TiO_2/SiO_2 composite was smaller , while the surface hydroxyl content was higher. They found that the photocatalytic activity of the TiO_2/SiO_2 composite thin films increased when the amount of SiO_2 was less than 5 mol%. However, when the amount of SiO_2 was greater than 10 mol%, the photocatalytic activity of TiO_2/SiO_2 began to decrease.

In 2003 Guan et al. [138] found that SiO_2 additions increased the surface acidity of SiO_2-TiO_2 film and increased the hydroxyl content at the surface, resulting in enhanced photo-hydrophilic properties. They found that the addition of 40 mol% of SiO_2 to TiO_2

was most effective for reducing the contact angle of water, and also found that SiO_2 had a suppressive effect on the crystal growth of TiO_2 in calcination and enhanced the transmittance of the composite films. Mills et al. [139] also showed that the photocatalytic layer was capable of removing stearic acid, which is a simulation of grime that oxidizes to H_2O and CO_2 through the photocatalytic reaction. This photocatalytic reaction showed extremely slow reaction kinetics compared to that of a sol-gel produced layer of TiO_2. The commercial film is designed for low light absorption at a wavelength of 365nm. The greater photocatalytic activity of the sol-gel films compared to Activ™ films upon irradiation was due to the thickness of the TiO_2 layer.

In 2004 Lee et al. [140] reported that the transformation from amorphous to anatase phase, as well as the transformation from anatase to rutile phase, were shifted toward higher temperatures when increasing the SiO_2 content during mixed film calcination.

Ren et al. [139] showed that SiO_2–TiO_2 thin films have excellent superhydrophilicity and it has been also a good adhesion to the substrate.

In 2005 Guan [97] used the sol-gel method to prepare films, in which different amounts of SiO_2 were added to TiO_2. They studied the relationship between the mutual effects of hydrophilicity, photocatalysis and the self-cleaning effect. He found that the amount of SiO_2 in mixed SiO_2–TiO_2 films had different influences on the photocatalysis and photohydrophilicity. TiO_2/SiO_2 film surfaces can have more photocatalytic activity and less superhydrophilic activity, or vice versa. He found that when adding 10-20 mol% of SiO_2, the films had optimum photocatalytic activity, while the addition of 30-40 mol% of SiO_2 yielded an optimum photohydrophilicity. He found that the contact angle of a

nano-layer of TiO_2 decreased almost to zero upon irradiation, thus achieving super-hydrophilicity. However, the contact angle was restored back to its original value, at a fast rate when the sample was placed in a dark area. This lessens the efficiency of the photocatalytic coating for rainfall at night. The incorporation of SiO_2 to form TiO_2/SiO_2 composite films achieved a more efficient hydrophilic state during dark hours, and also increased the photocatalysis reactivity of the coating.

In 2006, Masatoshi Nakamura [141] studied the hydrophilic and photocatalytic properties of SiO_2-TiO_2 double layers, and they determined the hydrophilicity of the double layers by the relative coverage of organic contaminants. Aguado et al. [142] showed the influence of the synthesis method on the physicochemical properties of SiO_2-TiO_2 mixtures, and consequently its effect on the photocatalytic activity of particles. It is the semiconductor behavior that explains the photoactivity of TiO_2-SiO_2 materials.

Zou et al. [143] found in their studies that TiO_2-SiO_2 pellets have a high adsorption capacity. They can serve dual functions as a photocatalyst and as an adsorbent in the hybrid photocatalysis and adsorption system. The results also demonstrated that porous photocatalysts with high adsorptive capacity enhance the subsequent photocatalysis reactions and led to a positive synergistic effect. The catalyst can be self-regenerated by photocatalytic oxidation of the adsorbed volatile organic compounds (VOC). Kim et al. studied the photocatalytic property of SiO_2-TiO_2 nanoparticles by sol-hydrothermal process [144]. In 2008, Liu et al. [145] prepared SiO_2-TiO_2 binary layer films with self-cleaning and antireflection properties. The bottom SiO_2 layer acts as an antireflection coating due to its lower refractive index, while the top TiO_2 layer acts as a self-cleaning

coating generated from its photocatalysis and photo-induced superhydrophilicity. They also found that after illumination by ultraviolet light, the SiO_2-TiO_2 binary layer films are superhydrophilic with water contact angle less than 2º, which greatly favors the self-cleaning function of the films.

Novotna et al. [146] studied the photocatalytic degradation of methylene blue by TiO_2/PDMS (poly dimethylsiloxane) and TiO_2/SiO_2 films. The results show that TiO_2/SiO_2 films exhibited higher degradation rates, which were probably due to higher crystallinity and high hydrophilicity. These qualities were further enhanced by the UV-illumination and the super-hydrophilic state of the film. Permpoon et al. [147] used sol-gel method to deposit SiO_2-TiO_2 and TiO_2-SiO_2 bi-layer films from a polymeric SiO_2 solution and either a polymeric TiO_2 solution or a TiO_2 crystalline suspension. They found that the water contact angle measurements for both types of bi-layer films exhibited superhydrophilicity, but did not maintain a zero contact angle for a long time of film aging.

In 2010 Tang et al. [148] developed a process for preparing SiO_2-TiO_2 fibers by means of a precursor transformation method from titanium modified polycarbosilane. The microstructure of the SiO_2-TiO_2 fibers is described as anatase-TiO_2 nanocrystallites with a mean size of ~10 nm embedded in an amorphous SiO_2 continuous phase. In 2011 Louis et al. [149] reported the synthesis and characterization of binary TiO_2-SiO_2 optical coatings prepared by a sol-gel method. They showed that the SiO_2 proportion was critical to the crystallization of TiO_2 as well as to the optical properties.

In 2013 Rasalingam et al. [150] pointed out that the content of Ti-O-Si species and appropriate distribution of TiO_2 on the SiO_2 support are the most effective parameters for

the photoactivity of these compounds. Tonooka and Kikuchi [151] used SiO_2-TiO_2 films, and a heat-resistant silver alloy to prepared hydrophilic and solar-heat-reflective coatings. The silver was deposited on glass substrates by radio-frequency sputtering. The bi-functional coating was a multilayer film and it was used to improve the spectral reflection and spectral transmission properties. The glass reflected most of the infrared light and simultaneously transmitted visible light.

In 2014 Fakin, Darinka, et al. [152] studied the effects of three TiO_2-SiO_2 nanoparticle dispersions on the hydrophilicity as well as coloration ability of polyester fabric during high temperature disperse dyeing. They found that the samples treated with TiO_2-3% SiO_2 or TiO_2-5% SiO_2 dispersions attained maximal water adsorption at shorter times as well as better hydrophilicity, lower contact angles, compared to the reference sample. In addition, the higher ratio of SiO_2 to TiO_2 resulted in elevated differences in brightness as well as reduced color strengths. They reported that the SiO_2-coated TiO_2 had a positive influence on the retardation of the oxidative dye fading under UV light by reducing the effective surface area of TiO_2 nanoparticles and, thus, suppressing their photocatalytic activity.

In 2015 Malnieks et al. [153] prepared TiO_2 - SiO_2 optical films that were deposited on an enamel surface using dip-coating techniques and calcined for different time from one hour to ten hours, in order to investigate the effect of calcination on self-cleaning. They found that calcination increased the grain size and decrease the surface area. Calcination also increased the water contact angle and decreased the porosity of the thin films. They

found that the TiO_2-SiO_2 films calcined for 1 h resulted in highly structured surfaces, which were found to increase the photocatalytic activity.

In 2016 Kim et al. [154] succeeded in using the sol-gel method to deposit TiO_2 (top)-SiO_2 (bottom) double-layer thin films by spin coating onto a glass substrate and then thermally treating at different temperatures. They reported that the thin films contained nanocrystalline anatase phase only. No rutile phase was observed up to 500˚C. The thin films showed superhydrophilicity switching after 15 min of UV irradiation. The photocatalytic activity of the films was studied by the photocatalytic degradation of methylene blue under UV light irradiations.

In 2017 Rosa Elena et al. [155] studied the macroscopic abrasion resistance of TiO_2-SiO_2 and SiO_2-TiO_2/SiO_2 thin films on soda-lime-silica (SLS) glass, according to an American Standard for safety glazing. They reported that the purpose of this was to increase the top active film durability in a bilayer system by understanding how film thickness and top film composition influence abrasion performance. They reported that the results showed that thinner top TiO_2 film thickness leads to SiO_2/TiO_2 bilayers with lower haze value and improved abrasion resistance. It was also found that SiO_2 addition to TiO_2 top film composition promoted thin film adhesion and sample durability against abrasive wear. Active top films based in a SiO_2-TiO_2 with molar ratio 2:8 and 1:9 pass the abrasion resistance criterion established by an American Automotive norm. Factors contributing to the improvement of the lifetime performance of TiO_2 and SiO_2-TiO_2 thin films were identified.

Chapter Four

Experimental Methodology and Procedure

4.1 Introduction

It is important to mention that the physical and chemical properties of SiO_2 and TiO_2 are strongly dependent on the preparation method. Basically, there are two different routes of preparation, i.e. gas-phase methods and solution methods. The solution methods include solvothermal method, precipitation method, microemulsion method, combustion synthesis, electrochemical synthesis and sol-gel method. Due to the several advantages which were explained previously, a sol-gel process was the preferred way to produce TiO_2-SiO_2 materials, where the preparation of titania sol and silica sol were carried out separately and then they were mixed at various ratios to achieve the desired outcome.

In this chapter, preparations of the following sols are explained: TiO_2, SiO_2, mixtures of TiO_2-SiO_2 and TiO_2-SiO_2-$Fe(NO_3)_3$). The sol-gel compositions were deposited on glass substrates using a dip-coating method. Thin films were subjected to heat treatment in a furnace at (100ºC) and characterized.

4.2 Precursors

All of the precursorss in this study were used as received: titanium (IV) butoxide $Ti(OCH_2CH_2CH_2CH_3)_4$, purity 97%, from Sigma-Aldrich, tetraethylorthosilicate (TEOS), [Si $(OC_2H_5)_4$], purity 98%, from Sigma-Aldrich, and iron (III) nitrate nonahydrate $Fe(NO_3)_3*9H_2O$, purity 99%, from Fisher ChemAlert Guide. The other reagents were

ethanol, C_2H_5OH, from Sigma-Aldrich, hydrochloric acid (HCl), 65%, from Fisher Scientific, and distilled-deionized water.

4.3 Preparation of the sol

The sol was prepared in a batch process as-needed. The equipment and supplies needed to prepare the sol are simple and consists of a flask containing the mixed solutions, a magnetic stirrer to ensure the mixture is uniform. The mixture is held at a constant temperature.

4.4 Synthesis of materials

Figure (4-1) is a flowchart of the sol-gel preparation by mixing the two components TiO_2 and SiO_2.

In the first step, the amount of TEOS listed in Table (4-1) and ethanol (40ml) were stirred for 6 hours. The beakers were covered to prevent premature evaporation. Then deionized water (90ml) was added to the mixture, followed by the addition 0.05ml of HCl dropwise as a catalyst. The solution was stirred with the aid of a magnetic stirrer until obtaining a homogeneous, transparent sol.

In the second step, the amounts of titanium (IV) butoxide listed in Table (4-1) and ethanol (40ml) were stirred for 6 hours. The beakers were covered to prevent premature evaporation. Then 0.05ml of HCl dropwise as a catalyst was added to the mixture. The solution was stirred with the aid of a magnetic stirrer until obtaining a homogeneous, transparent sol.

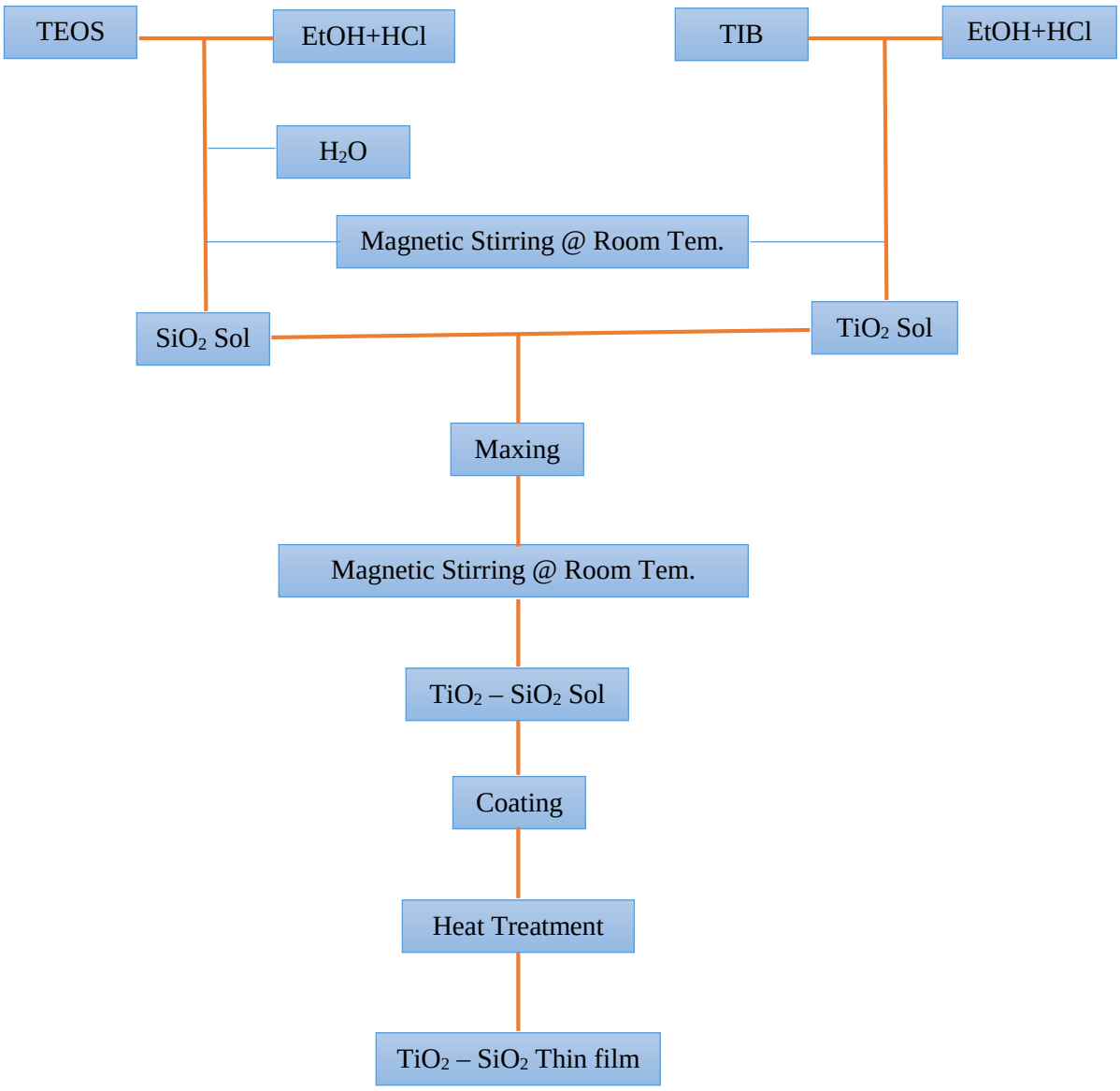

Figure 4-1: Flow Chart of preparing $TiO_2 – SiO_2$ Sol

Table 4-1: Sample compositions and dip coating conditions

Sample composite	Sample composite (TiO_2 : SiO_2)wt. ratio	Age days	Drying times	Temp. C°
Sample1	3 : 97 wt. %	0,5,10,15,20,25,30	24	100
Sample2	5 : 95 wt. %	0,5,10,15,20,25,30	24	100
Sample3	7.9 : 92.1 wt. %	0,5,10,15,20,25,30	24	100
Sample4	10 : 90 wt. %	0,5,10,15,20,25,30	24	100
Sample5	15 : 85 wt. %	0,5,10,15,20,25,30	24	100
Sample composite (TiO_2 : SiO_2 : $Fe(NO_3)_3$) wt. ratio	Sample composite (TiO_2 : SiO_2 : $Fe(NO_3)_3$) wt. ratio			
Sample6	10 : 90 : 0.0001 wt. %	0,5,10,15,20,25,30	24	100
Sample7	10 : 90 : 0.001 wt. %	0,5,10,15,20,25,30	24	100
Sample8	10 : 90 : 0.01 wt. %	0,5,10,15,20,25,30	24	100
Sample9	15 : 85 : 0.0001 wt. %	0,5,10,15,20,25,30	24	100
Sample10	15 : 85 : 0.001 wt. %	0,5,10,15,20,25,30	24	100
Sample11	15 : 85 : 0.01 wt. %	0,5,10,15,20,25,30	24	100

4.4.1 Synthesis of aqueous titania-silica sol

TiO_2-SiO_2 sol was prepared by mix the step one (silica precursor solution) with the step two (titania precursor solution) under magnetic stirring. The beakers were covered to prevent premature evaporation. The solution was stirred with the aid of a magnetic stirrer. A homogeneous, transparent and light yellow solution was obtained, as the shown in Figure (4-2). The sol was then aged for at least 24 hours at room temperature prior to use.

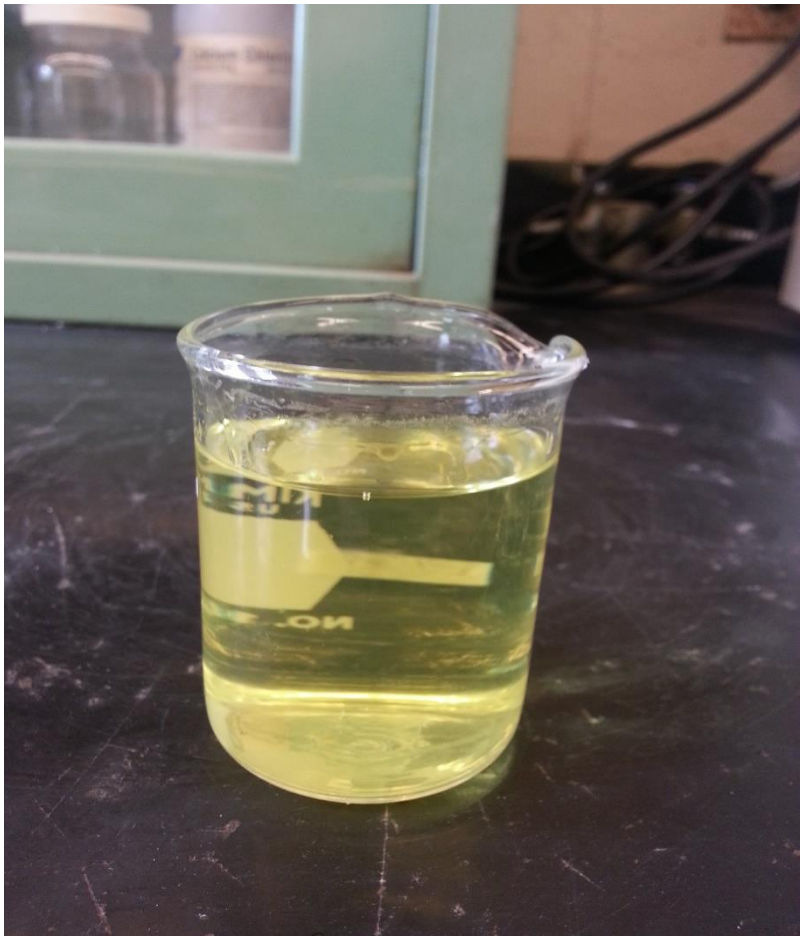

Figure 4-2: Typical homogeneous, transparent and light yellow sol

4.4.2 Synthesis of aqueous titania-silica-$Fe(NO_3)_3$ sol

The iron-doped sols were made in a similar fashion, except that the solution included different amounts of the doping material. The iron nitrate nonahydrate was first dissolved in ethanol and then added to the sol-gel precursor solution sample. The beakers were covered to prevent premature evaporation. Several weight amounts, 0.0001, 0.001, 0.01%, of $Fe(NO_3)_3$ were added to TiO_2–SiO_2 sol under a magnetic stirrer and the solution was stirred until obtaining a homogeneous sol. The amount of dissolved ions was calculated to be 0.0001%, 0.001%, and 0.01 mol% relative to the amount of TiO_2-SiO_2.

4 .5 Sol treatment prior to dipping

After mixing, the sols were left to stand, or age, before dipping. This allows the sols to begin to polymerize ensuring a better bond to the substrate. The sols were aged at room temperature. Aging times were 0, 5, 10, 15, 20, 25, 30 days. Sols aged for more than 30 days polymerized fully to gels and thus were of no use for dipping purposes.

4.6 Powder Preparation

Solutions of TiO_2-SiO_2 was poured into ceramic crucibles, kept in the furnace at 120°C for 3 hours to achieve drying and calcination. The solid pieces were reduced to powder by mortar and pestle.

4.7 Substrate Preparation

4.7.1 Preparation and cleaning of Substrates

Glass microscope slides with dimensions of 75mm x 38mm x 1mm was used as substrates. The cleaning of the surface of the substrate is a very important issue in thin film deposition technology. The exposure of the substrate surface to the atmosphere generates gaseous, liquid or solid contaminations which should be removed before the deposition process. When the substrates are not clean, the deposited film usually does not adhere well and the desired film properties are affected by the impurities on the surface of the substrate.

4.7.2 Steps of cleaning the glass substrates

Glass substrates first were rinsed with distilled-deionized water and technical grade ethanol. This was repeated with acetone instead of ethanol. Then this was repeated with water. Lastly, the washed slides were dried in 120°C oven for 10 minutes prior to coating.

4.8 Thin Film Fabrication

Thin films of sol-gel-derived materials were deposited on preconditioned substrates by immersing the substrates in the sol and withdrawing them at a constant speed using dip-coating method as discussed in Chapter One. The substrate was kept in the sol for one minute. After that, it was withdrawn with a fixed withdrawal rate. This technique produced a thin film of uniform thickness on the substrate. After dip-coating the samples were left to dry in air for a short period of time and then the drying treatment was performed at the end of each deposition in a furnace at 100ºC for 24 hours to produce thin films. Due to the dry environment of the oven, most of the reaction solvents are removed at this stage.

4.9 Methods of Characterization

Several methods of characterization were used to analyze the prepared materials and coatings. UV-VIS spectrophotometry was done to determine the optical transmittance of samples. The thickness of thin films was measured with A Zeiss-Sigma Scanning Electron Microscope (SEM). Sample preparation for SEM measurements involved splitting the thin film substrates perpendicular to the deposited thin film stack and mounting the exposed cross section of the sample on a vertical SEM specimen stub. Changes in coating thickness were obtained from this data.

FTIR spectroscopy was done to follow structural changes in titania-silica coatings and for identifying chemicals that are either organic or inorganic. The film phases and crystallite size was determined by a PANalytical X'Pert PRO high-resolution diffractometer with an alpha 1 configuration using CuKα1 radiation (1.5406 Å).

4.9.1 UV-vis spectroscopy

UV-vis spectroscopy probes the electronic transitions of molecules as they absorb light in the UV and visible regions of the electromagnetic spectrum [156]. The transmission spectra of the coatings deposited on glass slides substrates were measured using an EVOLUTION 300 UV-VIS spectrophotometer from Thermo Fisher Scientific. The measurements were carried out within the range 200 to 1100 nm. All measurements were done at room temperature. The transmission (T) was measured at normal incidence against air as reference.

4.9.2 Scanning electron microscopy (SEM)

The Zeiss Sigma field emission scanning electron microscope (FESEM, Thornwood, NY) with full digital image collection was used to investigate the thickness of thin films layer of the deposited films. The SEM was operated at 20 kV, and images were recorded at different magnifications.

4.9.3 X-ray diffraction (XRD)

The X-ray powder diffraction (XRD) patterns were obtained on a PANalytical X'Pert PRO high-resolution diffractometer with an alpha 1 configuration using CuKα1 radiation (1.5406 Å) in the range with a step size of 0.04º using a fully opened X'Celerator detector at room temperature. The X-ray diffractometer was operated at 45 kV and 40 mA. X-ray data were collected for a 2θ range of (10º - 90º). The data collection and analysis were carried out using the software supplied with the diffractometer.

The average crystallite size was determined from the broadening of the XRD peaks reflection by the Scherrer's equation:

$$D = K\lambda/\beta\cos\theta. \quad (4\text{-}1)$$

Where D is the crystallite size, K is a dimensionless constant called (particle shape factor) is related to the crystallite shape, usually taken as 0.9, λ is the wavelength of the X-ray radiation (CuKα = 1.5406 Å), β is the Full Width at Half-Maximum (FWHM) of the diffraction peak in radians and θ is the Bragg's diffraction angle in degrees [157]. Crystallite size is determined by measuring the broadening of a particular peak in a diffraction pattern associated with a particular planar reflection within the crystal unit cell.

It is inversely related to (FWHM) of individual peaks. The narrower the peak, the larger the crystallite size and vice versa [157].

4.9.4 Fourier Transform Infrared Spectroscopy (FT-IR)

The term Fourier Transform Infrared Spectroscopy (FT-IR) refers to the manner in which the data is collected and converted from an interference pattern to a spectrum [158]. The IR spectra of the powder samples were recorded using a FT-IR Perkin-Elmer Frontier^{TM} spectrometer with a 4 cm^{-1} resolution in the frequency range from 4000 to 400 cm^{-1} for each sample.

Chapter Five

Results and Discussions

5.1 Introduction

This chapter presents the results obtained from UV-Visible spectroscopy, Scanning Electron Microscope (SEM), X-ray diffraction patterns (XRD), and Fourier transform infrared spectroscopy (FT-IR).

5.2 Optical Properties

The optical properties depend on many parameters such as a substrate, sol, central wavelength, number of layers, optical thickness, aging time, porosity and heat treatment [159]. Optical characterizations were achieved through the transmission spectra and calculation of the thickness for the prepared films groups.

5.2.1 UV-Visible Spectroscopy

Stable, transparent, colorless and crack-free coatings have been obtained after heating at 100 ºC. A clean and uncoated glass substrate was used as the reference when measuring transmittance. Figures 5-1, 5-2, 5-3, 5-4, 5-5, and 5-6 show the transmittance spectra in the range 200-1100 nm. These Figures give a comparison of the visible light transmission spectra of the various combinations of thin films coated vs. the bare glass. As expected, the transmittance of the bare glass is the highest around ~ 97% in the wavelength range of 300-800 nm as shown in the Figure 5-1. It is worth noting that a thin layer of SiO_2

on the bare glass substrate has been used by others to limit the diffusion of sodium ions Na+ into the films from the glass slides during the heat treatment process [13,145,160].

The film thickness increased with the number of dip-coating cycles. Each cycle was followed by thermal treatment at 100ºC. Each layer covered an irregular surface, giving rise to an increase in the final thickness. The transmittance decreased with increasing number of dip coatings. This observation can be explained according to Beer-Lambert law. In addition, the reduction of transmittance is also due to light scattering for higher surface roughness and different grain size. The results of the transmittance measurements are in qualitative agreement with the film-thickness measurements.

Figures 5-2 through 5-6 exhibit fluctuations in the transmittance spectra, which are attributed to the interference between two optical interfaces: air-thin film and thin film substrate.

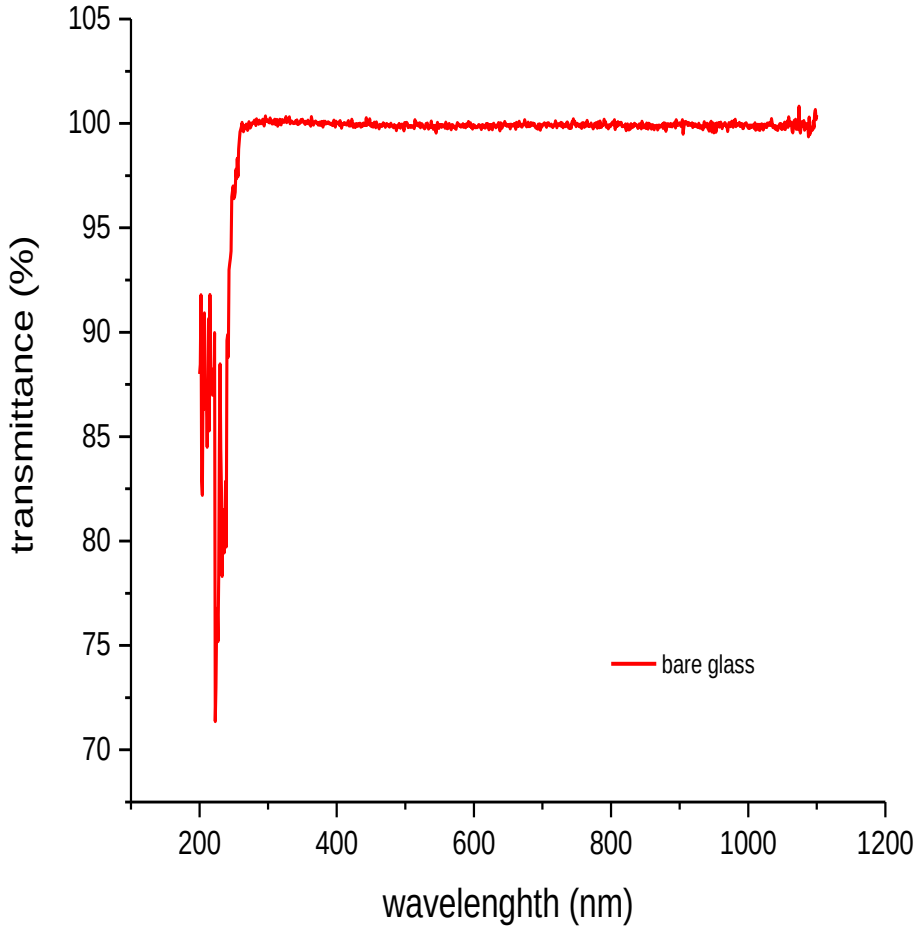

Figure 5-1: Transmittance spectra for the bare glass samples.

5.2.1.1 The composition of TiO_2- SiO_2 Groups

Transmission spectra for thin films prepared from TiO_2- SiO_2 solutions are shown in six groups, as listed in the Table 4.1. Each Figure shows of the UV-vis spectra from 200-1100 nm.

5.2.1.2 3% TiO_2 - 97% SiO_2

Figure (5-2) shows the transmission spectra for thin films with 1 and 3 dip-coatings of 3% TiO_2 + 97% SiO_2 with solution age (0, 5,15, and 25) days. The significant difference in transmittance behavior of the 3 layer sample, compared to 1 layer, was an increase in the spectral region 350-450nm that may be attributed to constructive interference since the constructive and destructive interference is more obvious in thin films with a large thickness. The transmittance after 3 layers is not as good as 1 layer. In terms of transmittance, 1 layer is better.

Also, from the Figure (5-3) and Figure (5-4), one can see that the transmittance of the as-deposited films at solution age 0 days for all layers 1 and 3 is higher than the transmittance for the solution aged 25 days. The age of the solution should be kept as low as is practical.

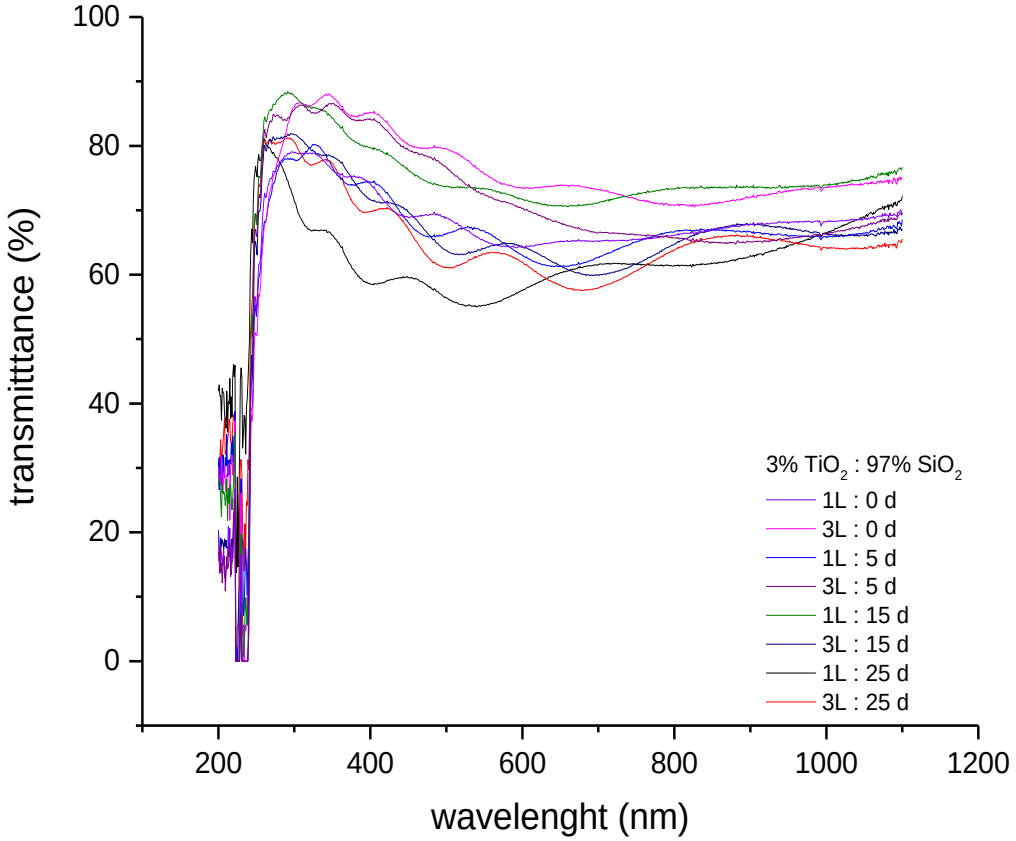

Figure 5-2: Transmittance spectra for the First group samples.

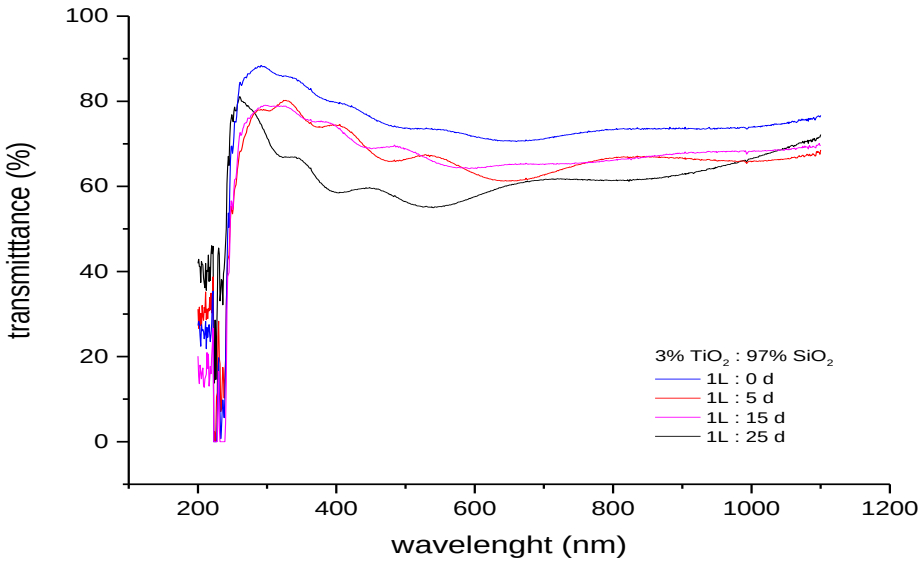

Figure 5-3: Transmittance spectra for the First group samples.

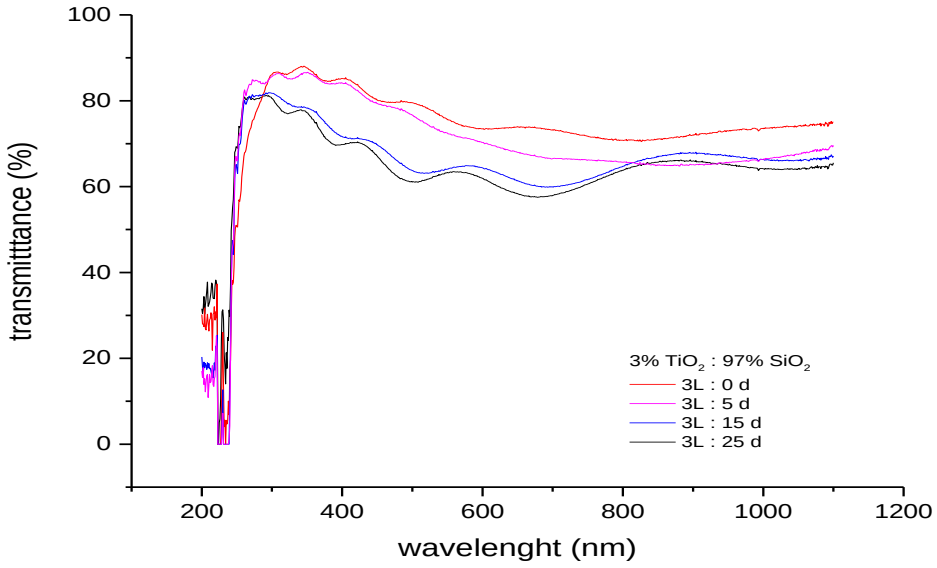

Figure 5-4: Transmittance spectra for the First group samples.

5.2.1.3 5% TiO_2 - 95% SiO_2

Figure 5-5 presents the UV-vis transmittance spectra for thin films with 1 and 3 dip-coatings of 5% TiO_2 + 95% SiO_2 with solution age 0, 5,15, and 25 days. The transmittance of thin films for this group is similar to the first group. The sample with 3 layers shows a high transmittance in the spectral region 650-750nm for the same reason as it was described for the sample of the first group. Hence, this sample is not recommended for further study. Also, it can be seen in Figures 5-6 and 5-7 that the transmittance behavior of the 1 and 3 layer sample at the solution age 25 days was decreased in the spectral region 650-750nm compared to solution age 0 days.

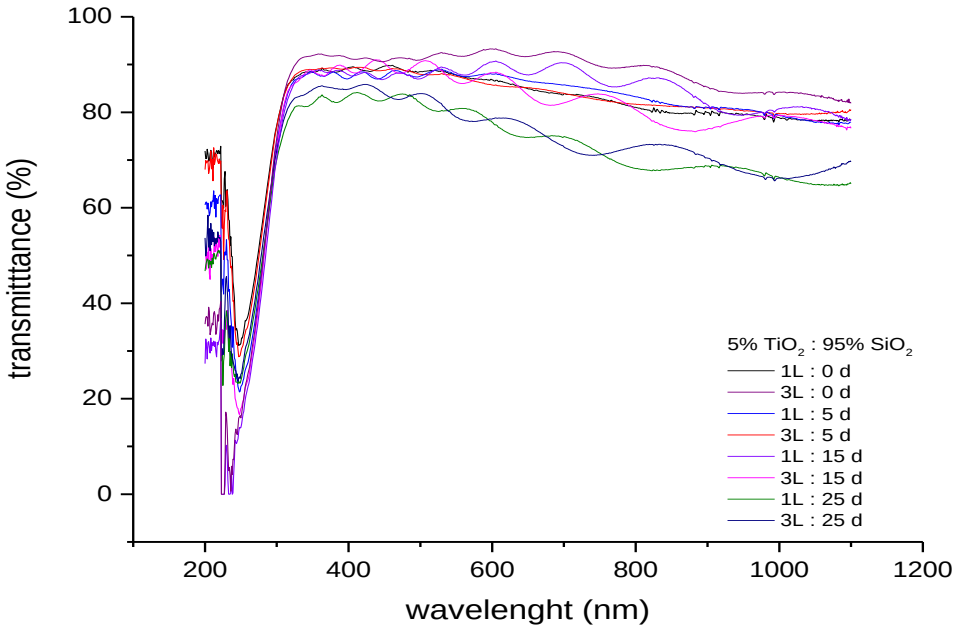

Figure 5-5: Transmittance spectra for the second group samples.

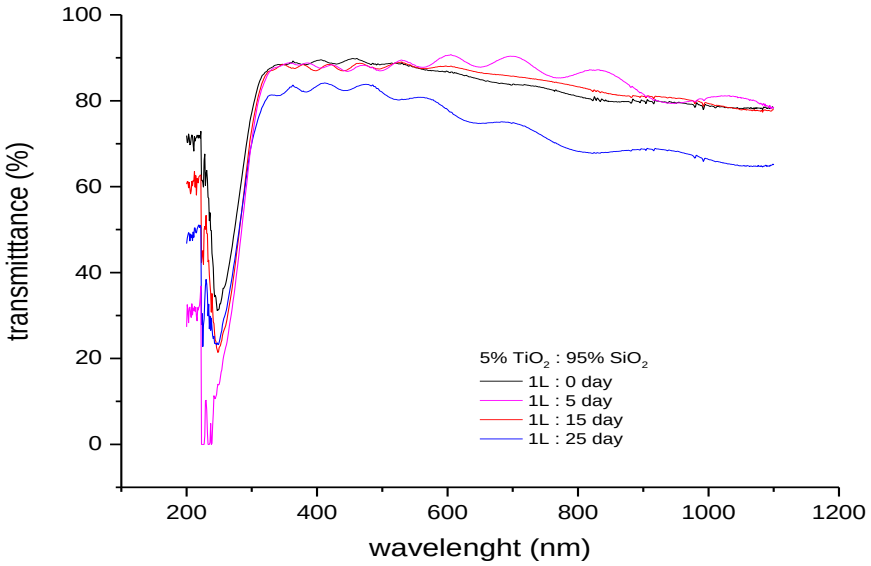

Figure 5-6: Transmittance spectra for the second group samples.

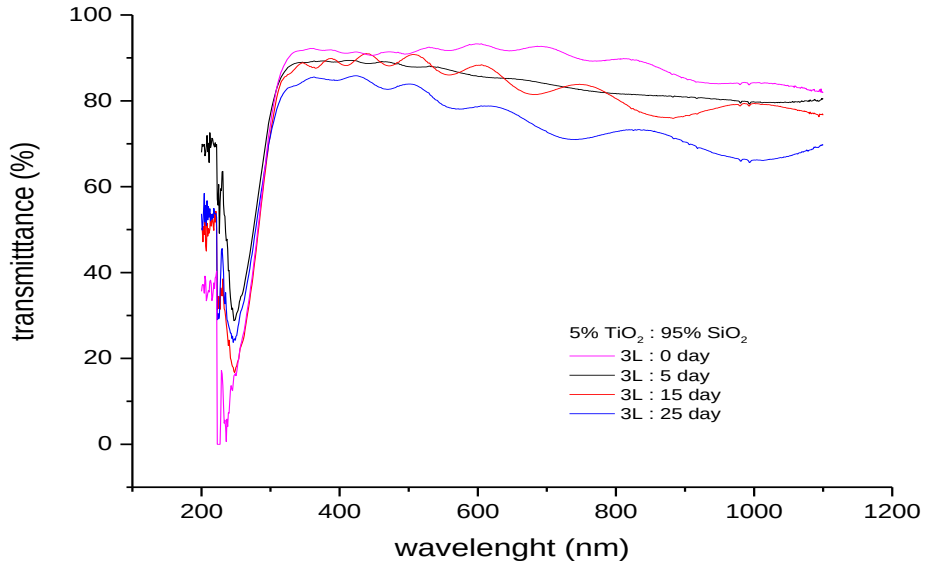

Figure 5-7: Transmittance spectra for the second group samples.

5.2.1.4 7.9% TiO_2 - 92.1% SiO_2

Figure 5-8 presents the UV-vis transmittance spectra for thin films with 1 and 3 dip-coatings of 7.9% TiO_2 + 92.1% SiO_2 with solution age 0, 5,15, and 25 days. The behavior of the transmittance of thin films for this group is similar to the first group. The sample with 3 layers shows a high transmittance in the spectral region 350-450 nm for the same reason as was described for the sample of the first group, but lower. Also, from the Figure 5-9 and Figure 5-10, the transmittance is higher for samples for all layers 1 and 3 at the age solution 0 days.

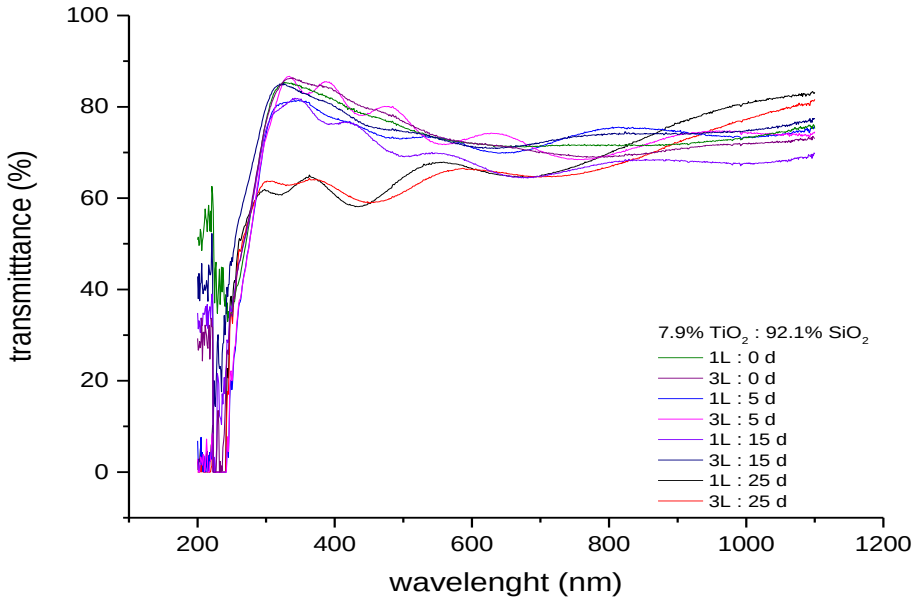

Figure 5-8: Transmittance spectra for the third group samples.

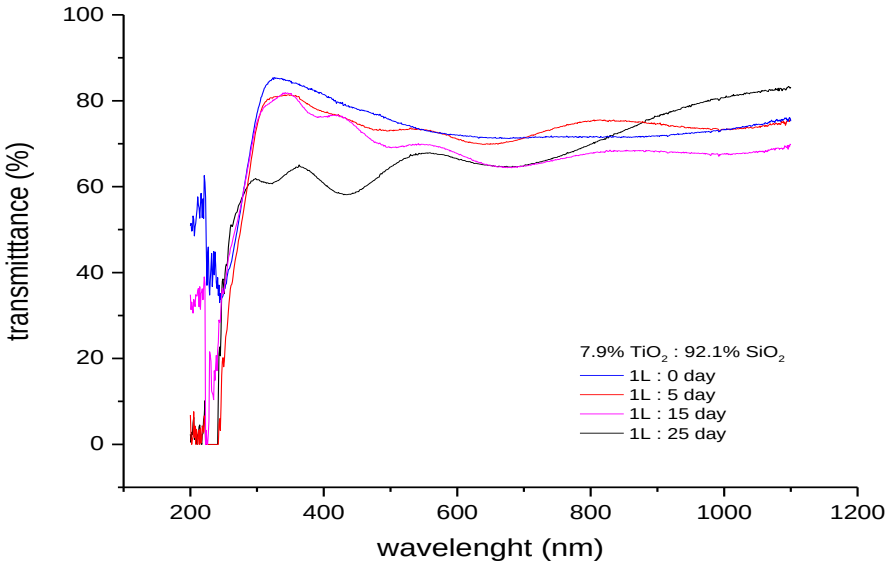

Figure 5-9: Transmittance spectra for the third group samples.

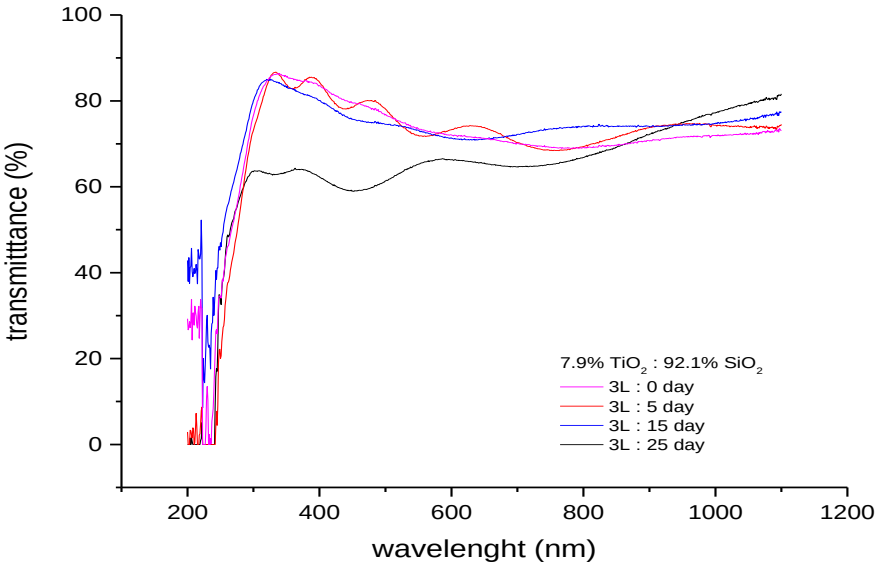

Figure 5-10: Transmittance spectra for the third group samples.

5.2.1.5 10% TiO_2 - 90% SiO_2

The transmission spectra for thin films with 1 and 3 dip-coatings of 10% TiO_2-90% SiO_2 with solution age 0, 5,15, and 25days are shown in the Figure. It can be seen in Figure 5-11 that the transmittance behavior of the 1 layer sample at 0 days aging was increased in the spectral region 400-600nm. Since the peak of the solar radiation spectrum lies in this important spectral region, the optical performance of this sample is promising. Therefore, it is the sample that will be studied further in terms of transmittance characteristics.

It can be seen in Figure 5-12 that film samples with age solution 0 days for all layers 1 and 3 have higher transmittance in comparison with the film samples at age solution 25 days in Figure 5-13. By comparing the two systems, it is seen that an increase of solution age decreases the transmittance of the films, because the sol becomes thicker than the original sol. So the age of the solution should be kept as low as possible in order to maintain the high transmittance obtained by TiO_2-SiO_2 nanoparticles.

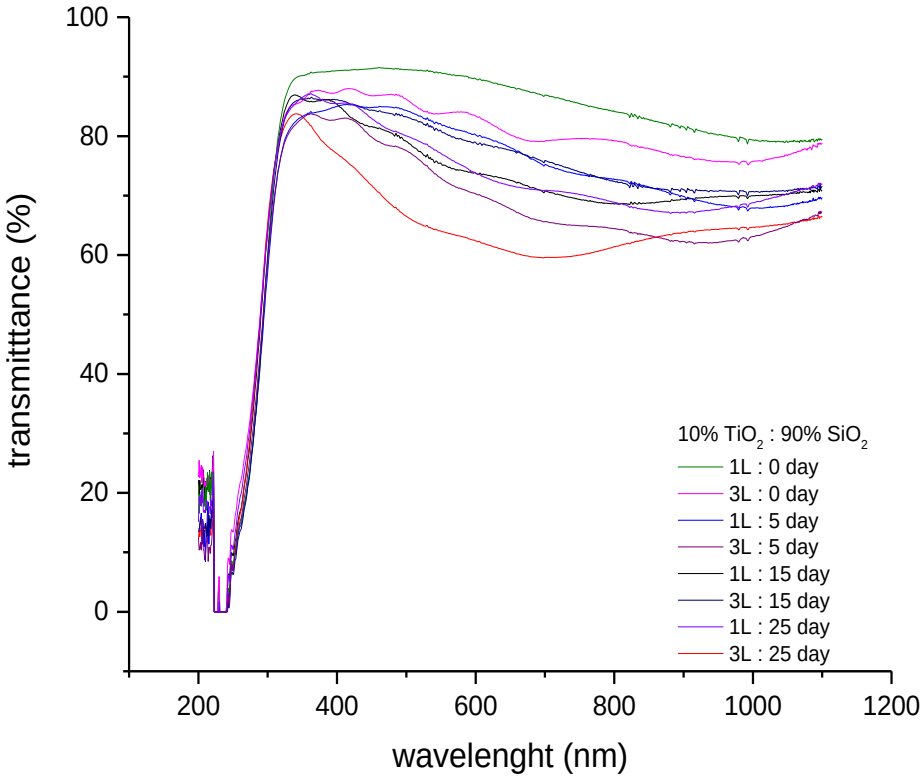

Figure 5-11: Transmittance spectra for the fourth group samples.

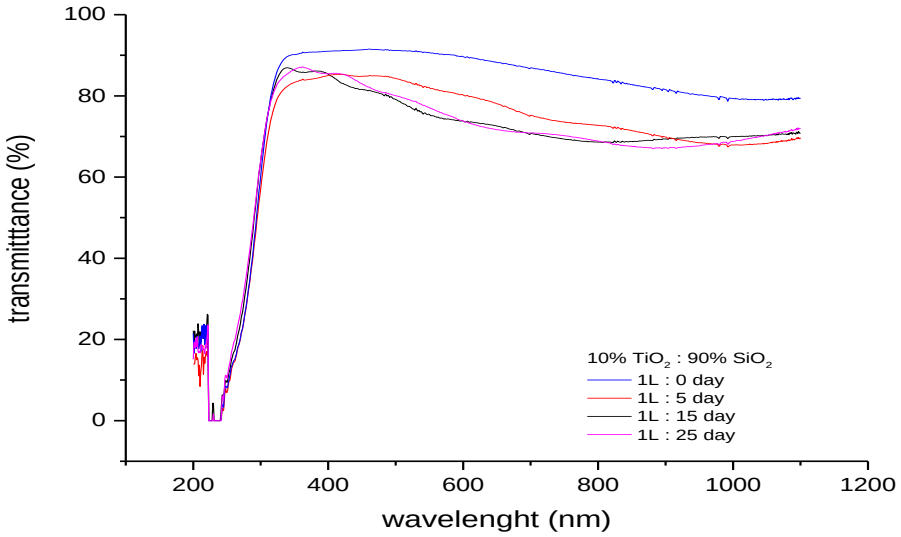

Figure 5-12: Transmittance spectra for the fourth group samples.

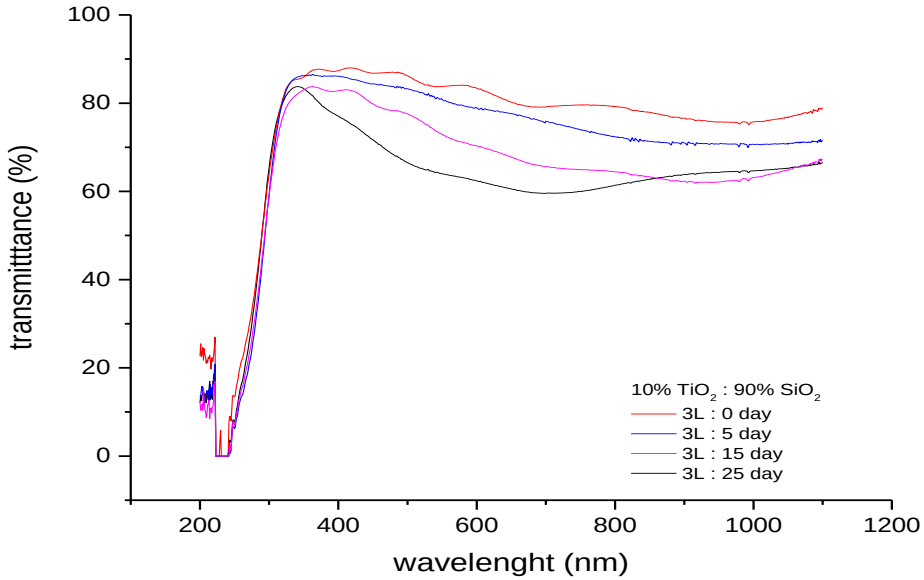

Figure 5-13: Transmittance spectra for the fouth group samples.

5.2.1.6 15% TiO_2 - 85% SiO_2

The transmission spectra for thin films with 1 and 3 dip-coatings of 15% TiO_2-85% SiO_2 with solution age 0 ,5, 15, and 25 days are shown in the Figure 5-14. The behavior of the transmittance of thin films for this group is similar to the fourth group except that the values of the transmittance are slightly lower, which may be attributed to the decreased amount of SiO_2 in the coating.

The 1 layer sample shows a high transmittance in the spectral region 400-550nm for the same reason as it was described for the sample in the fourth group, but lower transmittance compared to that of the sample. Hence, this sample for this group is the sample that will be studied further.

Also, it can be seen in Figure 5-16 that the transmittance of the 1 and 3 layer sample of the solution aged 25 days decreased in the spectral region 400-550nm in comparison with the same film samples at solution aged 0 days as the Figure 5-15. Both have shown a different trend of transmittance than that of the other samples with relatively lower transmission percentage. Nevertheless, the decrease of transmittance with an increase in the age solution indicates that the solution age should be kept as low as possible in order to maintain the high transmittance obtained by TiO_2-SiO_2 coating.

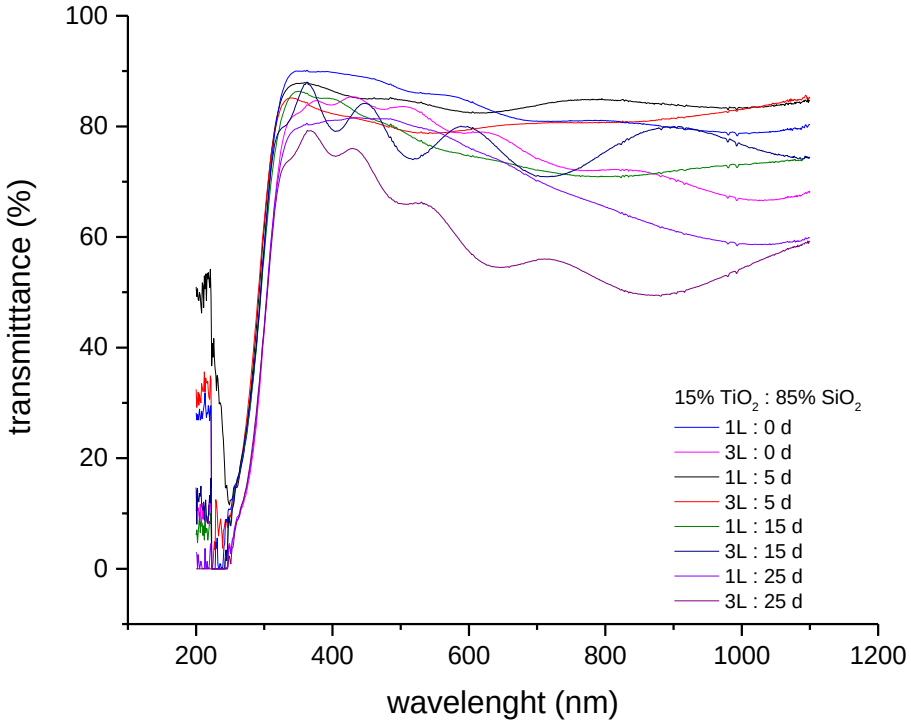

Figure 5-14: Transmittance spectra for the fifth group samples.

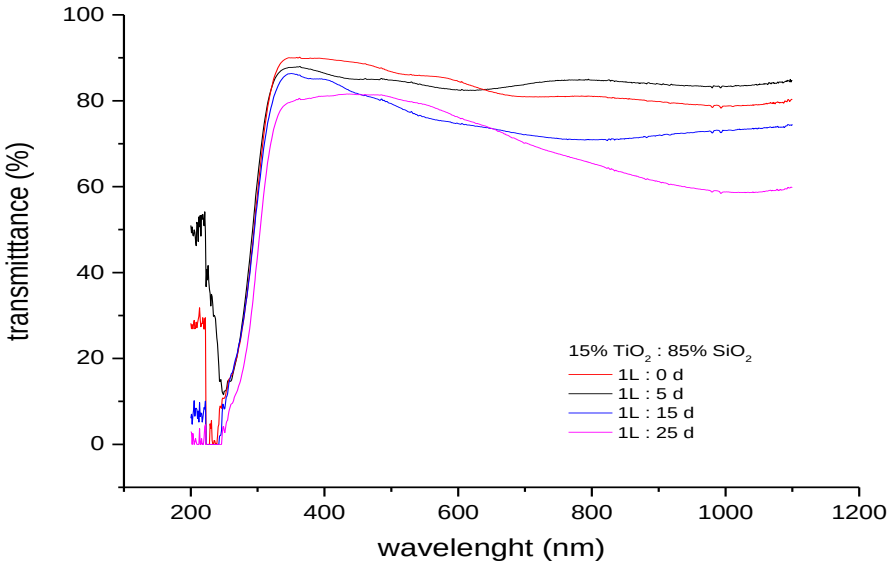

Figure 5-15: Transmittance spectra for the fifth group samples.

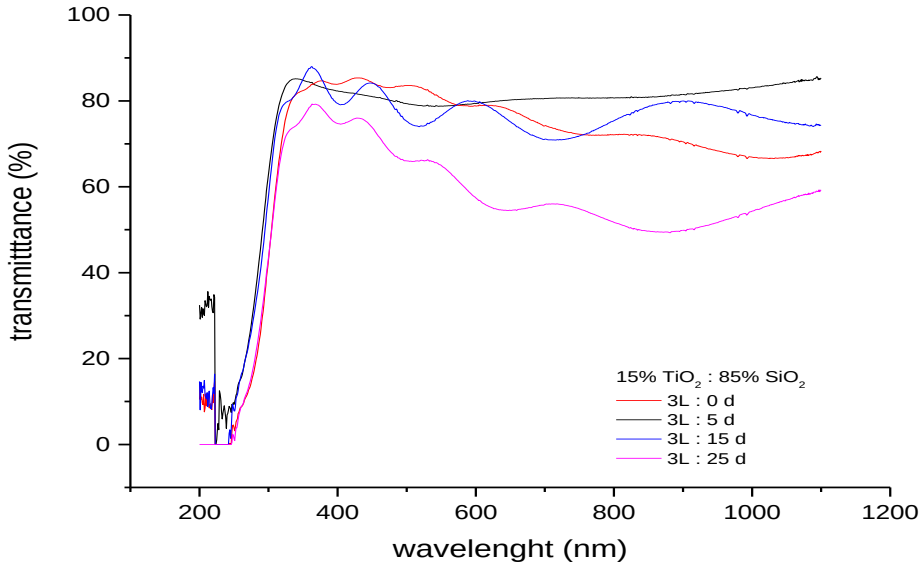

Figure 5-16: Transmittance spectra for the fifth group samples.

5.2.1.7 Iron (III) doped TiO_2-SiO_2 thin films

Transmission spectra for different amounts of $Fe(NO_3)_3$ doped TiO_2-SiO_2 thin films are shown in the Figures 5-17 and 5-18. The Iron (III) ions act as absorption centers so that the increase of their amount reduces the transmittance. The two Figures show that the film with lower weight amounts of $Fe(NO_3)_3$ (0.0001 %) exhibited higher transmittance than the other samples; hence this dopant amount has a negligible absorption influence. As the weight amount of $Fe(NO_3)_3$ increased the absorption effect became obvious, so that, the transmittance was reduced. In addition, a greater amount of iron may cause the agglomeration of iron particle clusters, resulting in the decrease in optical transmittance.

Doping $Fe(NO_3)_3$ into the TiO_2-SiO_2 thin film resulted in more electron excitation due to the surface plasmon resonance. As the weight amount of $Fe(NO_3)_3$ increased reaching 0.01%, the transmittance was reduced because the absorption of $Fe(NO_3)_3$ is higher. Also, there is some reflectance loss in the visible spectral region. The thin film with the amount 0.0001 % of $Fe(NO_3)_3$ dopant shows high transmittance in the spectral region 450nm - 550nm, which is the important region in solar applications. Thus, this thin film is considered as the optimized sample for this group for transparency consideration.

The same trend was seen in all groups. Longer aged solutions had reduced transmittance as seen in Figures 5-19 and 5-20. One can see that the transmittance of the deposited films for the solution aged 0 days for all layers 1 and 3 is higher than the transmittance of the deposited films for the solution aged 25 days.

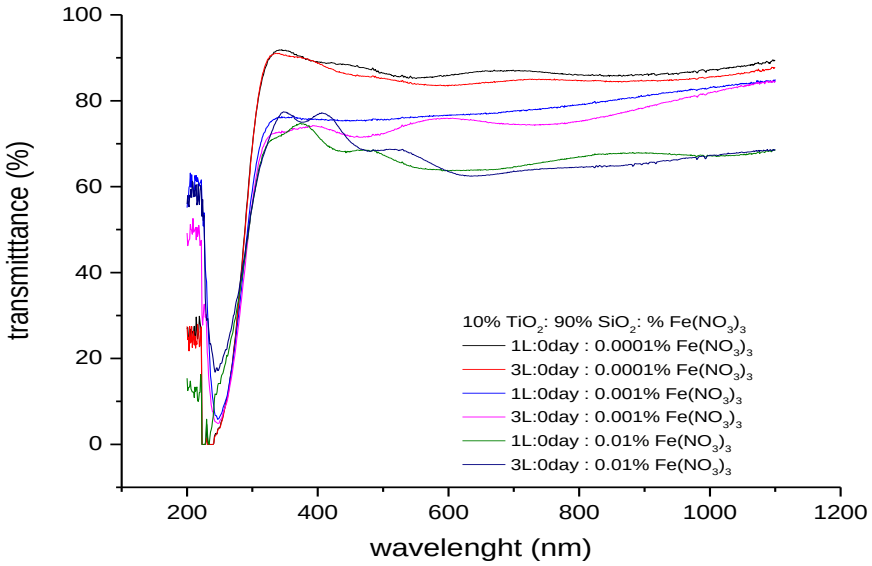

Figure 5-17: Transmittance spectra for the sixth group samples.

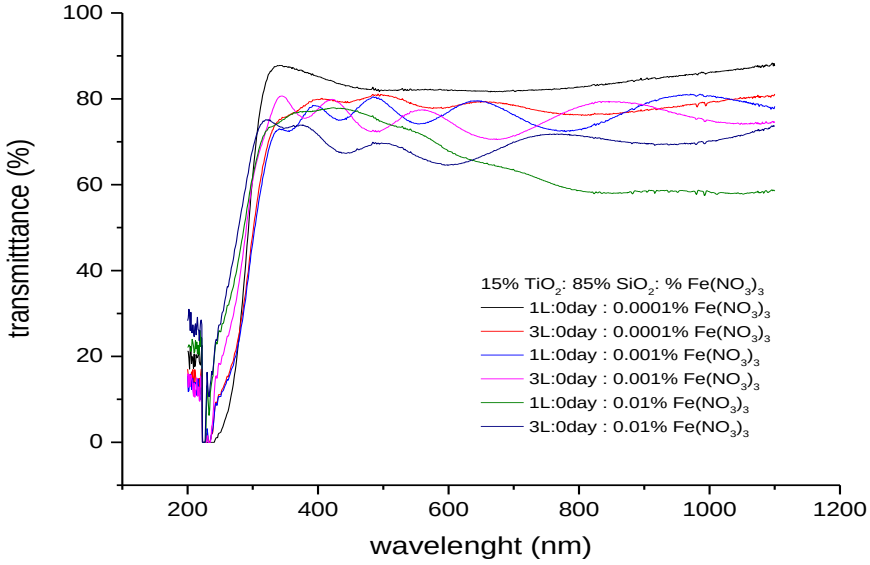

Figure 5-18: Transmittance spectra for the sixth group samples.

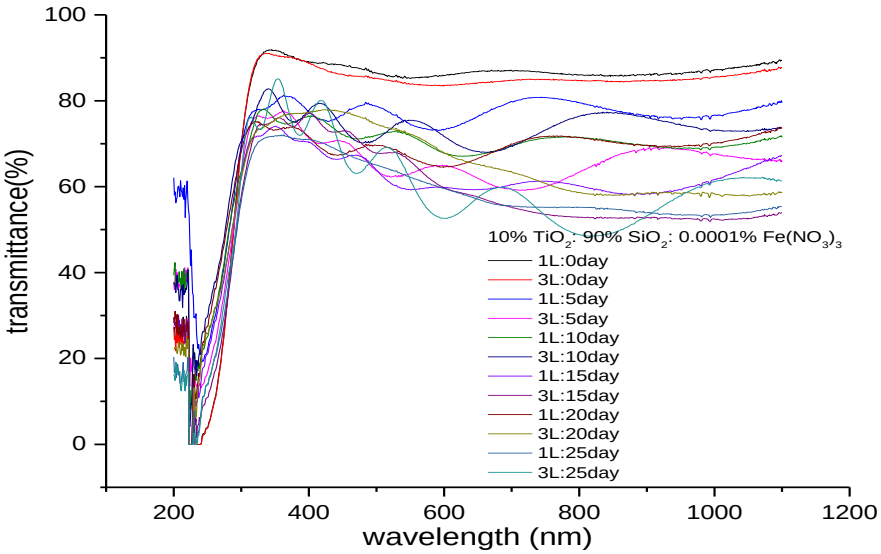

Figure 5-19: Transmittance spectra for the sixth group samples.

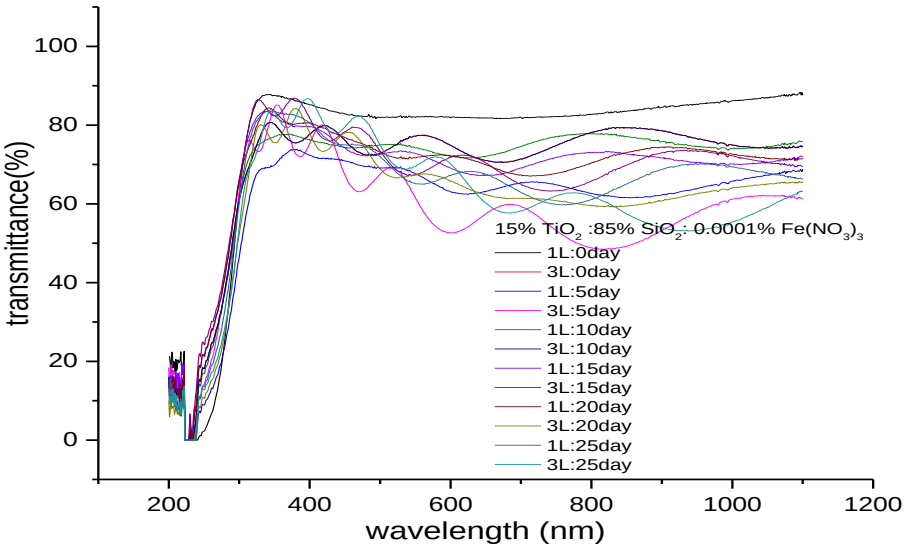

Figure 5-20: Transmittance spectra for the sixth group samples.

Based on this survey, the sample with 10% TiO_2-90% SiO_2 exhibits higher transmittance than any of the other compositions. Results from other researchers show that the transmittance increases as the percentage of SiO_2 increases. The cause of the decrease of transmittance is because of light scattering from small crystallites [138]. Additionally, the scattering from interfaces also results in decreasing the transmission in the mixed binary. It is observed in the XRD pattern that TiO_2-SiO_2 thin films are amorphous. However, the optical properties are indicative of microstructural properties, which depend on the process parameters and the composition of the materials used [161, 162]. In the current study, the sample with 10% TiO_2-90% SiO_2 does not appear to contain any crystallites and has the highest transmittance.

The values of transmittance for all prepared samples are summarized in Table 5-1. From the table, it can be seen that the sample of 10% TiO_2-90% SiO_2 and 0.0001% wt. $Fe(NO_3)_3$ dopant has higher transmittance than that of the other samples.

Table 5-1: The values of transmittance for all prepared samples

Group	Sample composite (TiO_2 : SiO_2)wt. ratio	No. of layers	The peak of the transmittance spectral region (nm)	The optical performance
1st	3 : 97 wt. %	3	350-450	Not promising
2nd	5 : 95 wt. %	3	650-750	Not promising
3rd	7.9 : 92.1 wt. %	3	350-450	Not promising
4th	10 : 90 wt. %	1	400-600	promising
5th	15 : 85 wt. %	1	400-550	promising
Group	Sample composite (TiO_2 : SiO_2 : $Fe(NO_3)_3$) wt. ratio	No. of layers	The peak of the transmittance spectral region (nm)	The optical performance
6th	10 : 90 : 0.0001 wt. %	1	350-450	promising
	10 : 90 : 0.001 wt. %	1	650-750	Not promising
	10 : 90 : 0.01 wt. %	1	350-450	Not promising
	15 : 85 : 0.0001 wt. %	1	400-600	promising
	15 : 85 : 0.001 wt. %	1	400-550	Not promising
	15 : 85 : 0.01 wt. %	1		Not promising

5.2.2 The thickness of Films

Thickness is a crucial parameter for thin films: the optical (transmission) and electronic properties (resistance, capacitance, leak current) of the film are highly dependent on its thickness and thickness uniformity. Applications in optics where optical interference effects are involved require the film thickness to be controlled within a small fraction of the wavelength of visible light [163]. The flexibility of the sol-gel process enables control of the thickness of the derived thin films through a number of techniques. There is the effect of varying film preparation parameters such as sol composition, annealing temperature, annealing time and dip speed on the thickness of the thin films.

The Zeiss Sigma field emission scanning electron microscope (FESEM, Thornwood, NY) with full digital image collection was used to observe the thickness of thin films layer of the deposited films. The SEM was operated at an accelerating voltage of 20 kV, and images were recorded at different magnifications.

At first, the thickness of thin films with 1 and 3 coatings on the glass substrate was measured without aging the solution. The samples with 5% TiO_2-95% SiO_2 had a thickness of 3.7μm for 1 layer and 6.2μm for 3 layers, as shown in the Figure 5-21. After aging the solution for 5 days, the thickness of the sample was 4.7μm for 1 layer and 7.9μm for 3 layers, as shown in the Figure 5-22.

The samples containing 10% TiO_2-90% SiO_2 without aging the solution had a thickness of 2.5μm for 1 layer and 5.6μm for 3 layers, as shown in the Figure 5-23. The thickness after aging the solution for 5 days is 3.5μm for 1 layer and 7.6μm for 3 layers as shown in the Figure 5-24.

The samples containing 15% TiO_2 - 85% SiO_2 without aging the solution had a thickness of 6.6µm for 1 layer and 23.1µm for 3 layers, as shown in Figure 5-25.

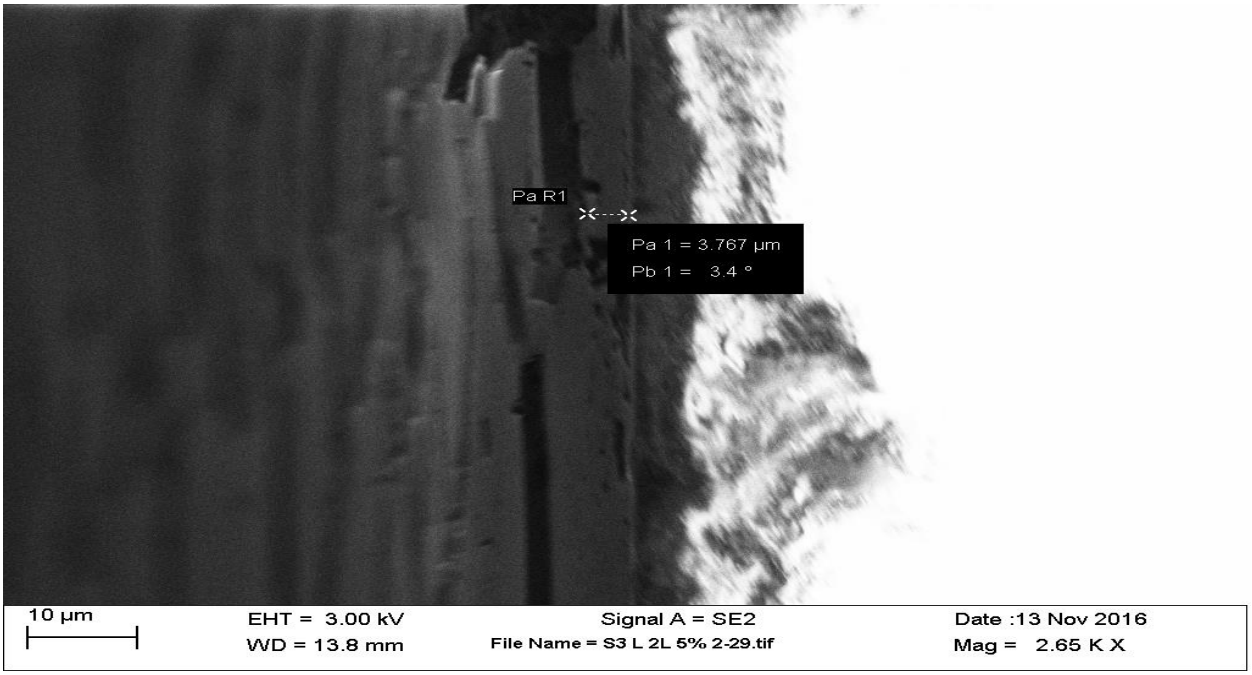

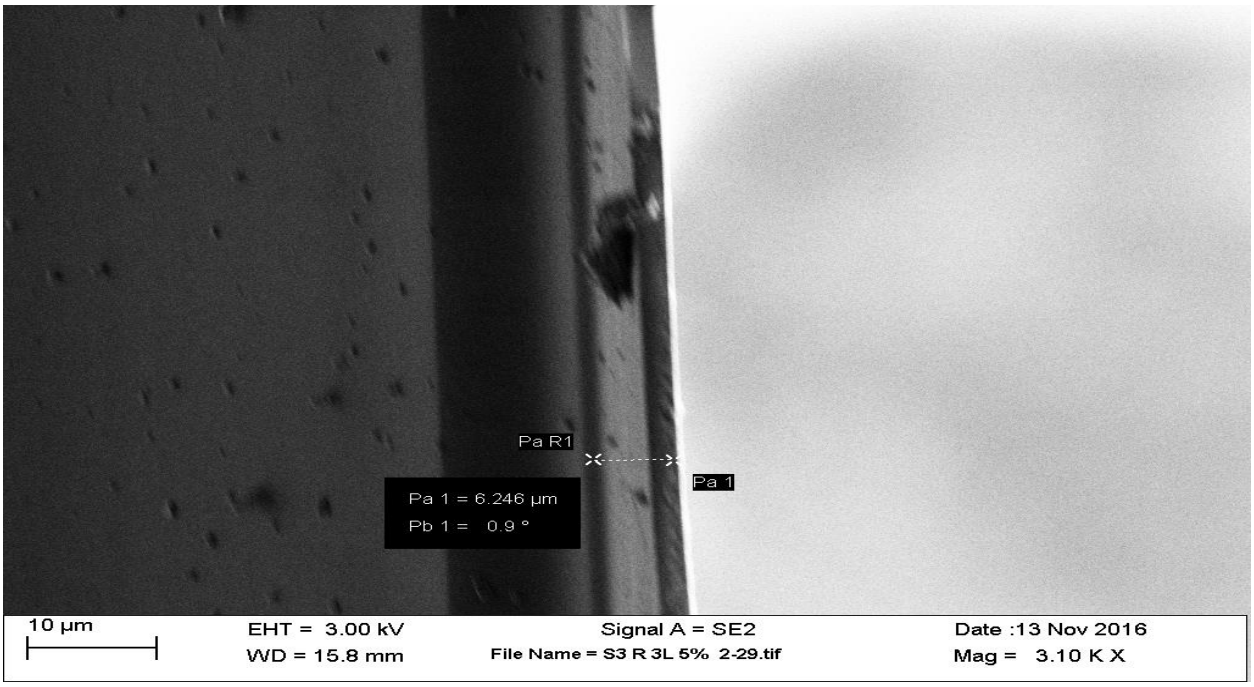

Figure 5-21: SEM micrograph of the sample 5% TiO_2 - 95% SiO_2, the thickness of one and three layers is equal to (3.7µm, 6.2µm) respectively.

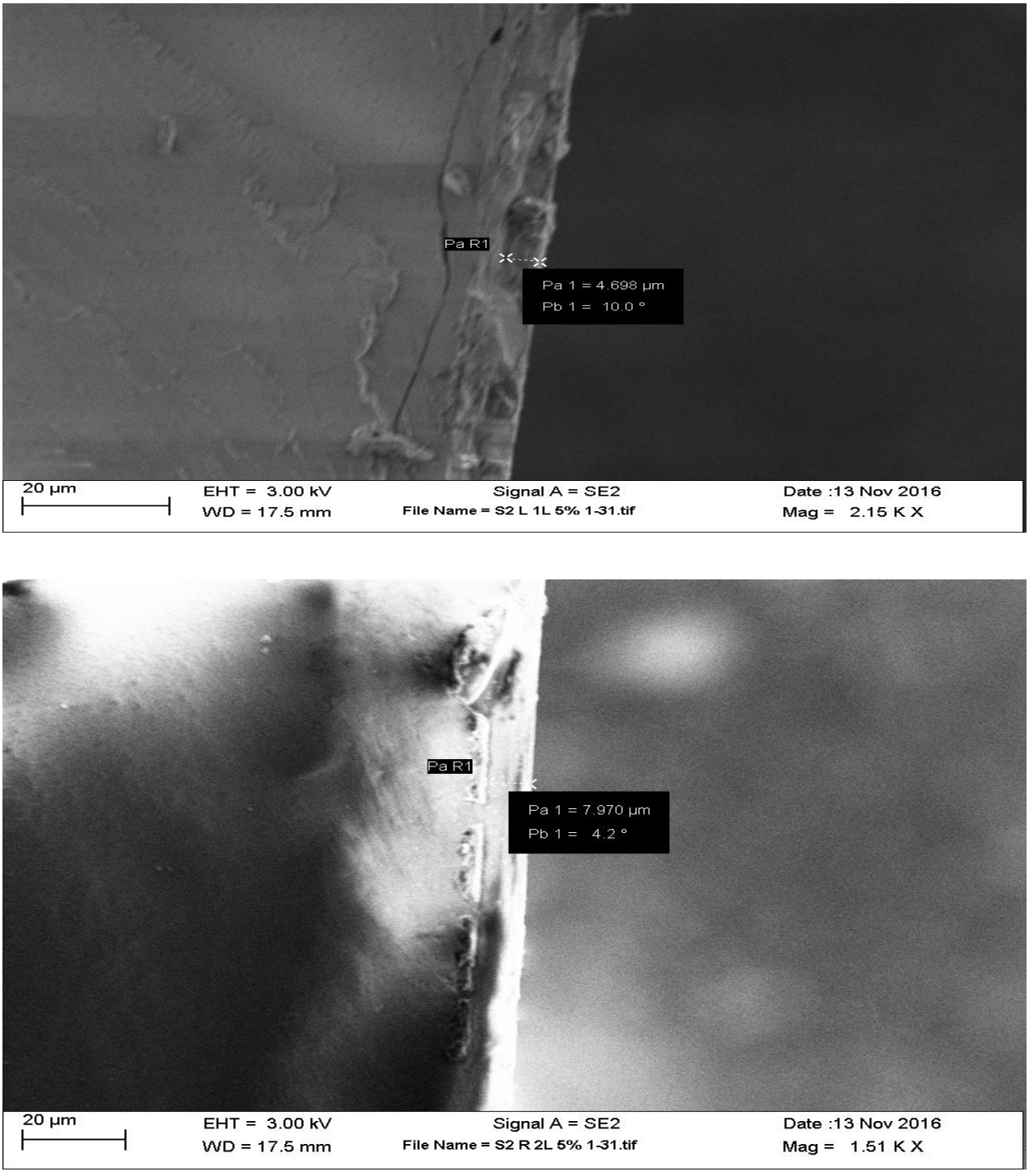

Figure 5-22: SEM micrograph of the sample 5% TiO_2 - 95% SiO_2, the thickness of one and three layers is equal to (4.7µm, 7.9µm) respectively.

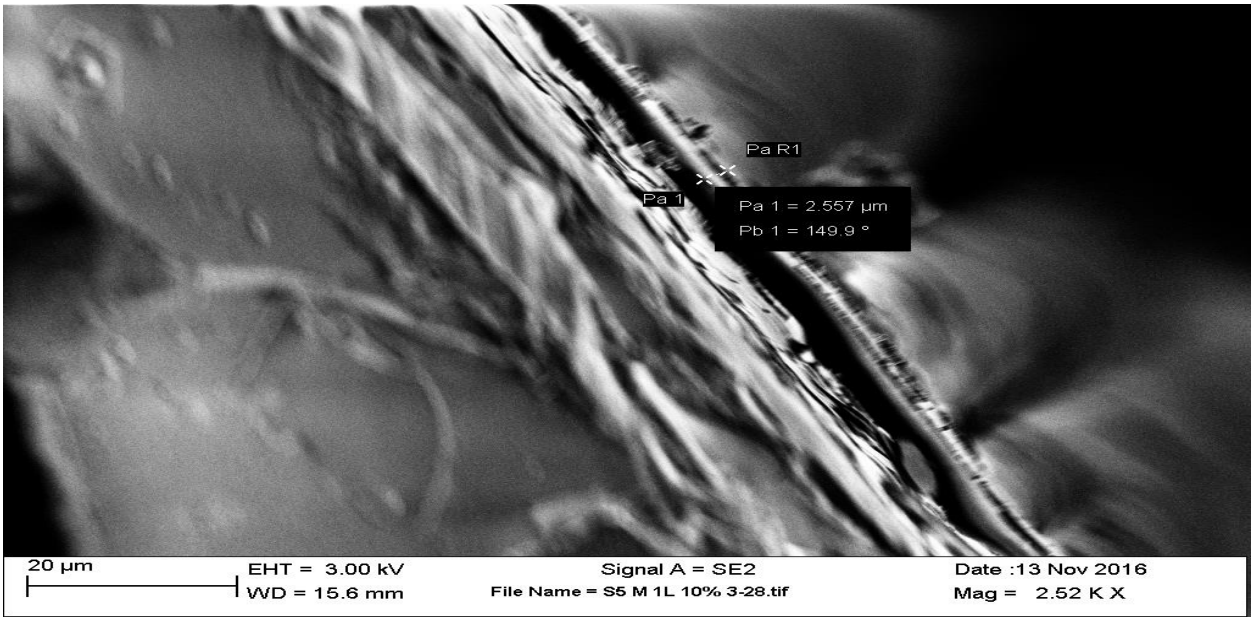

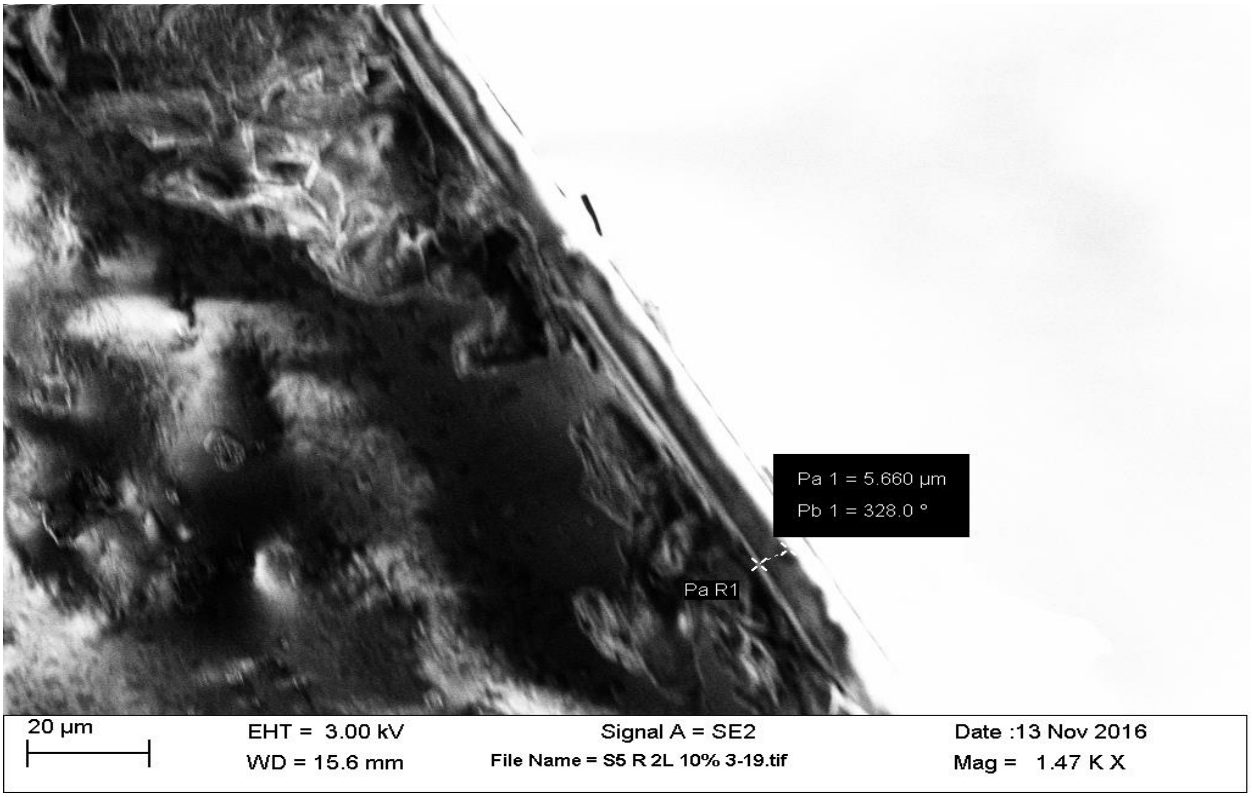

Figure 5-23: SEM micrograph of the sample 10% TiO_2 - 90% SiO_2, the thickness of one and three layers is equal to (2.5µm, 5.6µm) respectively.

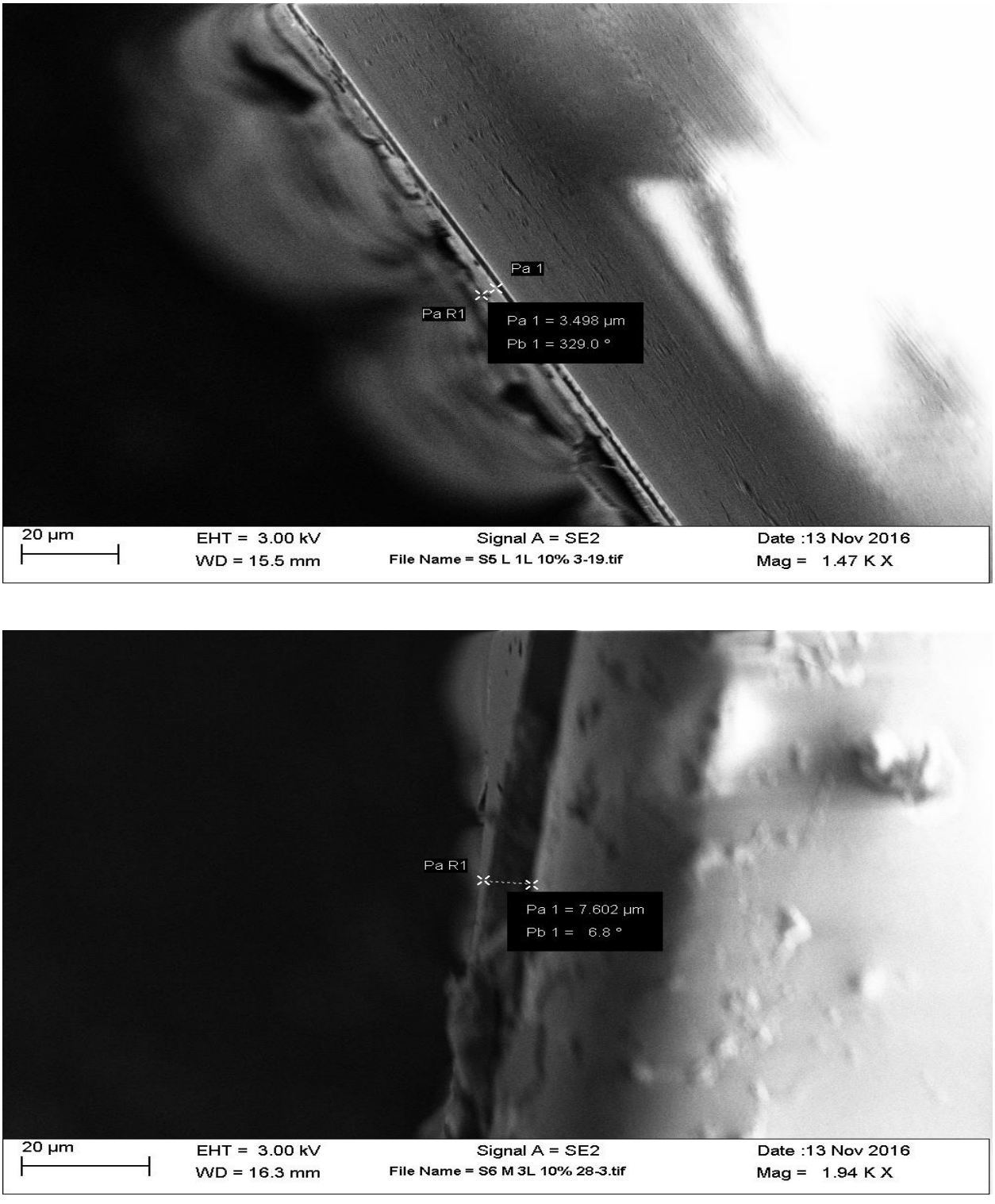

Figure 5-24: SEM micrograph of the sample 10% TiO_2 - 90% SiO_2, the thickness of one and three layers is equal to (3.5µm, 7.6µm) respectively.

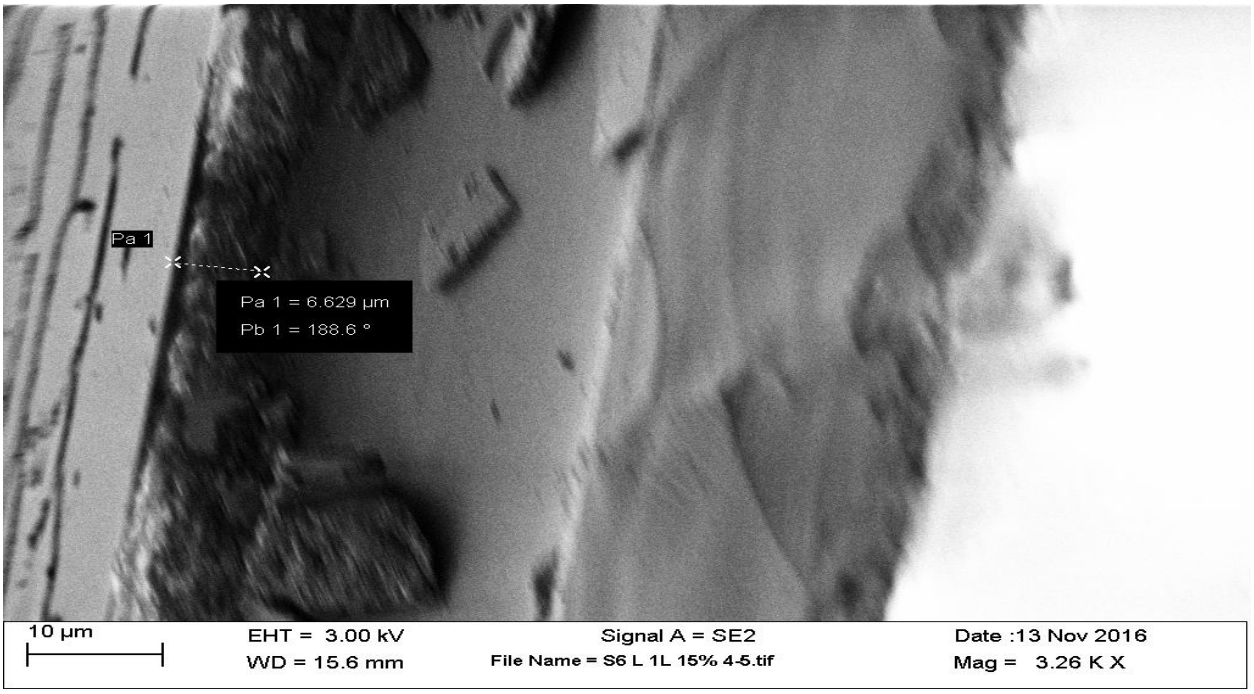

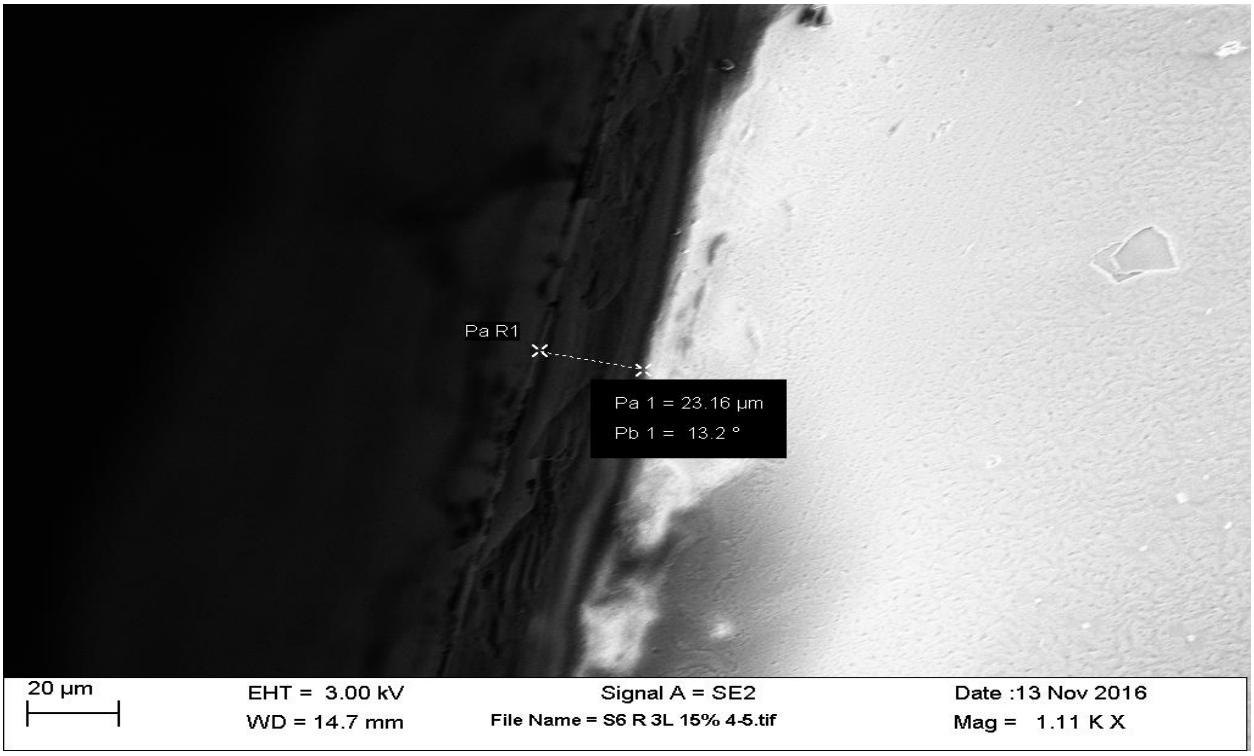

Figure 5-25: SEM micrograph of the sample 15% TiO_2 - 85% SiO_2, the thickness of one and three layers is equal to (6.6µm, 23.1µm) respectively.

The results of the film-thickness measurements agree with the transmittance measurement results, since the transmittance of samples with thinner TiO_2-SiO_2 coatings are expected to be higher.

The results of the thickness measurements from SEM of all observed thin films layer are summarized in table (5-2).

Table 5-2: Thickness of thin films layer for the samples

Sample	No. of Layers	Age(days)	Thickness(μm)
5% TiO_2 - 95% SiO_2	1 & 3	0	3.7 , 6.2
5% TiO_2 - 95% SiO_2	1 & 3	5	4.7 , 7.9
10% TiO_2 - 90% SiO_2	1 & 3	0	2.5 , 5.6
10% TiO_2 - 90% SiO_2	1 & 3	5	3.5 , 7.6
15% TiO_2 - 85% SiO_2	1 & 3	0	6.6 , 23.1

5.3 X-ray Diffraction analysis

The X-ray diffraction analysis was performed on the TiO_2-SiO_2 samples. Figure 1 shows the X-ray powder diffraction pattern for the TiO_2-SiO_2 precursor. It appears that powder is x-ray amorphous. As it can be seen, no characteristic crystalline peaks can be observed due to the amorphous behavior of the samples. The reaction of titania with silica nanoparticles may prevent the formation of titania nanocrystals. The absence of diffraction peaks in the film can be attributed to the low amount of TiO_2 in this system and a very broad and weak signal undetectable with XRD. The XRD pattern clearly shows a broad peak centered around 25^o as an indication of the amorphous or semi-amorphous structure of all samples. Relatively low annealing temperatures, for example, 100℃ does not cause anatase to-rutile crystal phase transformation. It is important to mention that there is no difference in the position of the amorphous phase between all the samples of the TiO_2-SiO_2 composite powders. In summary, for TiO_2-SiO_2 samples, the majority of the phase is amorphous. Crystal size was estimated by JADE software and ~ 0.3 nm. Crystallite size with less than 1 nm is probably signified short-range structure of the prepared thin film.

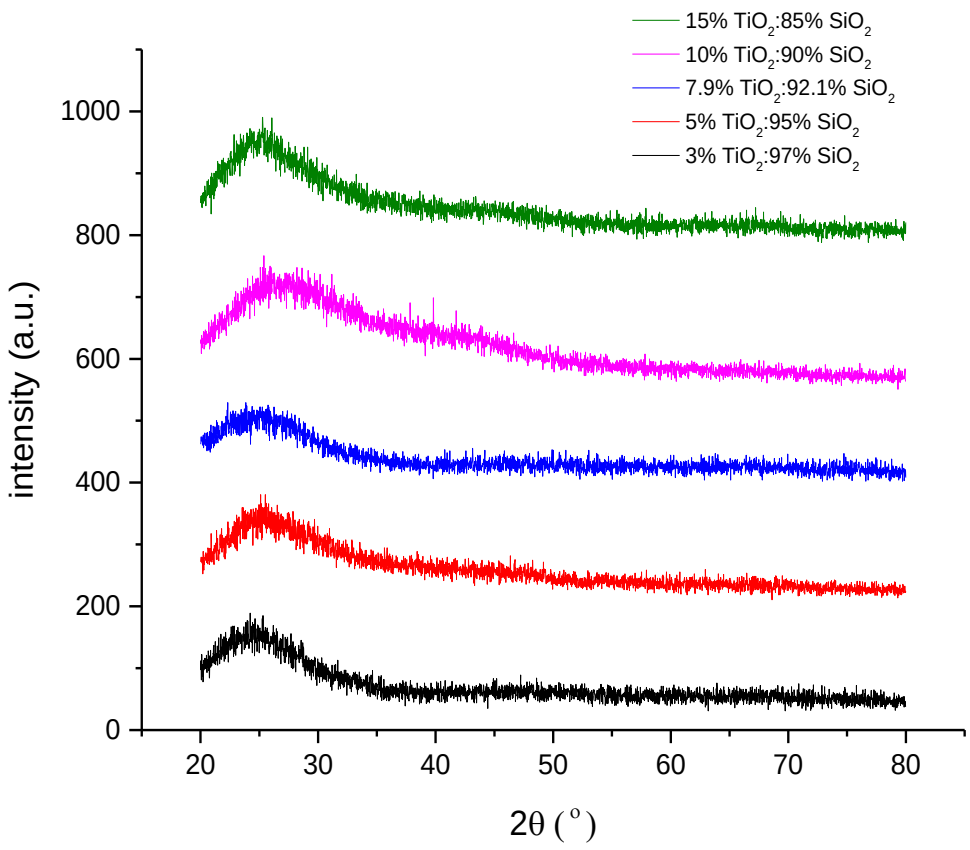

Figure 5-26: XRD pattern for the samples

5.4 XRD pattern for the sample of Fe doped TiO_2-SiO_2

The X-ray diffraction patterns for the samples Fe doped TiO_2-SiO_2 are shown in the Figures 5-27 and 5-28. The X-ray diffraction patterns illustrated that the structures of Fe doped 10% TiO_2-90% SiO_2 and Fe doped 15% TiO_2-85% SiO_2 powders are similar. As it was shown previously, in TiO_2-SiO_2 prepared powders, there is mainly amorphous phase. The amount of Fe ions had no significant effect on the crystal structure of the TiO_2-SiO_2. The broad peak indicates that the Fe doped TiO_2-SiO_2 films are amorphous. There is no

any sign of anatase, rutile or brookite. However, for Fe doped TiO_2-SiO_2, the hydroxyl groups associated with those of the Fe salt could react with silica or titania species, and inhibit crystallinity. It is important to mention that there is no difference in the position of the amorphous phase between the TiO_2-$SiO_2$and Fe doped TiO_2-SiO_2 powders. Crystal size was estimated by JADE software and ~ 0.3 nm.

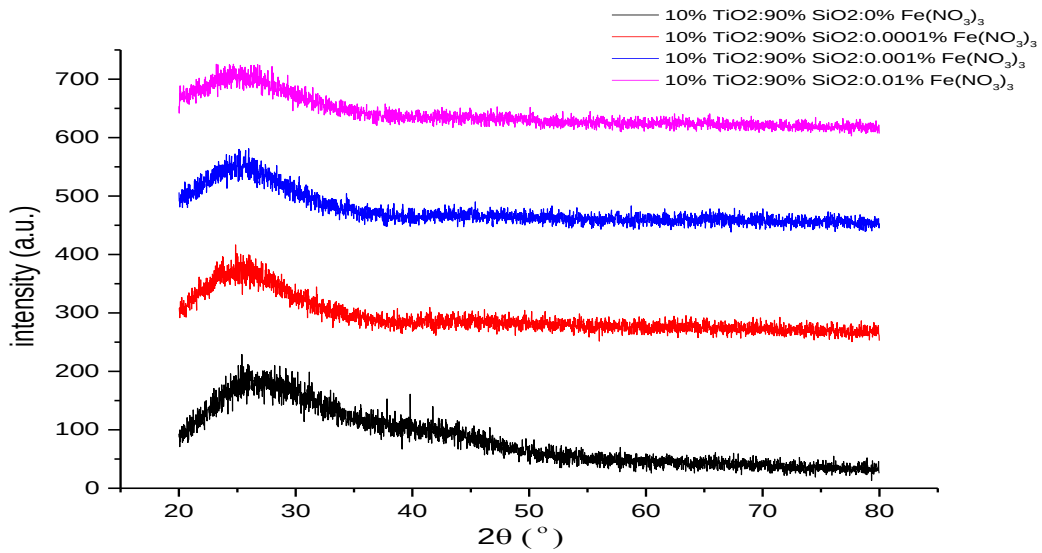

Figure 5-27: XRD pattern for the samples Fe-Doped (10%TiO_2-90%SiO_2)

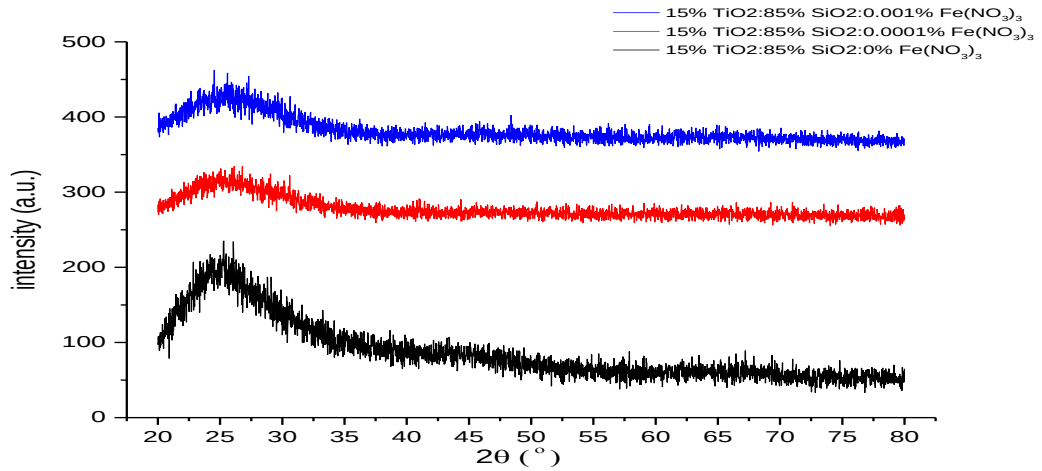

Figure 5-28: XRD pattern for the samples Fe-Doped (15%TiO_2-85%SiO_2)

5.5 Chemical Characterization

5.5.1 Fourier Transform Infrared Spectroscopy (FT-IR)

The FT-IR spectrum of TiO_2-SiO_2 film was measured to gain a better understanding of the chemical structure. Figures 5-29, 5-30, 5-31, 5-32, 5-33, and 5-34 are FT-IR spectra of all compositions of TiO_2-SiO_2 sol at 120 °C with the wavelength range from 4000 to 400 cm^{-1}. Figures 5-29 and 5-30 show the FT-IR spectra for 10% TiO_2-90% SiO_2 and 15% TiO_2-85% SiO_2 with different aging times, respectively. FT-IR spectra of Fe-doped 10% TiO_2-90% SiO_2, Fe-doped 15% TiO_2-85% SiO_2 with different iron percentage are shown in Figures 5-31 and 5-32, while spectra of Fe-doped 10% TiO_2-90% SiO_2, Fe-doped 15% TiO_2-85% SiO_2 with different aging times are shown in Figures 5-33 and 5-34. Spectra of all these samples look similar without any significant differences. However, some features need to be noted.

From all the Figures in all composition samples, one can observe a broad band centered at around 3300 cm^{-1} assigned to the fundamental stretching vibration of free or bonded hydroxyl groups belonging to adsorbed water. The peak occurred at about 1630 cm^{-1} was indexed to the O-H bending vibration of chemically adsorbed water [164,165,166,167,168].

The spectrum is characterized by a dominant band at 1051 cm^{-1} with a shoulder at 1130 cm^{-1}, and the band at ~795 cm^{-1} is assigned to longitudinal optical mode asymmetric stretching vibrations of the Si-O-Si, the shoulder is attributed to the transverse optical mode of the asymmetric stretching of Si–O–Si bonds, and symmetric stretching vibration of the Si-O-Si, respectively [167,169,170]. The band at 935 cm^{-1} is attributed to the stretching

mode of Si– OH or SiO^- groups [171], but in mixed materials, it is superimposed onto the band of the Si–O–Ti stretching mode confirming the linkage in TiO_2-SiO_2 material [171,172,173,164,174]. This particular bond plays an important role in the photocatalytic activity of TiO_2-SiO_2 compounds [150].

The spectral features of TiO_2 can be discerned at around 553 cm^{-1} and 446 cm^{-1}. The characteristic peaks of TiO_2 (553 cm^{-1} and 446 cm^{-1}) are attributed to Ti-O and Ti-O-Ti bonds [175, 176].

The addition of iron is shown by the peak of the ν Fe-O vibration band at ~ 420 cm^{-1} which is present only for sample with $Fe(NO_3)_3$[177].

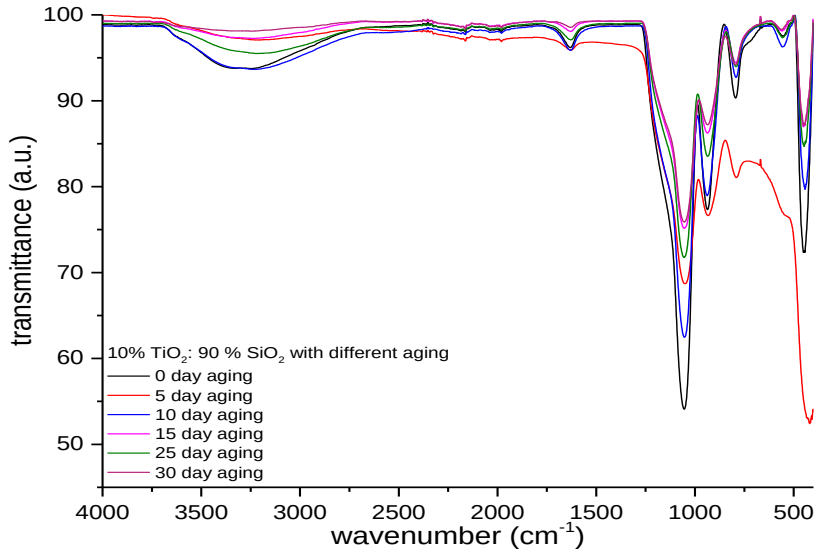

Figure 5-29: FT-IR spectrum of the (10% TiO_2-90% SiO_2) with different aging time

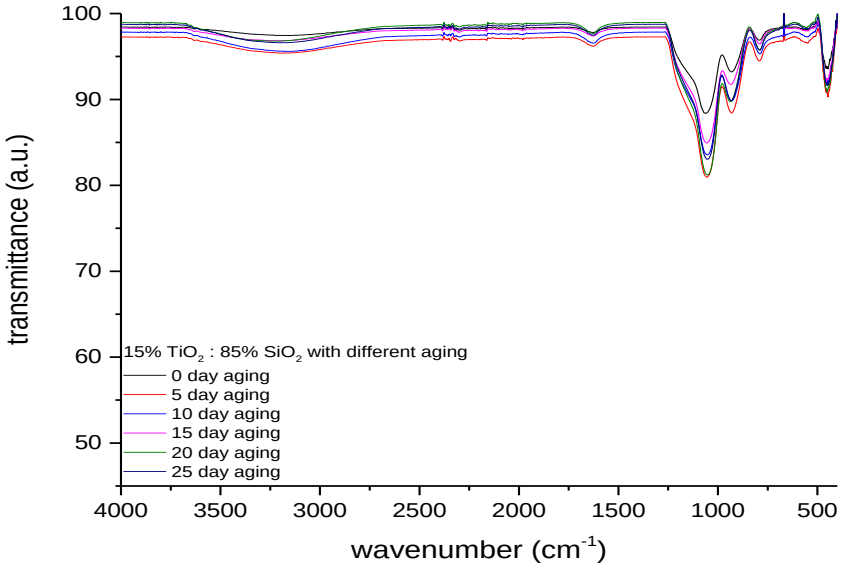

Figure 5-30: FT-IR spectrum of the (15% TiO_2-85% SiO_2) with different aging time

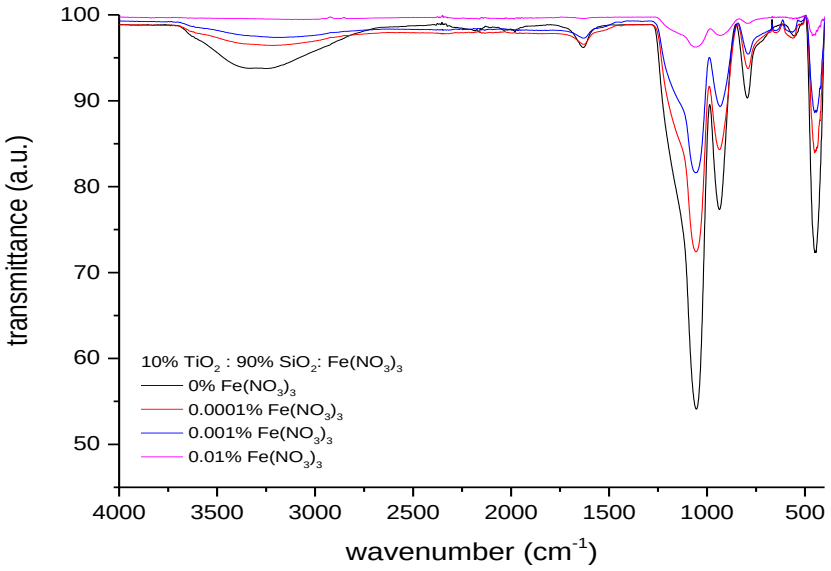

Figure 5-31: FT-IR spectra of Fe-Doped (10% TiO_2-90% SiO_2) with different Iron percentage

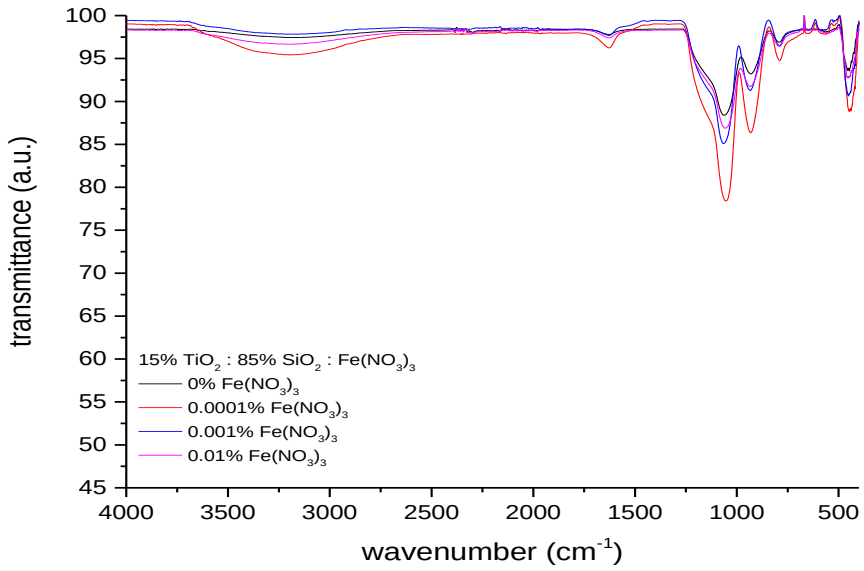

Figure 5-32: FT-IR spectra of Fe-Doped (15% TiO_2-85% SiO_2) with different Iron percentage

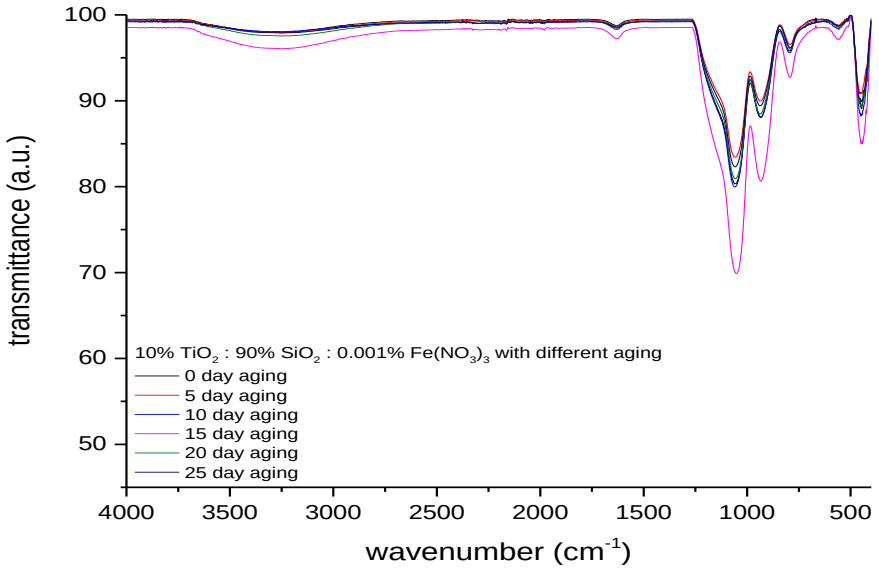

Figure 5-33: FT-IR spectra of Fe-Doped (10% TiO_2-90% SiO_2) with different aging time

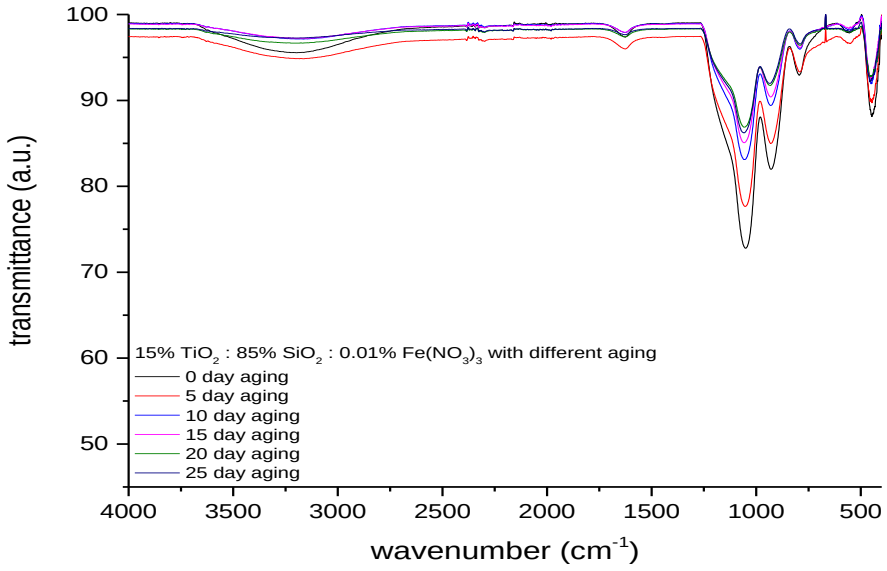

Figure 5-34: FT-IR spectra of Fe-Doped (15% TiO_2-85% SiO_2) with different aging time

Table 5-3: Peak Assignments of FT-IR Spectra for the (10% TiO_2-90% SiO_2) with different aging time

Peaks(cm^{-1})	(10% TiO2 – 90% SiO2) with different aged Days							
	0	5	10	15	20	25	Assignments	Ref.
	447	447	447	447	447	447	ν_s Ti-O-Ti	150,176
	552	552	552	552	552	552	ν Ti-O	150,176
	790	790	790	790	790	790	ν_s Si-O-Si	167,169,170
	935	935	935	935	935	935	νSi-OH and νSi-O-Ti	171,172,173,164,174,150
	1055	1055	1055	1055	1055	1055	ν_{as} Si-O-Si (LO Mode)	167,169,170
	1130	1130	1130	1125	1125	1125	ν_{as} Si-O-Si (TO Mode)	167,169,170
	1630	1630	1630	1630	1630	1630	δ HOH	164,165,166,159,168
	3290	3290	3290	3290	3290	3290	Structural OH^-	164,165,166,159,168

ν, stretching vibration; ν_s, symmetric stretching vibration; ν_{as}, antisymmetric stretching vibration; δ, deformation vibration; LO, longitudinal optical; TO, transversal optical.

Table 5-4: Peak Assignments of FT-IR Spectra for the (15% TiO_2-85% SiO_2) with different aging time

	(15% TiO_2 – 85% SiO_2) with different aged							
	Days							
Peaks(cm^{-1})	0	5	10	15	20	25	Assignments	Ref.
	447	447	447	447	447	447	ν_s Ti-O-Ti	150,176
	552	552	552	552	552	552	ν Ti-O	150,176
	790	790	790	790	790	790	ν_s Si-O-Si	167,169,170
	935	935	935	935	935	935	νSi-OH and νSi-O-Ti	171,172,173,164,174,150
	1055	1055	1055	1055	1055	1055	ν_{as} Si-O-Si (LO Mode)	167,169,170
	1130	1130	1130	1125	1125	1125	ν_{as} Si-O-Si (TO Mode)	167,169,170
	1630	1630	1630	1630	1630	1630	δ HOH	164,165,166,159,168
	3270	3270	3290	3270	3270	3270	Structural OH^-	164,165,166,159,168

ν, stretching vibration; ν_s, symmetric stretching vibration; ν_{as}, antisymmetric stretching vibration; δ, deformation vibration; LO, longitudinal optical; TO, transversal optical.

Table 5-5: Peak Assignments of FT-IR Spectra for Fe-Doped (10% TiO_2-90% SiO_2) with different Iron percentage

	Doped Fe- (10% TiO2 – 90% SiO2)						
Peaks(cm^{-1})	0% Fe	0.0001% Fe	0.001 Fe	0.01 Fe	Assignments	Ref.	
	447	447	447	447	ν_s Ti-O-Ti	150,176	
	-	422	422	422	ν Fe-O	177	
	525	559	566	566	ν Ti-O	150,176	
	790	790	790	790	ν_s Si-O-Si	167,169,170	
	935	935	935	935	νSi-OH and νSi-O-Ti	171,172,173,164,174,150	
	1055	1055	1056	1056	ν_{as} Si-O-Si (LO Mode)	167,169,170	
	1130	1125	1125	1125	ν_{as} Si-O-Si (TO Mode)	167,169,170	
	1630	1627	1627	1627	δ HOH	164,165,166,159,168	
	3290	3290	3290	3290	Structural OH^-	164,165,166,159,168	

ν, stretching vibration; ν_s, symmetric stretching vibration; ν_{as}, antisymmetric stretching vibration; δ, deformation vibration; LO, longitudinal optical; TO, transversal optical.

Table 5-6: Peak Assignments of FT-IR Spectra for Fe-Doped (15% TiO_2-85% SiO_2) with different Iron percentage

	Doped Fe- (15% TiO2 – 85% SiO2)						
	0% Fe	0.0001% Fe	0.001 Fe	0.01 Fe	Assignments	Ref.	
Peaks(cm^{-1})	447	447	447	447	ν_s Ti-O-Ti	150,176	
	-	422	422	422	ν Fe-O	177	
	555	550	566	566	ν Ti-O	153,181	
	790	790	790	790	ν_s Si-O-Si	167,169,170	
	940	935	935	935	νSi-OH and νSi-O-Ti	171,172,173,164,174,150	
	1055	1055	1056	1056	ν_{as} Si-O-Si (LO Mode)	167,169,170	
	1130	1124	1124	1125	ν_{as} Si-O-Si (TO Mode)	167,169,170	
	1630	1627	1627	1627	δ HOH	164,165,166,159,168	
	3300	3295	3295	3295	Structural OH^-	164,165,166,159,168	

ν, stretching vibration; ν_s, symmetric stretching vibration; ν_{as}, antisymmetric stretching vibration; δ, deformation vibration; LO, longitudinal optical; TO, transversal optical.

Table 5-7: Peak Assignments of FT-IR Spectra for Fe-Doped (10% TiO_2-90% SiO_2) with different aging time

Peaks(cm^{-1})	Doped Fe (10% TiO_2 – 90% SiO_2) with different aged							
	Days							
	0	5	10	15	20	25	Assignments	Ref.
	450	450	450	447	447	447	ν_s Ti-O-Ti	150,176
	430	430	425	425	425	425	ν Fe-O	177
	552	552	552	552	552	552	ν Ti-O	153,181
	790	790	790	790	790	790	ν_s Si-O-Si	167,169,170
	935	935	935	935	935	935	νSi-OH and νSi-O-Ti	171,172,173,164,174,150
	1055	1055	1055	1055	1055	1055	ν_{as} Si-O-Si (LO Mode)	167,169,170
	1130	1130	1130	1125	1125	1125	ν_{as} Si-O-Si (TO Mode)	167,169,170
	1630	1630	1629	1629	1629	1629	δ HOH	164,165,166,159,168
	3290	3290	3290	3290	3290	3290	Structural OH^-	164,165,166,159,168

ν, stretching vibration; ν_s, symmetric stretching vibration; ν_{as}, antisymmetric stretching vibration; δ, deformation vibration; LO, longitudinal optical; TO, transversal optical.

Table 5-8: Peak Assignments of FT-IR Spectra for Fe-Doped (15% TiO_2-85% SiO_2) with different aging time

	Doped Fe (15% TiO_2 – 85% SiO_2) with different aged							
	Days							
Peaks(cm^{-1})	0	5	10	15	20	25	Assignments	Ref.
	447	447	447	447	447	447	ν_s Ti-O-Ti	150,176
	419	419	419	419	419	419	ν Fe-O	177
	552	552	552	552	552	552	ν Ti-O	153,181
	790	790	790	790	790	790	ν_s Si-O-Si	167,169,170
	935	935	935	935	935	935	νSi-OH and νSi-O-Ti	171,172,173,164,174,150
	1055	1055	1055	1055	1055	1055	ν_{as} Si-O-Si (LO Mode)	167,169,170
	1130	1130	1130	1125	1125	1125	ν_{as} Si-O-Si (TO Mode)	167,169,170
	1627	1627	1626	1626	1626	1626	δ HOH	164,165,166,159,168
	3200	3200	3200	3200	3200	3200	Structural OH^-	164,165,166,159,168

ν, stretching vibration; ν_s, symmetric stretching vibration; ν_{as}, antisymmetric stretching vibration; δ, deformation vibration; LO, longitudinal optical; TO, transversal optical.

Chapter Six

Conclusions and Future Work

6.1. Conclusions

The sol-gel preparation of coatings from titania-silica and Fe-doped titania-silica has been studied. The coatings have been evaluated for functional applications. The TiO_2-SiO_2 sol was prepared from the titanium (IV) butoxide $Ti(OCH_2CH_2CH_2CH_3)_4$, and tetraethylorthosilicate (TEOS), [Si $(OC_2H_5)_4$]. The processes involved in the fabrication of sol-gel derived thin films.

Physical and chemical characterization of the thin films are discussed. A range of techniques such as UV-Visible spectroscopy, Scanning Electron Microscopy (SEM), X-ray diffraction (XRD), and Fourier transform infrared spectroscopy (FTIR) were used to determine parameters such as transmittance, the thickness of films, the presence or absence of crystals, and molecular structure.

Stable, transparent, colorless and crack-free coatings were obtained by using the dip coating technique with heating to 100 C° for 24hrs. Without heating, the films are cracked. Coatings dried at lower temperatures have better transmittance in the visible region comparing to those dried at a higher temperature. A clean and uncoated glass slide was used as the reference when measuring transmittance. As expected, the transmittance of the bare glass slide was ~ 97% in the wavelength range of 300-800.

According to the method of thin film preparation, the thickness increased with the number of dip-coating cycles. The transmittance decreased with increasing the number of

cycles for dip coating. The results of transmittance measurements are in accord with the film-thickness measurement results. This observation can be explained according to the Beer-Lambert law. In addition, the reduction of transmittance was due to light scattering from surface roughness and crystal size.

The transmission spectra for thin films with 1 and 3 dip-coatings of 3% TiO_2-97% SiO_2, 5% TiO_2-95% SiO_2 and 7.9% TiO_2-92.1% SiO_2 with solution age 0, 5, 15, and 25 days showed significant differences in transmittance behavior, especially between 3 layer samples, compared to 1 layer. These differences were in the spectral regions 350-450nm, and 650-750nm. This is attributed to constructive interference, since the constructive and destructive interference is more obvious in thin films with a large thickness. The transmittance after 3 layers was decreased, meaning that 1 layer was better for transmission, for the compositions with less than 10% TiO_2.

The transmission spectra for thin films with 1 and 3 dip-coatings of 10% TiO_2 - 90% SiO_2 and 15% TiO_2-85% SiO_2 with solution age 0, 5, 15, and 25 days showed that the transmittance behavior of the 1 layer sample at the age solution 0 days was higher in the spectral region 400-600nm. Since the peak of the solar radiation spectrum lies in this important spectral region, the optical performance of these samples is promising. These samples with greater than TiO_2 were studied further.

When $Fe(NO_3)_3$ is mixed into the sols, the nitrate is dissociated and the sols contain Fe^{3+} ions. If any particles remain after this dissolution, they are in the form of iron hydroxides. The absorption in the transmission spectra by the Fe^{3+} ions is apparent in all but the lowest amounts. Transmission spectra for different weight amounts of $Fe(NO_3)_3$

dopant showed that the film with the lowest weight amount 0.0001 % exhibited higher transmittance in the spectral region 450nm-550nm. This dopant amount has little absorption. As the weight amount of $Fe(NO_3)_3$ increased the absorption became obvious, so that the transmittance decreased. In addition, a greater amount of iron content resulted in agglomeration of iron clusters. When the weight amount of $Fe(NO_3)_3$ increased reaching 0.01%, the transmittance was reduced. Particles of FeOOH or $Fe(OH)_3$ contributed to scattering and reflectance in the visible spectral region. Thus, the lowestweight amount 0.0001 % of $Fe(NO_3)_3$ is the preferred level for transparency.

The transmittance of the as-deposited films at 0 days aged solution for 1 or 3 layer samples is higher than that the transmittance of the films with the 25 days aged solution. An increase of solution age decreases the transmittance of the films. The sol becomes thicker than the original sol. So the age of the solution should be kept as low as possible in order to maintain the high transmittance.

The thickness of thin films with 1 and 3 coatings was measured before and after aging the solution. The results of the film-thickness measurements support the trends in the transmittance measurements.

According to XRD analysis, the gels are amorphous. No characteristic crystalline peaks are observed. The absence of diffraction peaks for low amounts of TiO_2 indicates that the TiO_2-SiO_2 films are amorphous. It was found also that the Fe/TiO_2-SiO_2 films are amorphous and there is no sign of anatase or rutile or brookite. These results are promising for photocatalytic activity.

In the FT-IR analysis, spectra of all samples look similar. Hydroxyl groups were observed in all samples at around 3300 cm^{-1} and at about 1630 cm^{-1}. Siloxane bonds were also detected at different wavenumbers 1051, 1130, and 795 cm^{-1}. The spectral features of TiO_2 can be discerned at around 553 cm^{-1} and 446 cm^{-1}. The characteristic peaks of titania 553 cm^{-1} and 446 cm^{-1} are attributed to Ti-O and Ti-O-Ti bonds. The addition of iron can leads to the ν Fe-O vibration band at ~ 420 cm^{-1}, which appears distinctly only for sampleswith $Fe(NO_3)_3$. Finally, the linkage between TiO_2-SiO_2 was confirmed by the band at 935 cm-1 which is attributed to the Si-O-Ti stretching mode. This bond is said to play an important role in the photocatalytic activity of TiO_2-SiO_2 compounds.

6.2. Suggestions for Future Work

Some further work that could improve the understanding of these samples is given. To have a better understanding of the surface area and microstructure, further examination of the surface topography and surface roughness of the samples by atomic force microscope (AFM) and examination of the morphology of the samples by scanning electron microscopy (SEM) can be performed. This information will help to understand the optical transmission. Since transmission is the light that goes through the samples after accounting for absorption and reflection, the surface can be modified to increase transmission.

The surface roughness can be changed by using a different method of coating such as spin coating, instead of dip coating. Also, other precursors besides TEOS such as TMOS or mixtures of them with TiO_2 can be used to produce coatings with different roughnesses.

Finally, different substrates such as indium tin oxide (ITO) glass and silicon wafer may give different optical properties.

The original choice of TiO_2-SiO_2 coatings was to study the self-cleaning properties. Now that a method to produce the coatings has been studied, actual tests of the self-cleaning should be performed. One aspect that is important is the surface energy, which can be evaluated by measuring the contact angle of a water droplet placed on the surface of the prepared films. Then the photocatalytic activity can be tested using methylene blue dye as a pollutant model. Also, a study of the photo-oxidation power of the films by using several UV lamps to determine the appropriate wavelength for this process should be carried out, possibly using a different metal than Fe, such as Ag. Finally, for practical application, a study of the mechanical properties including adhesion, abrasion and resistance, hardness, and scratch resistance should be performed.

References

1. K. Chopra and I. Kaur. "Thin film Devices and Their Applications," (1983).

2. A. Elshabini, A.A. Elshabini-Riad and F.D. Barlow. *Thin film technology handbook;* McGraw-Hill Professional, 1998.

3. E. Wicke, J. R. Anderson, M. Boudart (Eds.): Catalysis, Science and Technology, Vol. 1-2, 1981; Springer Verlag, Berlin,

4. D. Talbot and J. Talbot. "Corrosion Science and Technology," (2007).

5. M.J. Madou and S.R. Morrison. *Chemical sensing with solid state devices;* Elsevier, 2012.

6. M. Ohring, S. Zarrabian and A. Grogan. "The materials science of thin films," Appl. Opt., **31,** 7162 (1992).

7. H. Tai-Ran, "MEMS & microsystems: design and manufacture," Mechanical Engineering Series, (2002).

8. H. Pulker and H. Pulker. *Coatings on glass;* Elsevier, 1999.

9. D. Glocker and S. Shah. *Handbook of Thin Film Process Technology*, IOP, 1995.

10. W.R. Grove, "LXXIX. On the electro-chemical polarity of gases," Philosophical Magazine **4,** 498-514 (1852).

11. W. Bryant, "The fundamentals of chemical vapor deposition" J. Mater. Sci. **12,** 1285-306 (1977).

12. R. Ghoshtagore, "Mechanism of CVD thin film SnO_2 formation" J. Electrochem. Soc. **125** 110-7 (1978).

13. H. Schroder, "Physics of Thin Films: Advances in Research and Developments 5, G. Hass and RE Thun (eds.) (1969).

14. Y. Jun, J. Choi and J. Cheon. "Shape control of semiconductor and metal oxide nanocrystals through nonhydrolytic colloidal routes," Angewandte Chemie International Edition **45** 3414-39 (2006).

15. J. Park, E. Lee, N. Hwang, et al. "One-nanometer-scale size-controlled synthesis of monodisperse magnetic Iron oxide nanoparticles," Angewandte Chemie, **117** 2932-7 (2005).

16. S.G. Kwon and T. Hyeon. "Colloidal chemical synthesis and formation kinetics of uniformly sized nanocrystals of metals, oxides, and chalcogenides" Acc. Chem. Res. **41** 1696-709 (2008).

17. J. Dutta, P. Roubeau, T. Emeraud, et al. "Application of pyrosol deposition process for large-area deposition of fluorine-doped tin dioxide thin films," Thin Solid Films **239** 150-5 (1994).

18. R. Chamberlin and J. Skarman. "Chemical spray deposition process for inorganic films" J. Electrochem. Soc. **113** 86-9 (1966).

19. J.B. Mooney and S.B. Radding. "Spray pyrolysis processing" Annual Review of Materials Science **12** 81-101 (1982).

20. B. Pamplin, "Spray pyrolysis of ternary and quaternary solar cell materials" Progress in Crystal Growth and Characterization **1** 395-403 (1979).

21. M. Tomar and F. Garcia. "Spray pyrolysis in solar cells and gas sensors," Progress in Crystal Growth and Characterization **4** 221-48 (1981).

22. D. Albin and S. Risbud. "Spray pyrolysis processing of optoelectronic materials," Advanced Ceramic Materials **2** (1987).

23. J. Ebelman, "Mémoire sur de nouvelles combinaisons de l'acide borique avec les éthers, et sur l'éther sulfureux," **57** 331 (1846).

24. A. Cossa, "Sull'Amalgama dell'Alluminio (On the Amalgam of Aluminum)," Il Nuovo Cimento, **3** 228 (1870).

25. L.C. Klein (ed.), *Sol-gel technology for thin films, fibers, preforms, electronics, and specialty shapes*; William Andrew Publishing, 1988.

26. C. J. Brinker, A. Hurd, G. Frye, K. Ward and C. Ashley. "Sol-gel thin film formation," J. Non Cryst. Solids **121** 294-302 (1990).

27. C. J. Brinker, A. Hurd, P. Schunk, G. Frye and C. Ashley. "Review of sol-gel thin film formation," J. Non Cryst. Solids **147** 424-36 (1992).

28. C.J. Brinker and George W. Scherer. Sol-gel science: the physics and chemistry of sol-gel processing pp. 908. Academic Press, San Diego, 1990.

29. L.C. Klein, "Sol-gel coatings," in *Thin Film Processes.* Elsevier, 1991 pp. 501-22.

30. X. Chen and S.S. Mao. "Titanium dioxide nanomaterials: synthesis, properties, modifications, and applications," Chem. Rev. **107** 2891-959 (2007).

31. A. Fujishima, X. Zhang and D.A. Tryk. "TiO_2 photocatalysis and related surface phenomena," Surface Science Reports **63** 515-82 (2008).

32. B.D. Fabes, B.J. Zelinski and D.R. Uhlmann. "Sol-gel derived ceramic coatings," Ceramic films and coatings, 224-75 (1993).

33. C. J. Brinker, G. Frye, A. Hurd and C. Ashley. "Fundamentals of sol-gel dip coating," Thin Solid Films **201** 97-108 (1991).

34. J. Lannutti and D. Clark. "Sol-Gel Derived Ceramic-Ceramic Composites Using Short Fibers," MRS Online Proceedings Library Archive **32** (1984).

35. C.J. Brinker and A.J. Hurd. "Fundamentals of sol-gel dip-coating," Journal de Physique III **4** 1231-42 (1994).

36. I. Strawbridge and P. James. "The factors affecting the thickness of sol-gel derived silica coatings prepared by dipping," J. Non Cryst. Solids **86** 381-93 (1986).

37. L. Landau and B. Levich. "Dragging of a liquid by a moving plate" Acta Phys.-Chim. URSS **17** 42-54 (1942).

38. L. Scriven, "Physics and applications of dip coating and spin coating," MRS Online Proceedings Library Archive **121,** (1988).

39. C. Lawrence, "The mechanics of spin coating of polymer films," The Physics of Fluids **31** 2786-95 (1988).

40. D. Meyerhofer, "Characteristics of resist films produced by spinning," J. Appl. Phys. **49** 3993-7 (1978).

41. S. Hellstrom, "Basic models of spin coating," Submitted as coursework for Physics **210** (2007) http://large.stanford.edu/courses/2007/ph210/hellstrom1/

42. T. Kyratsi, K. Chrissafis, J. Wachter, K.M. Paraskevopoulos and M.G. Kanatzidis. "KSb_5S_8: A Wide Bandgap Phase-Change Material for Ultra High Density Rewritable Information Storage," Adv Mater **15** 1428-31 (2003).

43. Y. Kim, A. DiVenere, G.K. Wong, J. Ketterson, S. Cho and J.R. Meyer. "Structural and thermoelectric transport properties of Sb 2 Te 3 thin films grown by molecular beam epitaxy," J. Appl. Phys. **91** 715-8 (2002).

44. J. Britt and C. Ferekides. "Thin-film CdS/CdTe solar cell with 15.8% efficiency," Appl. Phys. Lett. **62** 2851-2 (1993).

45. J. D. Mackenzie, "Sol-gel optics," Journal of the Ceramic Society of Japan **101** 1-10 (1993).

46. M. Nogami in "Sol–Gel Optics: Processing and Applications," L.C. Klein (ed.) Kluwer Academic, Hingham, MA, (1994).

47. L. Klein and G. Garvey. "Kinetics of the sol/gel transition," J. Non Cryst. Solids **38** 45-50 (1980).

48. B. E. Yoldas, "Introduction and effect of structural variations in inorganic polymers and glass networks," J. Non Cryst. Solids **51** 105-21 (1982).

49. M. Schraml-Marth, K. Walther, A. Wokaun, B. Handy and A. Baiker. "Porous silica gels and TiO_2/SiO_2 mixed oxides prepared via the sol-gel process: characterization by spectroscopic techniques," J. Non Cryst. Solids **143** 93-111 (1992).

50. F. Brunet and B. Cabane. "Populations of oligomers in sol-gel condensation," J. Non Cryst. Solids **163** 211-25 (1993).

51. A. Rampaul, I.P. Parkin, S.A. O'Neill, J. DeSouza, A. Mills and N. Elliott. "Titania and tungsten doped titania thin films on glass; active photocatalysts," Polyhedron **22** 35-44 (2003).

52. U. Diebold, "The surface science of titanium dioxide," Surface Science Reports **48** 53-229 (2003).

53. A. Czanderna, C.R. Rao and J. Honig. "The anatase-rutile transition. Part 1.—Kinetics of the transformation of pure anatase," Transactions of the Faraday Society **54** 1069-73 (1958).

54. B. Grzmil, B. Kic and M. Rabe. "Inhibition of the anatase-rutile phase transformation with addition of K_2O, P_2O_5, and Li_2O," Chem. Pap. **58** 410-4 (2004).

55. S. Mo and W. Ching. "Electronic and optical properties of three phases of titanium dioxide: Rutile, anatase, and brookite," Physical Review B **51** 13023 (1995).

56. K. I. Hadjiivanov and D.G. Klissurski. "Surface chemistry of titania (anatase) and titania-supported catalysts," Chem. Soc. Rev. **25** 61-9 (1996).

57. O. Carp, C.L. Huisman and A. Reller. "Photoinduced reactivity of titanium dioxide," Progress in Solid State Chemistry **32** 33-177 (2004).

58. K. Tanaka, M.F. Capule and T. Hisanaga. "Effect of crystallinity of TiO_2 on its photocatalytic action," Chemical Physics Letters **187** 73-6 (1991).

59. G. Li, L. Chen, M.E. Graham and K.A. Gray. "A comparison of mixed phase titania photocatalysts prepared by physical and chemical methods: the importance of the solid–solid interface," Journal of Molecular Catalysis A: Chemical **275** 30-5 (2007).

60. N.T. Nolan, "Sol-Gel Synthesis and Characterisation of Novel Metal Oxide Nanomaterials for Photocatalytic Applications," Doctoral Thesis, Dublin Institute of Technology (2010).

61. R. Benedix, F. Dehn, J. Quaas and M. Orgass. "Application of titanium dioxide photocatalysis to create self-cleaning building materials," Lacer **5** 157-68 (2000).

62. X. Li and F. Li. "Study of Au/Au^{3+}-TiO_2 photocatalysts toward visible photooxidation for water and wastewater treatment," Environ. Sci. Technol. **35** 2381-7 (2001).

63. K.P. Kumar, K. Keizer and A.J. Burggraaf. "Textural evolution and phase transformation in titania membranes: Part 1.—Unsupported membranes," Journal of Materials Chemistry **3** 1141-9 (1993).

64. B. O'Regan and M. Grätzel. "A low-cost, high-efficiency solar cell based on dye-sensitized colloidal TiO_2 films," Nature **353** 737 (1991).

65. A. Fujishima, T.N. Rao and D.A. Tryk. "Titanium dioxide photocatalysis," Journal of Photochemistry and Photobiology C: Photochemistry Reviews **1** 1-21 (2000).

66. K. Hashimoto, H. Irie and A. Fujishima. "TiO_2 photocatalysis: a historical overview and future prospects," Japanese Journal of Applied Physics **44** 8269 (2005).

67. Y. Guo, Y. Hu and J. Maier. "Synthesis of hierarchically mesoporous anatase spheres and their application in lithium batteries," Chemical Communications, 2783-5 (2006).

68. E. Da Costa, C. Avellaneda and A. Pawlicka. "Alternative Nb_2O_5-TiO_2 thin films for electrochromic devices," J. Mater. Sci. **36** 1407-10 (2001).

69. S. Yamazaki, S. Matsunaga and K. Hori. "Photocatalytic degradation of trichloroethylene in water using TiO_2 pellets," Water Res. **35** 1022-8 (2001).

70. L. L. Hench and J.K. West. "The sol-gel process," Chem. Rev. **90** 33-72 (1990).

71. K. Unger, "Porous Silica (Journal of Chromatography Library, Vol. 16)," Elsevier (1979).

72. E. Pope and J. Mackenzie. "Sol-gel processing of silica: II. The role of the catalyst," J. Non Cryst. Solids **87** 185-98 (1986).

73. B. E. Yoldas, "Monolithic glass formation by chemical polymerization," J. Mater. Sci. **14** 1843-9 (1979).

74. E. Matijevic, "Monodispersed colloids: art and science," Langmuir **2** 12-20 (1986).

75. C. J. Brinker and S. Mukherjee. "Conversion of monolithic gels to glasses in a multicomponent silicate glass system," J. Mater. Sci. **16** 1980-8 (1981).

76. M. Dubois and B. Cabane. "Light-scattering study of the sol-gel transition in silicon tetraethoxide," Macromolecules **22** 2526-33 (1989).

77. R.J. Davis and Z. Liu. "Titania−silica: a model binary oxide catalyst system," Chemistry of Materials **9** 2311-24 (1997).

78. J. Calvino, M. Cauqui, G. Cifredo, et al. "Ultrasound as a tool for the preparation of gels: effect on the textural properties of TiO_2-SiO_2 aerogels," J. Mater. Sci. **28** 2191-5 (1993).

79. S. Gontier and A. Tuel. "Synthesis and characterization of Ti-containing mesoporous silicas," Zeolites **15** 601-10 (1995).

80. M. Kruk, M. Jaroniec and A. Sayari. "Structural and surface properties of siliceous and titanium-modified HMS molecular sieves," Microporous Materials **9** 173-82 (1997).

81. M. Cauqui and J. Rodriguez-Izquierdo. "Application of the sol-gel methods to catalyst preparation," J. Non Cryst. Solids **147** 724-38 (1992).

82. M.M. Haridas, S. Datta and J.R. Bellare. "Time and temperature based gellability zones in modified titanium alkoxide sols," Ceram. Int. **25** 601-6 (1999).

83. X. Gao and I.E. Wachs. "Titania–silica as catalysts: molecular structural characteristics and physico-chemical properties," Catalysis Today **51** 233-54 (1999).

84. T. Kamegawa, Y. Masuda, N. Suzuki, Y. Horiuchi and H. Yamashita. "Design of Single-Site Ti Embedded Highly Hydrophilic Silica Thin Films with Macro–Mesoporous Structures," ACS Applied Materials & Interfaces **3** 4561-5 (2011).

85. G. Xu, Z. Zheng, Y. Wu and N. Feng. "Effect of silica on the microstructure and photocatalytic properties of titania," Ceram. Int. **35** 1-5 (2009).

86. D. Lee and S. Choi. "Preparation of photocatalytic TiO_2−SiO_2 thin film by sol-gel coating," Metals and Materials International **10** 357-60 (2004).

87. G. Copley, A. Redmond and B. Yates. "Influence of titania upon thermal expansion of vitreous silica," Physics and Chemistry of Glasses **14** 73-6 (1973).

88. I. Salvado and J. Navarro. "Titania-silica glasses prepared by the alkoxide route" J. Non-Cryst. Solids **147&148** 256 (1992).

89. A. Alvarez-Herrero, G. Ramos, F. Del Monte, E. Bernabeu and D. Levy. "Water adsorption in porous TiO_2–SiO_2 sol–gel films analyzed by spectroscopic ellipsometry," Thin Solid Films **455** 356-60 (2004).

90. R. M. Almeida, X. M. Du, D. Barbier and X. Orignac. "Er^{3+}-doped multicomponent silicate glass planar waveguides prepared by sol-gel processing," J. Sol Gel Sci. Technol. **14** 209-16 (1999).

91. N. Carmona, M. Villegas and J. F. Navarro. "Protective silica thin coatings for historical glasses," Thin Solid Films **458** 121-8 (2004).

92. G. Helsch, E. Rädlein and G. Frischat. "On the origin of the aging process of porous SiO_2 antireflection coatings," J. Non Cryst. Solids **265** 193-7 (2000).

93. Y. Xu, W. Zheng and W. Liu. "Enhanced photocatalytic activity of supported TiO_2: dispersing effect of SiO_2," J. Photochem. Photobiol. A. **122** 57-60 (1999).

94. C. H. Kwon, H. Shin, J. H. Kim, W. S. Choi and K .H. Yoon. "Degradation of methylene blue via photocatalysis of titanium dioxide," Mater. Chem. Phys. **86** 78-82 (2004).

95. Z. Wu, D. Lee, M. F. Rubner and R. E. Cohen. "Structural color in porous, superhydrophilic, and self-cleaning SiO_2/TiO_2 Bragg stacks," Small **3** 1445-51 (2007).

96. K. Guan, "Relationship between photocatalytic activity, hydrophilicity and self-cleaning effect of TiO_2/SiO_2 films," Surface and Coatings Technology **191** 155-60 (2005).

97. F. Ghodsi, F. Tepehan and G. Tepehan. "Influence of pH on the optical and structural properties of spin coated CeO_2–TiO_2 thin films prepared by sol–gel process," Surf. Sci. **601** 4497-501 (2007).

98. S. Lien, D. Wuu, W. Yeh and J. Liu. "Tri-layer antireflection coatings (SiO_2/SiO_2–TiO_2/TiO_2) for silicon solar cells using a sol–gel technique," Solar Energy Mater. and Solar Cells **90** 2710-9 (2006).

99. X. Wang, G. Wu, B. Zhou and J. Shen. "Thermal annealing effect on optical properties of binary TiO_2-SiO_2 sol-gel coatings," Materials **6** 76-84 (2012).

100. P. Klankaw, C. Chawengkijwanich, N. Grisdanurak and S. Chiarakorn. "The hybrid photocatalyst of TiO_2–SiO_2 thin film prepared from rice husk silica," Superlattices and Microstructures **51** 343-52 (2012).

101. Z. Jiwei, Y. Xi and Z. Liangying. "Characterization and optical propagation loss of sol-gel derived TiO_2/SiO_2 films," J. Phys. D **33** 3013 (2000).

102. M. Galan-Fereres, L.J. Alemany, R. Mariscal, M.A. Banares, J.A. Anderson and J.L. Fierro. "Surface acidity and properties of titania-silica catalysts," Chemistry of Materials **7** 1342-8 (1995).

103. A.P. Gerola, J. Semensato, D.S. Pellosi, et al. "Chemical determination of singlet oxygen from photosensitizers illuminated with LED: new calculation methodology considering the influence of photobleaching," J. Photochem. Photobiol. A. **232** 14-21 (2012).

104. I. Rodrigues and J. Sanches. "Photoblinking/photobleaching differential equation model for intensity decay of fluorescence microscopy images," IEEE Int. Symp. Biomedical Imaging 1265-8 (2010).

105. A. Hopt and E. Neher. "Highly nonlinear photodamage in two-photon fluorescence microscopy," Biophys. J. **80** 2029-36 (2001).

106. J. Widengren and R. Rigler. "Mechanisms of photobleaching investigated by fluorescence correlation spectroscopy," Bioimaging **4** 149-57 (1996).

107. F. Müller, *Numerical simulations of fluorescence recovery after photobleaching experiments;* https://code.google.com/archive/p/frap-quant/ , 2005.

108. M. Ebelman, "Untersuchungen uber die Verbindung der Borsaure und Kieselsaure mit Aether.," Annales de Chimie et de Physique, **57** 319-355 (1846).

109. W. Geffcken and E. Berger. "Verfahren zur änderung des reflexionsvermögens optischer gläser," Deutsches Reichspatent, assigned to Jenaer Glaswerk Schott & Gen., Jena, **736,** 411 (1939).

110. R. Roy and E. Osborn. "The system Al_2O_3-SiO_2-H_2O" Am.Mineralogist **39** 853-86 (1954).

111. D. M. Roy and R. Roy. "An experimental study of the formation and properties of synthetic serpentines and related layer silicate minerals," Am. Mineral. **39** 957-75 (1954).

112. R. Roy, "Aids in hydrothermal experimentation: II, Methods of making mixtures for both “dry” and “wet” phase equilibrium studies," J Am Ceram Soc, **39** 145-6 (1956).

113. H. Schroeder, "Properties and applications of oxide layers deposited on glass from organic solutions," Opt. Acta **9** 249-54 (1962).

114. H. Schroeder, "Oxide layers deposited from organic solutions," Physics of Thin Films **5** 87-141 (1969).

115. W. Stöber, A. Fink and E. Bohn. "Controlled growth of monodisperse silica spheres in the micron size range," J. Colloid Interface Sci. **26** 62-9 (1968).

116. V. Chiola, J. Ritsko and C. Vanderpool. Process for producing low-bulk density silica, US Patent 3,556,725, January 19, 1971

117. H. Dislich, "New routes to multicomponent oxide glasses," Angewandte Chemie International Edition **10** 363-70 (1971).

118. H. Schroeder, and G. Gliemeroth. Method for producing glass compositions. U.S. Patent 3,597,252; August 3, 1971.

119. H. Dislich, P. Hinz, and R. Kaufmann, Process for the Manufacture of Multicomponent substances. U.S. Patent 3,759,683; Sept. 18, 1973.

120. L. Levene and I.M. Thomas. Process of converting metalorganic compounds and high purity products obtained therefrom, US Patent 3,640 093; February 8, 1972.

121. G.L. Wilkes, "Ceramers: Hybrid Materials Incorporating Polymeric/Oligomeric Species into Inorganic Glasses Utilizing a Sol-Gel Approach," Polym.Prepr. **26** 300-1 (1985).

122. H. Schmidt, "New type of non-crystalline solids between inorganic and organic materials," J. Non Cryst. Solids, **73** 681-91 (1985).

123. G. Philipp and H. Schmidt. "New materials for contact lenses prepared from Si- and Ti-alkoxides by the sol-gel process," J. Non Cryst. Solids **63** 283-92 (1984).

124. L.L. Hench, *Sol-gel silica: properties, processing and technology transfer;* William Andrew, 1998.

125. M. Anpo, H. Nakaya, S. Kodama, Y. Kubokawa, K. Domen and T. Onishi. "Photocatalysis over binary metal oxides. Enhancement of the photocatalytic activity of titanium dioxide in titanium-silicon oxides," J. Phys. Chem. **90** 1633-6 (1986).

126. Q. Xu and M.A. Anderson. "Synthesis of porosity controlled ceramic membranes," J. Mater. Res. **6** 1073-81 (1991).

127. S. Satoh, K. Susa, I. Matsuyama, "Sol-gel-derived binary silica glasses with high refractive index" J. Non-Cryst. Solids 146 121-128 (1992).

128. T. Liu and T. Cheng. "Effects of SiO_2 on the catalytic properties of TiO_2 for the incineration of chloroform," Catalysis Today **26** 71-7 (1995).

129. C. Anderson and A.J. Bard. "An improved photocatalyst of TiO_2/SiO_2 prepared by a sol-gel synthesis," J. Phys. Chem. **99** 9882-5 (1995).

130. C. Anderson and A.J. Bard. "Improved photocatalytic activity and characterization of mixed TiO_2/SiO_2 and TiO_2/Al_2O_3 materials," The Journal of Physical Chemistry B **101** 2611-6 (1997).

131. X. Orignac, H. Vasconcelos, X. Du and R. Almeida. "Influence of solvent concentration on the microstructure of SiO_2-TiO_2 sol-gel films," J. Sol Gel Sci. Technol. **8** 243-8 (1997).

132. M. Machida, K. Norimoto, T. Watanabe, K. Hashimoto and A. Fujishima. "The effect of SiO_2 addition in super-hydrophilic property of TiO_2 photocatalyst," J. Mater. Sci. **34** 2569-74 (1999).

133. K.Y. Jung and S.B. Park. "Enhanced photoactivity of silica-embedded titania particles prepared by sol–gel process for the decomposition of trichloroethylene," Applied Catalysis B: Environmental **25** 249-56 (2000).

134. H. Chun, W. Yizhong and T. Hongxiao. "Preparation and characterization of surface bond-conjugated TiO_2/SiO_2 and photocatalysis for azo dyes," Applied Catalysis B: Environmental **30** 277-85 (2001).

135. J. Yu, X. Zhao, C.Y. Jimmy, G. Zhong, J. Han and Q. Zhao. "The grain size and surface hydroxyl content of super-hydrophilic TiO_2/SiO_2 composite nanometer thin films," J. Mater. Sci. Lett. **20** 1745-8 (2001).

136. C.Y. Jimmy, J. Yu, W. Ho and J. Zhao. "Light-induced super-hydrophilicity and photocatalytic activity of mesoporous TiO_2 thin films," J. Photochem. Photobiol. A. **148** 331-9 (2002).

137. J. Yu, C.Y. Jimmy and X. Zhao. "The effect of SiO_2 addition on the grain size and photocatalytic activity of TiO_2 thin films," J. Sol Gel Sci. Technol. **24** 95-103 (2002).

138. K. Guan, B. Lu and Y. Yin. "Enhanced effect and mechanism of SiO_2 addition in super-hydrophilic property of TiO_2 films," Surface and Coatings Technology **173** 219-23 (2003).

139. A. Mills, A. Lepre, N. Elliott, S. Bhopal, I.P. Parkin and S. O'Neill. "Characterisation of the photocatalyst Pilkington Activ™: a reference film photocatalyst?" J. Photochem. Photobiol. A. **160** 213-24 (2003).

140. H.J. Lee, S.H. Hahn, E.J. Kim and Y.Z. You. "Influence of calcination temperature on structural and optical properties of TiO_2-SiO_2 thin films prepared by sol-gel dip coating," J. Mater. Sci. **39** 3683-8 (2004).

141. M. Nakamura, "Hydrophilic and photocatalytic properties of the SiO_2/TiO_2 double layers," Thin Solid Films **496** 131-5 (2006).

142. J. Aguado, R. Van Grieken, M. Lopez-Munoz and J. Marugán. "A comprehensive study of the synthesis, characterization and activity of TiO_2 and mixed TiO_2/SiO_2 photocatalysts," Applied Catalysis A: General **312** 202-12 (2006).

143. L. Zou, Y. Luo, M. Hooper and E. Hu. "Removal of VOCs by photocatalysis process using adsorption enhanced TiO_2-SiO_2 catalyst," Chemical Engineering and Processing: Process Intensification **45** 959-64 (2006).

144. C.M. Whang, Y. Kim, J. Kim, W.I. Lee and Y. Kim. "Photocatalytic Activity of SiO_2-TiO_2 Nanoparticles Prepared by Sol-Hydrothermal Process," Materials Science Forum **449** 1117-20 (2004).

145. Z. Liu, X. Zhang, T. Murakami and A. Fujishima. "Sol–gel SiO_2/TiO_2 bilayer films with self-cleaning and antireflection properties," Solar Energy Mater. and Solar Cells **92** 1434-8 (2008).

146. P. Novotna, J. Zita, J. Krýsa, V. Kalousek and J. Rathouský. "Two-component transparent TiO_2/SiO_2 and TiO_2/PDMS films as efficient photocatalysts for environmental cleaning," Applied Catalysis B: Environmental **79** 179-85 (2008).

147. S. Permpoon, M. Houmard, D. Riassetto, et al. "Natural and persistent superhydrophilicity of SiO_2/TiO_2 and TiO_2/SiO_2 bi-layer films," Thin Solid Films **516** 957-66 (2008).

148. X. Tang, Y. Yu and D. Yang. "SiO_2/TiO_2 fibers from titanium-modified polycarbosilane," J. Mater. Sci. **45** 2670-4 (2010).

149. B. Louis, N. Krins, M. Faustini and D. Grosso. "Understanding crystallization of anatase into binary SiO_2/TiO_2 sol− gel optical thin films: An in situ thermal ellipsometry analysis," Journal of Physical Chemistry C **115** 3115-22 (2011).

150. S. Rasalingam, H.S. Kibombo, C. Wu, et al. "Influence of Ti-O-Si hetero-linkages in the photocatalytic degradation of Rhodamine B," Catalysis Communications, **31** 66-70 (2013).

151. K. Tonooka and N. Kikuchi. "Super-hydrophilic and solar-heat-reflective coatings for smart windows," Thin Solid Films **532** 147-50 (2013).

152. D. Fakin, K.S. Kleinschek, M. Kurečič and A. Ojstršek. "Effects of nanoTiO_2–SiO_2 on the hydrophilicity/dyeability of polyester fabric and photostability of disperse dyes under UV irradiation," Surface and Coatings Technology, **253** 185-93 (2014).

153. K. Mālnieks, G. Mezinskis, I. Pavlovska, L. Bidermanis and A. Pludons. "Optical, photocatalytical and structural properties of TiO_2-SiO_2 sol-gel coatings on high content SiO_2 enamel surface," Materials Science **21** 100-4 (2015).

154. B. Kim, H.M. Yadav and J. Kim. "Self-cleaning performance of sol–gel-derived TiO_2/SiO_2 double-layer thin films," Journal of Coatings Technology and Research, **13** 905-10 (2016).

155. R.E. Ramírez-García, J.A. González-Rodríguez, M. Arroyo-Ortega, S.A. Pérez-García and L. Licea-Jiménez. "Engineered TiO_2 and SiO_2-TiO_2 films on silica-coated glass for increased thin film durability under abrasive conditions," International Journal of Applied Ceramic Technology, **14** 39-49 (2017).

156. P. Misra and M.A. Dubinskii. *Ultraviolet spectroscopy and UV lasers;*CRC Press, 2002.

157. R. Jenkins and R. Zinder. *Introduction to X-ray Powder Diffractometry*, John Wiley & Sons, 1996.

158. J.R. Ferraro and L.J. Basile. *Fourier transform infrared spectra: applications to chemical systems* Academic Press, New York, 1978.

159. D.A. Hanaor and C.C. Sorrell. "Review of the anatase to rutile phase transformation," J. Mater. Sci., **46** 855-74 (2011).

160. M. Addamo, V. Augugliaro, A. Di Paola, et al. "Photocatalytic thin films of TiO_2 formed by a sol–gel process using titanium tetraisopropoxide as the precursor," Thin Solid Films **516** 3802-7 (2008).

161. M. Lottiaux, C. Boulesteix, G. Nihoul, et al. "Morphology and structure of TiO_2 thin layers vs. thickness and substrate temperature," Thin Solid Films **170** 107-26 (1989).

162. R. Mechiakh, F. Meriche, R. Kremer, R. Bensaha, B. Boudine and A. Boudrioua. "TiO_2 thin films prepared by sol–gel method for waveguiding applications: correlation between the structural and optical properties," Optical Materials **30** 645-51 (2007).

163. J.E. Mahan, *Physical vapor deposition of thin films*, Wiley-Interscience, New York 2000.

164. A. Nilchi, S. Janitabar-Darzi and S. Rasouli-Garmarodi. "Sol-gel preparation of nanoscale TiO_2/SiO_2 composite for eliminating of Con Red azo dye," Materials Sciences and Applications **2** 476-80 (2011).

165. M. Kanna and S. Wongnawa. "Mixed amorphous and nanocrystalline TiO_2 powders prepared by sol–gel method: characterization and photocatalytic study," Mater. Chem. Phys. **110** 166-75 (2008).

166. M. Nag, P. Basak and S.V. Manorama. "Low-temperature hydrothermal synthesis of phase-pure rutile titania nanocrystals: Time temperature tuning of morphology and photocatalytic activity," Mater. Res. Bull. **42** 1691-704 (2007).

167. H. Ding, H. Sun and Y. Shan. "Preparation and characterization of mesoporous SBA-15 supported dye-sensitized TiO_2 photocatalyst," J. Photochem. Photobiol. A. **169** 101-7 (2005).

168. K.S. Babu, A.R. Reddy and K.V. Reddy. "Controlling the size and optical properties of ZnO nanoparticles by capping with SiO_2," Mater. Res. Bull., **49** 537-43 (2014).

169. E. Kamitsos, A. Patsis and G. Kordas. "Infrared-reflectance spectra of heat-treated sol-gel-derived silica," Physical Review B **48** 12499 (1993).

170. M. Raileanu, M. Crian, C. Petrache, et al. "Sol-gel Fe_xO_y-SiO_2 nanocomposites," Rom. Journ. Phys **50** 595-606 (2004).

171. C. Gonzalez-Oliver, P.F. James and H. Rawson. "Silica and silica-titania glasses prepared by the sol-gel process," J. Non Cryst. Solids **48** 129-52 (1982).

172. H. Gobara, R. El-Salamony, D. Mohamed, M. Mishrif, Y. Moustafa and T. Gendy. "Use of SiO_2-TiO_2 nanocomposite as photocatalyst for the removal of trichlorophenol: a kinetic study and numerical evaluation," Chemistry and Materials Research **6** 63-81 (2014).

173. T. Ohsaka, F. Izumi and Y. Fujiki. "Raman spectrum of anatase, TiO_2," J. Raman Spectrosc. **7** 321-4 (1978).

174. L. Yang, Y. Lai, J. Chen, P. Tsai, C. Chen and C.J. Chang. "Compositional tailored sol-gel SiO_2-TiO_2 thin films: Crystallization, chemical bonding configuration, and optical properties," J. Mater. Res. **20** 3141-9 (2005).

175. S. Vives and C. Meunier. "Influence of the synthesis route on sol–gel SiO_2-TiO_2 (1: 1) xerogels and powders," Ceram. Int. **34** 37-44 (2008).

176. D. C. L. Vasconcelos, V.C. Costa, E. H. M. Nunes, A.C.S. Sabioni, M. Gasparon and W.L. Vasconcelos. "Infrared spectroscopy of titania sol-gel coatings on 316L stainless steel." (2011) http://repositorio.ufop.br/handle/123456789/1110

177. D. Predoi, O. Crisan, A. Jitianu, et al. "Iron oxide in a silica matrix prepared by the sol–gel method," Thin Solid Films **515** 6319-23 (2007).